ANDRÉ FERREIRA RODRIGUES

INSIGHTS INTO THE CANOPY-RAINFALL INTERACTIONS: NEW EXPERIENCES FROM A LONG-TERM NEOTROPICAL FOREST MONITORING

LAVRAS-MG
2022

ANDRÉ FERREIRA RODRIGUES

INSIGHTS INTO THE CANOPY-RAINFALL INTERACTIONS: NEW EXPERIENCES FROM A LONG-TERM NEOTROPICAL FOREST MONITORING

Tese apresentada à Universidade Federal de Lavras, como parte das exigências do Programa de Pós-Graduação em Recursos Hídricos, área de concentração em Hidrologia, para obtenção do título de Doutor.

Prof. Dr. Carlos Rogério de Mello
Orientador

LAVRAS-MG
2022

Ficha catalográfica elaborada pelo Sistema de Geração de Ficha Catalográfica da Biblioteca Universitária da UFLA, com dados informados pelo(a) próprio(a) autor(a).

Rodrigues, André Ferreira.

Insights into the canopy-rainfall interactions: New experiences from a long-term Neotropical forest monitoring / André Ferreira Rodrigues. - 2022.

181 p. : il.

Orientador(a): Carlos Rogério de Mello.

Tese (doutorado) - Universidade Federal de Lavras, 2022.

Bibliografia.

1. Ecohydrology. 2. Droughts. 3. Modeling. I. de Mello, Carlos Rogério. II. Título.

ANDRÉ FERREIRA RODRIGUES

PERCEPÇÕES NA INTERAÇÃO CHUVA-DOSSEL: NOVAS EXPERIÊNCIAS A PARTIR DO MONITORAMENTO DE LONGO PRAZO DE UMA FLORESTA NEOTROPICAL

INSIGHTS INTO THE CANOPY-RAINFALL INTERACTIONS: NEW EXPERIENCES FROM A LONG-TERM NEOTROPICAL FOREST MONITORING

Tese apresentada à Universidade Federal de Lavras, como parte das exigências do Programa de Pós-Graduação em Recursos Hídricos, área de concentração em Hidrologia, para obtenção do título de Doutor.

APROVADA em 18 de fevereiro de 2022.

Dr. Marcelo Ribeiro Viola – DRH/UFLA
Dra. Marcela de Castro Nunes Santos Terra – DCF/UFLA
Dr. José Alves Junqueira Junior – IF SUDESTEMG
Dra. Kelly Cristina Tonello – DCA/UFSCAR

Prof. Dr. Carlos Rogério de Mello
Orientador

LAVRAS-MG
2022

A todos aqueles que acreditam na ciência como instrumento para moldar a sociedade

Dedico

AGRADECIMENTOS

Aos meus pais, José Geraldo e Marluci, pelo apoio incondicional e por não terem medido esforços para que eu pudesse estudar.

À minha irmã, Bárbara, pela amizade, cumplicidade e por proporcionar momentos ótimos de descontração.

À minha esposa, Bruna, por ser suporte nos momentos de frustração e companheira nas conquistas. Sem você, nada seria possível. Amo-te.

À minha família por ter me ensinado o valor do trabalho e da dedicação.

Aos meus amigos de infância (Z.F.C) por terem sido companheiros em todos esses anos.

Ao esporte por ter sido crucial no meu desenvolvimento e por ter me direcionado para o caminho certo.

Aos amigos do programa de pós-graduação por serem os únicos capazes de entender os diversos sentimentos que passamos ao longo deste período.

A todos os mestres que tive o prazer de trocar conhecimentos e que foram fundamentais para o meu crescimento intelectual.

Ao professor Carlos Rogério pelos ensinamentos, conselhos e amizade.

Ao técnico em hidrologia Renato pela amizade e profissionalismo.

A todos os colaboradores por terem dedicado parte do seu tempo na construção da presente tese.

À Universidade Federal de Lavras pela qual serei eternamente grato.

Ao Programa de Pós-Graduação em Recursos Hídricos.

À Coordenação de Aperfeiçoamento de Pessoal do Nível Superior (CAPES) pelo apoio financeiro.

Muito obrigado!

RESUMO

A interceptação da precipitação pelos dosséis florestais é um dos processos hidrológicos mais importantes da zona crítica. As interações dossel-precipitação conduzem os ciclos da água e de nutrientes ao redistribuir a precipitação tanto no tempo quanto no espaço. Tais interações definem vários processos hidrológicos tais como a dinâmica da água no solo, a evapotranspiração, o escoamento superficial, os padrões espaço-tempo dos nutrientes, a recarga subterrânea, dentre outros. As relações dossel-precipitação ainda são pouco conhecidas em vários biomas florestais, principalmente no tocante aos efeitos de condições climáticas severas (e.g., secas) nessas interações. Neste sentido, o presente estudo objetivou investigar a partição da precipitação em uma floresta Neotropical durante uma seca prolongada. A partição da precipitação se inicia com a interceptação da chuva pelo dossel dando início ao escoamento pelo tronco e precipitação interna. Precipitação interna e escoamento pelo tronco são as parcelas da precipitação que alcançam o solo e, juntas, são conhecidas como precipitação efetiva. Outra parcela da precipitação retorna à atmosfera por evaporação durante e após o evento. A evaporação do dossel e a precipitação interna são as maiores parcelas da partição da precipitação, podendo chegar a 99,5% em florestas tropicais e, por isso, são as variáveis analisadas nesse estudo. Modelos físicos imitam a realidade e são ferramentas essenciais para avançar no entendimento de processos físicos complexos como a interceptação da precipitação. Os modelos de Liu e Gash tiveram atuações satisfatórias modelando a interceptação da chuva em diferentes climas e florestas. Porém, eles nunca haviam sido aplicados para condições de seca. O modelo de Liu sobressaiu ao de Gash na floresta Neotropical por representar melhor a estratificação do dossel. Em períodos sem seca, a radiação solar e a energia armazenada no interior da floresta (ar e biomassa) são responsáveis pela evaporação do dossel. Além dessas fontes de energia, a advecção de áreas circunvizinhas tem atuação mais importante e aumenta a evaporação nas secas. Outra consideração importante é o comportamento da distribuição espacial da precipitação interna durante secas. O índice de estabilidade temporal foi utilizado para avaliar o comportamento da variabilidade espacial da precipitação interna ao longo do tempo e destacar a possível influência da dinâmica climática e florestal. Interpretações equivocadas da estabilidade temporal da precipitação interna foram observadas em estudos anteriores porque as mudanças estruturais da floresta e em padrões climáticos não foram consideradas. Biomassa, a dominância de algumas espécies e a ocupação por árvores são características florestais que conduzem a distribuição espacial e a estabilidade temporal da precipitação interna. Essas estruturas mudam devido a sucessões ecológicas ou recuperando de alguma perturbação (e.g., secas), o que altera a distribuição espacial da precipitação interna. Ademais, as intensidades máximas das precipitações são diferentes durante as secas, alterando os processos de saturação/instauração do dossel e, portanto, a estabilidade temporal. Assim, secas modificam as interações dossel-precipitação aumentando a evaporação do dossel e alterando a distribuição espacial da precipitação interna ao longo do tempo.

Palavras-chave: Partição da Precipitação. Mata Atlântica. Modelagem. Balanço de Energia. Dinâmica Florestal

ABSTRACT

One of the most important processes in the hydrology of the critical zone is the rainfall interception by forest canopies. The canopy-rainfall interactions drive the water and nutrient cycles by redistributing rainfall in both time and space. This defines the fate of many hydrological processes, such as soil water dynamics, evapotranspiration, streamflow, spatiotemporal pattern of nutrients, and groundwater recharge. Although the canopy-rainfall interactions are well-known in many forests worldwide, there is still a knowledge gap in the effects of extreme weather (e.g., droughts) on these interactions. In this regard, the present study aims to improve the understanding regarding rainfall partitioning in a Neotropical forest during a prolonged drought. Rainfall partitioning starts with the canopy intercepting the rainfall and splitting it into stemflow and throughfall. Throughfall and stemflow is the amount of water that reaches the floor, known as net rainfall. A parcel of the intercepted water returns to the atmosphere by evaporation during and after the event. The canopy evaporation and throughfall are the most significant part of the rainfall partitioning, summing up to 99.5% in some tropical forests. Therefore, they are the subject of the present study. Physical models mimic reality and are key tools to advance the knowledge of complex physical processes such as rainfall interception. The Liu and Gash models have presented adequate performances to model the rainfall interception in different climates and forests. However, they had never been applied to drought conditions. The Liu model overcame the Gash model in the Neotropical forest because it better represents the stratified canopy. In non-drought periods, solar radiation and the energy stored in biomass and the air inside the forest are responsible for canopy evaporation. Besides the abovementioned energy sources, the energy advection from surrounding areas plays a more important role and increases canopy evaporation during droughts. Another important consideration is the spatial distribution of throughfall and how it behaves during droughts. The time stability index was considered to assess the behavior of the spatial variability of throughfall over time to highlight the likely influence of forest and weather dynamics on it. Misinterpretation of time stability of throughfall was observed in prior studies because the changes in forest structure and weather patterns had not been considered. Biomass, the dominance of some species, and tree occupation are forest characteristics driving the spatial distribution and time stability of throughfall. These structures change due to ecological succession or regenerating from a disturbance (e.g., droughts), which modify the spatial distribution of throughfall. Moreover, maximum rainfall intensities are different in drought periods, changing the canopy's saturation/unsaturation processes, and therefore the time stability. In this sense, droughts modify the canopy-rainfall interactions by enhancing canopy evaporation and changing the spatial distribution of throughfall over time.

Keywords: Rainfall Partitioning. Atlantic Forest. Modeling. Energy Balance. Forest Dynamics.

SUMMARY

1 Introduction

Forests connect soil to the atmosphere by intermediating mass and energy exchanges. Among the processes encompassing the soil-forest-atmosphere continuum (e.g., evapotranspiration, soil moisture dynamics, root water uptake, preferential pathway formation, groundwater recharge), the rainfall-canopy interactions deserve a special attention because they are the genesis of the water and nutrient cycles. The forest canopy attenuates the gross rainfall and works as a reservoir, which may reach saturation depending on the rainfall amount, weather condition, and storage capacity. The stored water is redistributed toward the floor by dripping from the canopy or running down on the trunks. The raindrops can also splash water from the canopy and pass freely through the gaps. The drip, splash, and free water are known as throughfall, whereas the stemflow is the water draining on the trunk. These processes are part of the canopy water balance and are responsible for the soil moisture dynamics, spatial distribution of tree species, formation of hotspots for groundwater recharge, increasing the soil biodiversity, driving evapotranspiration, among others.

Part of the water stored on the canopy returns to the atmosphere by evaporation during the rainfall event. This amount represents an unavailable fraction of water and is known as canopy interception. Although this fraction varies with weather conditions and canopy structure, it can reach up to 35% of gross (or incident) rainfall in tropical forests. This amount is likely to increase in the upcoming decades as more intense and prolonged droughts are expected in tropical regions. Canopy evaporation is likely to increase in dry years due to a drier and hotter atmosphere. In this regard, to attain the sustainable goals for water resources management, it is straightforward the importance of understanding the canopy interception under drought conditions, which have not been accounted for up to now.

Although field experiments and remote sensing techniques have been applied to assess canopy interception worldwide, the development of physical models accelerated the understanding of the rainfall-canopy interactions. It enabled the forecasting of water loss by evaporation. However, such models have not been applied in droughts yet. Drought is likely to increase evaporation due to a greater energy availability, which increases the atmosphere dynamics. Besides the well-known sources of energy that drive canopy evaporation in normal conditions (such as air temperature and solar radiation), droughts may provide new sources of energy that are barely known yet.

Therefore, assessing rainfall interception in these conditions is mandatory to understand the water availability as long as droughts become more frequent and intense (as in the case of climate change).

Canopy evaporation and the spatial and temporal distribution of throughfall are likely to change during droughts. Throughfall represents the most significant parcel of the canopy water balance and is the driving force of the water and nutrient cycles. Throughfall has already been recognized as a function of weather characteristics (e.g., rainfall amount, intensity, wind velocity, and air temperature) and canopy structure (e.g., leaf properties, storage capacity, branch architecture, and canopy hydrophobicity). However, the importance of forest structure (e.g., species diversity, dominance, biomass, number of individuals) has not been fully understood yet. Forests are dynamic environments in constant successional development and adapting to some disturbance (e.g., droughts, logging, and fire). The effects of these dynamics on the spatial distribution of throughfall should be assessed because they may change the water and nutrient cycles. Therefore, not considering the temporal changes of the spatial distribution of throughfall can lead to misinterpretation of the rainfall-canopy interception, which will obscure the relationships between weather, forests, and hydrology.

In this sense, this thesis aims to advance in the knowledge regarding the canopy-rainfall interactions and the effects of droughts by (i) applying physically-based models to model rainfall interception in drought conditions, (ii) improving the understanding of the energy dynamics in the canopy-atmosphere interactions, and (iii) assessing the importance of forest structure and droughts on the spatial variability of throughfall. The study was carried out in a semi-deciduous Atlantic forest remnant throughout seven years of monitoring. This forest is in an advanced conservation stage and can provide meaningful insight into the importance of its preservation for water resources purposes. Moreover, this semi-deciduous Atlantic forest remnant has been the subject of many studies recently. These studies encompass soil water dynamics (JUNQUEIRA JUNIOR et al., 2017; OLIVEIRA et al., 2021; RODRIGUES et al., 2020), nutrient inputs (MANTOVANI et al., 2021), water balance (RODRIGUES et al., 2021b), rainfall interception (JUNQUEIRA JUNIOR et al., 2019; RODRIGUES et al., 2021a), rainfall water quality (MARQUES et al., 2019), stemflow (TERRA et al., 2018) and throughfall (RODRIGUES et al., 2022) dynamics, spatial variability of net precipitation

(RODRIGUES et al., 2020), and ecological succession (SOUZA et al., 2021). Therefore, studying this remnant has provided significant insights into the importance of the Atlantic Forest for local meteorology, hydrology, and biodiversity so far.

2 Theoretical Framework

2.1 Atlantic Forest

The Brazilian Atlantic Forest is one of the world's most biodiverse areas (MYERS et al., 2000), with remarkable endemism and hydrological importance (MELLO et al., 2019; RODRIGUES et al., 2021b). However, this biome has been highly degraded by the historical expansion of urban and agricultural activities (DEAN, 1995; JOLY et al., 2014; RIBEIRO et al., 2009). The degree of threat, and its importance for species conservation, guaranteed the title of "biodiversity hotspot" to the Atlantic Forest (MYERS et al., 2000). Therefore, the Atlantic Forest is a priority biome for conservation.

The Atlantic Forest initially encompassesd15% of the Brazilian territory (17 out of 27 Brazilian federative units). However, only 12.4% of the original extent remains in remnants greater than 3 ha (SOS Mata Atlântica, access link: https://www.sosma.org.br/), which points out the biome devastation degree. Moreover, Atlantic Forest is home to 72% of the Brazilian people and is responsible for 70% of the Brazilian Gross Domestic Product (GPD) (SOS Mata Atlântica, access link: https://www.sosma.org.br/). These characteristics highlight the importance of this biome since most of the Brazilian economy depends on it. Fortunately, the largest remaining Atlantic Forest patches are located in mountain ranges, which are advantageous environments for water yield (MELLO et al., 2019; TEIXEIRA et al., 2021) and hazard mitigation (NEHREN et al., 2019). This reinforces the importance of the Atlantic Forest for water management due to its close relationship with water availability (TERRA et al., 2018b).

Therefore, studies that highlight the importance of the Atlantic Forest biome as a provider of ecosystem services (such as water yield and biodiversity shelter) are crucial to support stakeholders and decision-makers in taking the best actions. They also provide supporting evidence to increase preserved areas to guarantee people's well-being and livelihood.

2.2 Rainfall partitioning

Precipitation falling on a forest canopy takes different pathways on its way to the forest floor. The incident (or gross) rainfall is routed to the subcanopy by throughfall and stemflow (CROCKFORD; RICHARDSON, 2000; GUO et al., 2020). Throughfall (TF) is defined as the most significant fraction of gross rainfall (GR) that passes directly through the canopy along with the portions that drip and splash from it. Stemflow is the minor fraction of GR that drains from outlying leaves and branches and is channeled to the bole (or stem) of plants (LEVIA; GERMER, 2015; LIU et al., 2018; LLORENS; DOMINGO, 2007). Such rainfall redistribution is driven by weather and forest characteristics (VAN STAN et al., 2020, YAN et al., 2021; ZHANG et al., 2015). Rainfall intensity, duration, and amount under different wind speeds and directions have been recognized as the main meteorological drivers of rainfall redistribution in forests (e.g., NANKO et al., 2011). On the other hand, the structure and architecture of the forest canopy are generally considered the most critical biotic features controlling rainfall redistribution in forests (STAELENS et al., 2006; TERRA et al., 2018a).

The complexity of tropical forests is another characteristic driving the spatial and temporal patterns of rainfall partitioning. The diversity of species addresses heterogeneity on canopy storage capacity due to the variety of leaf shape, orientation, and texture, canopy hydrophobicity, and bark roughness (LEVIA; FROST, 2006; NANKO et al., 2014; POORTER et al., 2006; TERRA et al., 2018a). Moreover, the species-specific characteristics that improve (or decrease) canopy drainage (LEVIA; FROST, 2006) are unevenly distributed throughout the forest, which creates a particular time for starting canopy drainage (ALLEN et al., 2013). For instance, reduced canopy interception is observed in young trees due to their small crown (TERRA et al., 2018a; WULLAERT et al., 2009), funnel-shaped branches (GERMER et al., 2006; SU et al., 2019), and greater canopy openness (MARTINS et al., 2004). The importance of

canopy gaps to decrease canopy interception is even greater in lower rainfall amounts (STAELENS et al., 2006), highlighting the importance of canopy openness during small events (ZIMMERMAN et al., 2009). This provides different conditions to intercept and route water, depending on rainfall characteristics (intensity, amount, and duration).

Rainfall intensity increases splash throughfall (LEVIA et al., 2019) and decreases canopy storage capacity (CALDER et al., 1996). The time interval between rainfall events also influences rainfall redistribution because of canopy dryness levels (Allen et al., 2013). The importance of pre-event canopy storage on throughfall formation was highlighted by Allen et al. (2013) using isotopic tracers. Wind speed and direction also drive throughfall due to the canopy shaking (decreasing canopy storage capacity; ZHANG et al., 2019) and the rain shadow effects. Greater rainfall interception in the windward than the leeward canopy was observed by Fan et al. (2014), creating "dry" spots in the forest.

Such heterogeneity of rainfall redistribution entails different spatial and temporal dynamics of forest hydrology and biogeochemistry dynamics (METZGER et al., 2021) that deserves further investigation. For instance, Stogsdill et al. (1986) assessed the relationship between thinning and throughfall input to improve soil water availability in a Pinus plantation. However, the complexity of rainfall redistribution increases in tropical forests because TF probably interacts and responds to the traits of several trees before reaching the floor (AUBRY-KIENTZ et al., 2019; GUAN et al., 2013). This greater interaction with the stratified canopy of tropical forests defines the fate of nutrient input (MANTOVANI et al., 2021; TONELLO et al., 2021), soil moisture (JUNQUEIRA JUNIOR et al., 2017; OLIVEIRA et al., 2021), distribution of tree species (PRESSLAND, 1976; TERRA et al., 2018b), evapotranspiration (GUSWA; SPENCE, 2011; RODRIGUES et al., 2021b), and groundwater recharge (BIALKOWSKI; BUTTLE, 2015; GUSWA; SPENCE, 2011).

2.3 Physical models

2.3.1 Rutter model (1971)

Rutter et al. (1971) proposed the first physics-based model, which relies on both climate and canopy characteristics. The model performs a running water balance, in which the balance between rainfall and evaporation drives both throughfall and canopy interception. Moreover, a portion of rain may reach the soil directly since gaps are present in forest canopies (RODRIGUES et al., 2021):

$$\Delta C = (1 - p) \int R\, dt - \int D\, dt - \int E\, dt \quad (1)$$

where ΔC is the change in canopy water storage in the interval dt; p is the free throughfall coefficient (i.e., the rainfall that reaches the forest floor without touching the canopy); R is the rainfall rate; D is the rate of water dripping (or draining) from the canopy, and E is the evaporation rate. Throughfall (*TF*) is composed of direct rainfall and dripping water:

$$TF = p \int R\, dt + \int D\, dt \quad (2)$$

Dripping is modeled by an empirical relationship with canopy water storage (C) and only happens when $C \geq S$ (VALENTE; DAVID; GASH, 1997). S is defined as the minimum water necessary to saturate the canopy (i.e., the canopy storage capacity):

$$D = \begin{cases} D_s \exp[b(C - S)] & if\ C \geq S \\ 0 & if\ C < S \end{cases} \quad (3)$$

D_s is the minimum drainage rate (for $C = S$), and b is an empirical coefficient. From 5-minutes observations of R and T in a Corsian pine forest, Rutter et al. (1971) defined $D_s = 0.002$ mm min^{-1}. Since D_s was empirically determined, Rutter, Morton, and Robins (1975) proposed an improvement by relating the minimum drainage rate to the leaf area index (LAI), enabling the extrapolation for other forests. Moreover, these authors also observed that stemflow can be an important fraction of rainfall and should be considered apart from the canopy. Therefore, the trunk storage capacity (S_t) and the proportion intercepted by the trunks (p_t) were introduced to define a second reservoir:

$$\Delta C = (1 - p - p_t) \int R\, dt - \int D\, dt - \int E\, dt \quad (4)$$

$$\Delta C_t = p_t \int R\, dt - \int E_t\, dt \quad (5)$$

where ΔCt is the change in trunk water storage; and E_t the evaporation rate from the trunks. Differently from the canopy drainage (or dripping), when $C_t > S_t$, the excess is promptly drained from the trunks as stemflow (RUTTER; MORTON; ROBINS, 1975).

Rutter, Morton, and Robins (1975) considered that there are potential evaporation rates (E_p and E_{pt} for the canopy and trunk, respectively) which are controlled by the available water in both reservoirs:

$$E = E_p \frac{C}{S} \tag{6}$$

$$E_t = E_{pt} \frac{C_t}{S_t} \tag{7}$$

$$E_{pt} = e\, E_p \tag{8}$$

where *e* is an empirical ratio parameter. Rutter, Morton, and Robins (1975) and Valente, David, and Gash, (1997) argued that the potential evaporation from the trunks is way lower than that from the canopy and could be well represented by fitting the parameter *e* to the observed stemflow.

Although there are many methods to retrieve the potential evaporation, the Penman-Monteith method was considered in the model's conception because it is a physics-based approach, agreeing with the former assumptions (RUTTER et al., 1971). Since potential evaporation only happens when the canopy is saturated, transpiration can be neglected, and the resistance imposed by the stomata sets to zero (i.e. $r_s = 0$):

$$E_P = \frac{\Delta R_n + \rho_a c_p g_a (e_s - e_a)}{\lambda(\Delta + \gamma)} \tag{9}$$

where Δ is the slope of the saturation vapor pressure curve; R_n is the net radiation; ρ_a is the mean air density at constant pressure; c_p is the specific heat of the air; g_a is the aerodynamic conductance; e_s is the saturation vapor pressure; e_a is the actual vapor pressure; $(e_s - e_a)$ is known as the vapor pressure deficit; λ is the latent heat for water vaporization, and γ is the psychrometric constant. The other methods and some assumptions that should be considered before applying the Penman-Monteith techniques will be further described in the appropriate topic.

2.3.2 Sparse Rutter model (1997)

There were some inconsistencies in the original formulation of the Rutter model, which impaired the canopy interception modeling of sparse forests (VALENTE;

DAVID; GASH, 1997). Gash, Lloyd, and Lachaud (1995) argued that portioning the rainfall rate as $(1 - p - p_t)R$ is unsuitable because two problems arise in sparse forests:

- Gaps are more significant in sparse forests, and therefore p increases. In these conditions, the canopy may never reach saturation whether $(1 - p - p_t)R \leq E$.
- Since $\bar{E}$ is calculated per unit of the total plot area, the evaporation per unit of canopy area increases proportionally with canopy sparseness (with p). As $p \rightarrow \infty$, E follows its pattern ($E \rightarrow \infty$), which is physically impossible.

Moreover, the total canopy evaporation was inconsistent with the energy balance in the original formulation. The evaporation was split between the canopy (Equation 6) and the trunk (Equation 8), which encompass the entire plot area. Thus, the total evaporation per unit plot area was $(1+e)E_p$. This problem had been neglected because of the small values of e (VALENTE; DAVID; GASH, 1997). Valente, David, and Gash, (1997) fixed it by rewriting canopy evaporation as $(1–e)E_p$.

To address the preceding problems, Valente, David, and Gash (1997) split the total plot area into covered (canopy + trunks) and open (gaps) subareas. The same rainfall intensity reaches both areas, and the evaporation (usually calculated with the Penman-Monteith method) regards only the covered area. Therefore, the evaporation from gaps is zero, (neglecting the evaporation from the understory). The canopy and trunk storage capacity were rewritten to model canopy interception having the canopy area as reference (GASH; LLOYD; LACHAUD, 1995).

$$S_c = \frac{S}{c} \tag{10}$$

$$S_{t,c} = \frac{S_t}{c} \tag{11}$$

where S_c is the canopy storage capacity per unit canopy area and $S_{t,c}$ is the trunk storage capacity per trunk area. Valente et al. (1997) simplified the drainage function (Equation 3) by considering that all excess water (C > S) is promptly routed to the floor. This change was made to eliminate the empirical parameters (D_s and b). A portion is designated to the trunk (pd) reservoir from this drainage and will further generate stemflow. One can realize that the trunk reservoir starts filling only after the canopy is saturated (VALENTE; DAVID; GASH, 1997). The sparse Rutter model can be written as:

$$TF = (1 - c)GP + c(1 - p_d) \int D_c dt \quad (12)$$

$$SF = c\left(p_d \int D_c\, dt - S_{t,c} - \int E_{t,c} dt\right) \quad (13)$$

$$cGP = c\left(\int E_c dt + \int D_c\, dt + S_c\right) \quad (14)$$

where SF is the stemflow, D_c is the drainage per canopy area, and $E_{t,c}$ is the evaporation rate per unit trunk area.

2.3.3 Gash model (1979)

Despite the advantages that the Rutter model had attained, there were some shortcomings to be addressed. First, the Rutter model demands a high temporal resolution of both rainfall and meteorological data, in which an hourly step produces the best results (MUZYLO et al., 2009; RUTTER; MORTON; ROBINS, 1975). Such a temporal resolution is far from the reality of many studies, mainly those in tropical forests. These forests are primarily found in developing countries with problems in research funding and technical staff. Therefore, a more straightforward model was necessary. Second, prior knowledge in programming was necessary to build the running water balance, which limited its widespread application (GASH, 1979). In this regard, Gash (1979) proposed a simpler rainfall interception model without losing the physical description of the rainfall-canopy interactions. It is also known as the analytical form of the Rutter model because a series of discrete storms represent the rainfall events with sufficient time between them to enable canopy and trunk to dry completely (GHIMIRE et al., 2017a; JUNQUEIRA JUNIOR et al., 2019; RODRIGUES et al., 2021).

The model can be split into three phases: (i) the wetting phase, where the canopy is still unsaturated; (ii) the saturation phase; and (iii) the drying phase, where rainfall has already finished. Moreover, to simplify the Rutter model, some assumptions were considered:

- The meteorological conditions of both the wetting and saturation phases are the same for each event, and their average can represent the meteorology of all events throughout the study period. Therefore, rainfall and evaporation means

computed during the saturation phase represents the overall meteorological condition;

- There is no drip from the canopy before saturation. The excess of water is promptly drained from the canopy, remaining only the saturation capacity (S) at the end of a storm. This configures the water-box approach.
- The interval between rainfall events must be sufficient to guarantee the complete dryness of the canopy and trunk, i.e., the reservoir (canopy + trunks) is empty before any rainfall.

Canopy interception is the portion of rainfall returning into the atmosphere through evaporation. This evaporation happens in the three abovementioned phases (for each rainfall event) and can be written as follows:

$$CI = \int_0^{t'} E\ dt + \int_{t'}^{t} E\ dt + S \tag{10}$$

CI is the rainfall canopy interception of an event n; t' is the time necessary for canopy saturation; t is the event duration; E is the evaporation rate for each time step dt, and S is the canopy storage capacity. The first member on the right-hand side is the wetting up phase, the second is the saturation phase, and the third is the drying phase. Considering the first assumption, mean evaporation and rainfall rates can be set to represent the meteorological conditions of all events:

$$\bar{E} = \frac{1}{(t - t')} \int_{t'}^{t} E\ dt \tag{11}$$

$$\bar{R} = \frac{1}{(t - t')} \int_{t'}^{t} R\ dt \tag{12}$$

where $\bar{E}$ and $\bar{R}$ are the mean evaporation and rainfall rates for an event n. The mean rainfall rate can also be written in terms of the total rainfall that fell during the saturation phase (t – t'):

$$GP - P'_G = \bar{R}(t - t') \quad (13)$$

where P'_G is the minimum rainfall necessary for canopy saturation, the second assumption made by Gash (1979) is that there is no drip from the canopy before saturation (i.e., the water-box approach), and therefore P'_G can be set as:

$$(1 - p - p_t)P'_G = S + \int_0^{t'} E\ dt \quad (14)$$

where p and p_t are the free throughfall coefficient and the rainfall portion derived to the trunks (RUTTER et al., 1971; RUTTER; MORTON; ROBINS, 1975), respectively. Therefore, canopy interception is defined by integrating and rearranging the preceding equations:

$$CI = \int_0^{t'} E\ dt\ + \frac{\bar{E}}{\bar{R}}(GP - P'_G) + S \quad (15)$$

Since this equation represents the rainfall canopy interception for one event, the total water intercepted by the forest canopy is the sum of all events throughout the study period:

$$\sum_{j=1}^{n} CI_J = \sum_{j=1}^{n} \left[\int_0^{t'} E\ dt + \frac{\bar{E}}{\bar{R}}(GP - P'_G) \right] + nS \quad (16)$$

where n is the number of rainfall events in the study period. Equation 6 represents the three phases for all rainfall events and will be further described in the following sections.

2.3.3.1 The wetting phase

Two magnitudes of events are considered to model the rainfall canopy interception in the wetting phase: (i) those which saturate the canopy and (ii) those

insufficient for saturation (i.e., GP < P'_G). Equation 14 can be integrated to all events able to saturate the canopy:

$$\sum_{j=1}^{n} CI_j = \sum_{j=1}^{n} \left[\int_0^{t'} E \, dt \right] = (1 - p - p_t) \sum_{j=1}^{n} P'_{G_j} - nS \tag{17}$$

The m events insufficient to saturate the canopy are represented by the portion of the gross precipitation that reaches the canopy (1 – p – p_t)*GP. Therefore, the final equation joining both events' magnitude is:

$$\sum_{j=1}^{n+m} CI_j = (1 - p - p_t) \sum_{j=1}^{n} P'_{G_j} - nS + (1 - p - p_t) \sum_{j=1}^{m} GP_j \tag{18}$$

2.3.3.2 The saturation phase

This phase only happens for those n events able to saturate the forest canopy (i.e., GP ≥ P'_G) and ends when rainfall ceases:

$$\sum_{j=1}^{n} CI_J = \frac{\bar{E}}{\bar{R}} \sum_{j=1}^{n} \left(GP_j - P'_{G_j} \right) \tag{19}$$

2.3.3.3 The drying phase

For those events which saturate the canopy, the remaining water only leaves the canopy by evaporation after rainfall ceasing (water-box assumption). In this regard, the canopy storage capacity is added up to the n events as nS.

2.3.3.4 Trunk interception and evaporation

The rainfall is derived to the trunks as soon as it reaches the canopy, being not considered in its water balance (RUTTER et al., 1971). The water-box approach also applies to the trunks because stemflow only occurs after S_t is satisfied (GASH, 1979). For GP ≥ S_t/p_t, the trunk saturates, and the exceedance is promptly converted to stemflow. Since evaporation from the trunks is much lower than that from the canopy

(RUTTER; MORTON, 1977; VALENTE; DAVID; GASH, 1997) in the course of the rainfall event, it is neglected in the Gash model. Therefore, the water stored on the trunks is the only to be evaporated (GASH, 1979):

$$\sum_{j=1}^{n+m} CI_j = qS_t + p_t \sum_{j=1}^{n+m-q} GP_j \tag{20}$$

where q is the number of rainfall events that satisfy $GP \geq S_t/p_t$.

All the foregoing equations consider that the interval between rainfall events is sufficient to dry completely both canopy and trunk, i.e., every time a rainfall starts, the reservoirs (canopy + trunk) are empty. Finally, the original Gash model can then be written as:

$$\begin{aligned}\sum_{j=1}^{n+m} CI_j = (1-p-p_t)\sum_{j=1}^{n} P'_{G_j} + \frac{\bar{E}}{\bar{R}}\sum\nolimits_{j=1}^{n}\left(GP_j - P'_{G_j}\right) \\ + (1-p-p_t)\sum_{j=1}^{m} GP_j + qS_t + p_t \sum_{i=1}^{m+n-q} GP_j\end{aligned} \tag{21}$$

2.3.3.5 The minimum rainfall to canopy saturation

The only definition remaining is the minimum rainfall necessary to saturate the canopy (P'_G). It relies on the canopy water balance in the wetting phase, having the canopy storage (C) from Rutter et al. (1971) as the dependent variable.

$$\frac{dC}{dt} = (1-p-p_t)\bar{R} - E \tag{22}$$

where E is the evaporation rate from the partially saturated canopy. Following Rutter et al. (1971), E can be written as a function of canopy storage $E = \frac{C}{S} * E_p$. Considering the assumption that mean evaporation and rainfall during the saturation phase can represent the overall meteorological condition, E is set as $E = \frac{C}{S} * \bar{E}$. Therefore,

$$\frac{dC}{dt} = (1 - p - p_t)\bar{R} - \frac{C}{S}\bar{E} \quad (23)$$

and the solution:

$$C(t) = (1 - p - p_t)\frac{\bar{R}S}{\bar{E}}\left[1 - e^{-\bar{E}t/S}\right] \quad (24)$$

where C(t) is the canopy storage at each moment t between rainfall onset and canopy saturation. Equation 24 is valid for the interval [0, t']. At t', canopy saturation is fulfilled and the rainfall amount can be defined by $P'_{G_j} = \bar{R}t'$. P'_G is set by replacing these two conditions in Equation 24 and manipulating it algebraically. It is worth mentioning that P'_G is constant for the analyzed period. To further details on the definition of P'_G, readers should extend their attention to Gash (1979).

$$P'_G = -\frac{\bar{R}S}{\bar{E}} ln\left[1 - \frac{\bar{E}}{\bar{R}(1 - p - p_t)}\right] \quad (25)$$

2.3.4 Liu model

Liu (1997) concentrated his efforts on developing a rainfall interception model without the empirical canopy drainage of the running model of Rutter et al. (1971) (Equation 3), and that was as simple as the Gash model (GASH, 1979). Canopy interception can be written as a function of the change in the canopy storage and the evaporation throughout the rainfall events:

$$CI = \Delta C + EV \quad (26)$$

where ΔC is the change in the canopy storage (in the Liu model represents both canopy and trunks) and EV is the canopy evaporation throughout the rainfall event.

2.3.4.1 Change in canopy storage (ΔC)

The canopy is quickly filled in a rainfall event due to its storage capacity, and therefore the evaporation can be disregarded (LIU, 1997). In this initial phase, changes in rainfall after passing through the canopy are only due to the increase in canopy storage ΔC, i.e.

$$\Delta C = -(TF - GP) \tag{27}$$

Liu (1997) described the changes in rainfall (TF – GP) as a function of rainfall intensity and duration, canopy dryness, and the canopy cover fraction:

$$(TF - GP) = cRD\Delta T' \tag{28}$$

where R is the rainfall intensity, D is the canopy dryness, and $\Delta T'$ is the small time-step where evaporation can be neglected (LIU, 1997). Canopy dryness is another way to describe the canopy reservoir by representing its emptiness:

$$D = 1 - \frac{C}{C_m} \tag{29}$$

where C_m is the storage capacity (canopy + trunk).

By rearranging and integrating Equations 27, 28, and 29, canopy dryness is expressed as a function of rainfall amount and the emptiness before the event had started (D_i):

$$D = D_i e^{-cGP/C_m} \tag{30}$$

Equation 30 can be rewritten as a function of canopy storage to better understand the canopy water balance (Equation 31). Moreover, the overall representation of canopy storage changing (ΔC) should take into consideration some antecedent storage (C_i), i.e., $\Delta C = C - C_i$, where $C_i = C_m(1 - D_i)$ (Equation 32).

$$C = C_m\left(1 - D_i e^{-cGP/C_m}\right) \tag{31}$$

$$\Delta C = C_m D_i \left(1 - e^{-cGP/C_m}\right) \tag{32}$$

2.3.4.2 Evaporation

As previously discussed (LIU, 1997), evaporation (E) is the integration of the product of the evaporation rate (E) and the wetness of the canopy (1 – D):

$$EV = \int_0^T E(1 - D)dt \tag{33}$$

$$EV = \int_0^T E\left(1 - D_i e^{-cPt/C_m}\right)dt \tag{34}$$

where T is the duration of the rainfall event and P is the rainfall intensity in each time-step dt. Therefore, the running form (LIU, 2001) of the canopy water balance developed by Liu (1997) is:

$$CI = C_m D_i \left(1 - e^{-cGP/C_m}\right) + \int_0^T E\left(1 - D_i e^{-cPt/C_m}\right)dt \tag{35}$$

2.3.4.3 Assumptions and the analytical form

Although the running form of the Liu model (Equation 35) is more straightforward than that of Rutter et al. (1971), it still demands computational efficiency and a detailed dataset. In this regard, an analytical form of the Liu model was developed (LIU, 1997) to simulate the rainfall canopy interception on either a single-storm or multiple-storm scale (LIU, 2001). To start the derivation of the analytical form of the Liu model, Equation 36 can be rewritten as follows:

$$CI = C_m D_i \left(1 - e^{-\frac{cGP}{C_m}}\right) + \int_0^T E dt - \int_0^T E D_i e^{-\frac{cPt}{C_m}} dt \tag{36}$$

Liu (1997) assumed that the evaporation and rainfall rates could be represented by their average ($E \cong \overline{E}$ and $P \cong \overline{R}$, respectively) throughout the rainfall event (GASH, 1979). Moreover, the rainfall events are individuals, in which the canopy reservoir is empty (dry) before each rainfall onset (GASH, 1979). When the canopy is dry, $D_i = 1$. Following this assumption, the integral could be solved analytically (from equation 37 to 39):

$$CI = C_m\left(1 - e^{-\frac{cGP}{C_m}}\right) + \int_0^T \bar{E}\,dt - \int_0^T \bar{E}e^{-\frac{c\bar{R}t}{C_m}}dt \tag{37}$$

$$CI = C_m\left(1 - e^{-\frac{cGP}{C_m}}\right) + \bar{E}t_0^T - \left\{-\bar{E}\left[\frac{C_m}{c\bar{R}}e^{\frac{-c\bar{R}t}{C_m}}\right]\right\}_0^T \tag{38}$$

$$CI = C_m\left(1 - e^{-\frac{cGP}{C_m}}\right) + \bar{E}T - \left\{\frac{\bar{E}C_m}{c\bar{R}}\left[1 - e^{\frac{-c\bar{R}T}{C_m}}\right]\right\} \tag{39}$$

where $T = \frac{GP}{\bar{R}}$. Rearranging Equation 39, the single-storm analytical form of the Liu model is defined as (LIU, 1997, 2001):

$$CI = C_m\left[1 - e^{-\frac{cGP}{C_m}}\right]\left[1 - \frac{\bar{E}}{\bar{R}c}\right] + \frac{\bar{E}}{\bar{R}}GP \tag{40}$$

The multiple-storm is the summation of each single-storm CI:

$$CI = C_m\left[n - \sum_{i=1}^{n} e^{-\frac{cGP}{C_m}}\right]\left[1 - \frac{\bar{E}}{\bar{R}c}\right] + \frac{\bar{E}}{\bar{R}}\sum_{i=1}^{n} GP \tag{41}$$

where n is the number of rainfall events with sufficient time between them to enable the canopy to dry completely.

2.4 Stochastic models

2.4.1 Calder model (1986)

Instead of considering the forest canopy as a reservoir from which water is routed toward the forest floor (GASH, 1979; RUTTER et al., 1971), Calder (1986) proposed a stochastic hypothesis to model rainfall canopy interception. Such a hypothesis relies on splitting the canopy into elemental areas which have the same probability of being struck by raindrops (CALDER, 1986). The Poisson distribution describes the probability of 0, 1, 2, …, r drops reach each elemental area during a rainfall event, respectively:

$$e^{-m}, \frac{m}{1!}e^{-m}, \frac{m^2}{2!}e^{-m}, \dots, \frac{m^r}{r!}e^{-m} \tag{42}$$

where m is the mean raindrop strikes per elemental area (disregarding evaporation). The non-exceedance probability of raindrops reaching the elemental areas is then written as:

$$\sum_{x=0}^{r} Prob_x = e^{-m} + \frac{m}{1!}e^{-m} + \frac{m^2}{2!}e^{-m}, + \cdots + \frac{m^r}{r!}e^{-m} \tag{43}$$

Intuitively, the exceedance probability is:

$$Prob_{x>r} = 1 - \sum_{x=0}^{r} Prob_{x<r} \tag{44}$$

Each elemental area has a maximum drop storage capacity (q), which can be a non-integer number (CALDER, 1986). The excess of drops (r – q) pours from the elemental areas when r > q. On the other hand, all r drops are stored for r ≤ q. From these concepts, the mean number of drops stored on the elemental areas (n) can be defined by:

$$n = \left(1 - \sum_{x=0}^{r} Prob_{x<r}\right) q + \frac{m}{1!}e^{-m} + 2\,\frac{m^2}{2!}e^{-m}, + \cdots + r\frac{m^r}{r!}e^{-m} \tag{45}$$

where the first right-hand side term represents the saturated elemental areas, whereas the other terms regard partially wet ones.

The formulations described the rainfall canopy interception for the elemental scale, which is not interesting for water management purposes. Decision-makers need information on a forest scale to simulate and forecast the rainfall canopy interception (PAGE et al., 2020). In this regard, it was necessary to upscale the Calder model to the canopy scale. Calder (1986) introduced the number of elemental areas per unit ground area (L), the mean volume of the raindrops (v), and inserted evaporation (which was disregarded in the elemental model).

2.4.1.1 From elemental to canopy scale

The canopy storage per unit of ground area (C) can then be calculated:

$$C = nvL \tag{46}$$

and the maximum canopy storage capacity (C_{max}) is:

$$C_{max} = qvL \tag{47}$$

In the rescaled model, the mean number of raindrops striking the canopy during a rainfall event can be related to the gross rainfall amount as:

$$m = \frac{GP}{vL} \tag{48}$$

2.4.1.2 Inserting evaporation

As the evaporation withdraws water from the canopy reservoir (C), the stored water reduces simultaneously. Therefore, the changes in canopy storage are equivalent to the evaporation per unit ground area (CI):

$$\frac{dC}{dCI} = -1 \tag{49}$$

From differentiating equation 46 and replacing equation 49, the change in the mean number of drops stored in the elemental area regarding the evaporation is:

$$\frac{dn}{dCI} = \frac{dC}{dCI} \cdot \frac{dn}{dC} = -\frac{1}{vL} \tag{50}$$

Calder (1986) applied a finite differencing approach (Equation 51) to describe the changes in the mean number of raindrops striking the elemental areas (m) as a function of the balance between gross rainfall (GP) and evaporation (CI). Calder (1986) renamed the m variable the *elemental* mean number of raindrops because it represents the equivalent number of raindrops striking the elemental areas discounting those drops leaving by evaporation.

$$\Delta m = \frac{dm}{dGP}\Delta GP + \frac{dn}{dCI} \cdot \frac{dm}{dn}\Delta CI \tag{51}$$

$$\Delta m = \frac{1}{vL}\Delta GP - \frac{1}{vL}\left\{1 \Big/ \left[qe^{-m} + \frac{(1-q)}{1!}(1-m)e^{-m} + \frac{(2-q)}{2!}(2m-m^2)e^{-m} + \cdots + \frac{(r-q)}{r!}(rm^{r-1}-m^r)e^{-m}\right]\right\}\Delta CI \tag{52}$$

where the evaporation increment (ΔCI) is calculated from the Penman-Monteith equation (CALDER, 1996) with the surface resistance set to zero to represent wet canopy conditions (GASH; VALENTE; DAVID, 1999). For more details regarding the step-by-step application of this model, we encourage readers to access the works of Calder (1986; 1996).

2.4.1.3 Calder two-layer model (CALDER, 1996)

To account for the observed influence of drop size on canopy storage capacity (CALDER, 1986) and to deal with some shortcomings (e.g., a single canopy layer), Calder (1996) proposed an improved model, in which the parameter q could vary with rainfall intensity, drop size, and drop kinetic energy since such relationships were highlighted by Calder (1986) but not inserted into the model. Furthermore, the new

version also considered the canopy interception to occur in a two-layer environment. The rainfall drops (the primary drops) reach the top layer directly, whereas the bottom layer is only stricken by the shed drops of the top layer (secondary drops) (CALDER, 1996).

The improvement started with the definition of the maximum elemental volume (v_e), which is a vegetation-specific parameter. For drops reaching the canopy with zero kinetic energy, we can write the maximum elemental volume as:

$$v_{e0} = qv_0 \tag{53}$$

where v_{e0} and v_0 are the maximum elemental volume and the mean drops volume for drops with zero kinetic energy, respectively. Upscaling to the canopy, the maximum storage capacity (C_{max}), when drops have no kinetic energy is:

$$C_{max} = v_{e0}L = v_0qL \tag{54}$$

However, drops have some kinetic energy (further described as a function of rainfall intensity), which decrease the maximum canopy storage capacity (C_m):

$$C_m = v_eL = vqL \tag{55}$$

Rearranging Equations 54 and 55, Calder (1996) wrote the maximum elemental volume for drops with non-zero kinetic energy as a function of the maximum elemental volume with zero kinetic energy:

$$v_e = \frac{C_m}{C_{max}} v_{e0} \tag{56}$$

Then, the dependence of the maximum drop retention number (q) to rainfall kinetic energy is written as:

$$q = \frac{C_m}{C_{max}} \frac{v_{e0}}{v} \quad (57)$$

The values of C_{max} and v_{e0} can be defined for a particular vegetation type (CALDER, 1996; CALDER et al., 1996), whereas the relationship of C_m/C_{max} with v was determined using an experiment with a rainfall simulator as:

$$\frac{C_m}{C_{max}} = 1 \quad for\ v < 0.065 \quad (58)$$

$$\frac{C_m}{C_{max}} = 0.5 + 0.73e^{-5.5v} \quad for\ v \geq 0.065 \quad (59)$$

Equations 58 and 59 highlight the dependence of canopy storage capacity on raindrops volume (Figure 1). Greater raindrops happen in intense rainfall, and therefore regions with more convective storms tend to intercept less rainfall than those with frontal systems (CALDER, 1996).

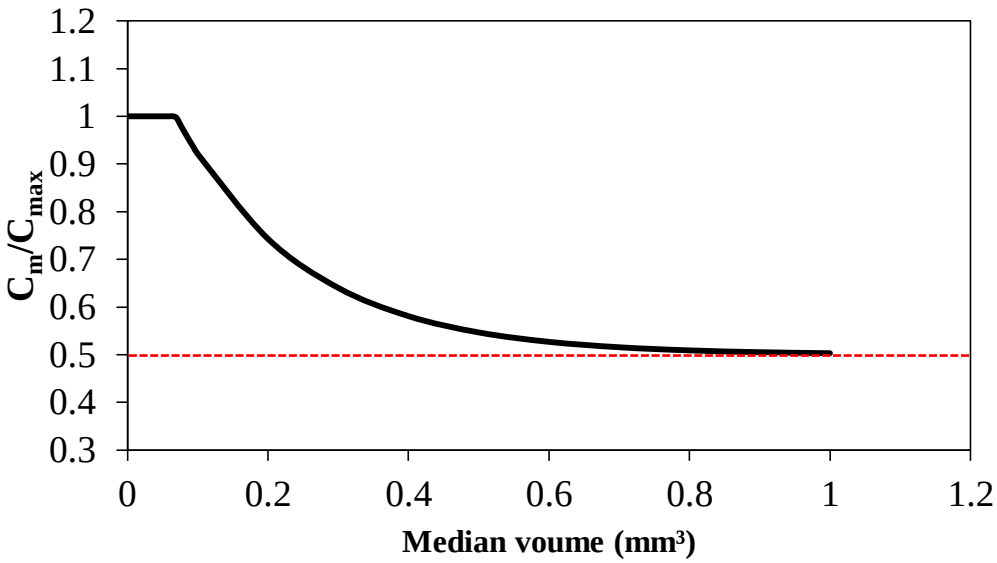

Figure 1. Relationship of Cm/Cmax with v, highlighting the asymptotic pattern of decreasing maximum canopy storage capacity with raindrop size. Adapted from Calder (1996).

Torres, Porra, and Creutin (1994) proposed a relationship between the median raindrop diameter (D_0) and rainfall intensity based on the Marshall and Palmer distribution (MARSHALL; PALMER, 1948):

$$D_0 = \alpha R^{\beta} \tag{60}$$

where α and β are empirical parameters, which must obey α + 4β = 1. The drop volume reaching the top layer can be calculated from rainfall intensity, whereas those reaching the bottom layer are related to the canopy characteristic volume (CALDER, 1996).

The two-layer approach relies on splitting the projected canopy area index (L_p) into the top (L_{p1}) and bottom (L_{p2}) layers using Beer's law:

$$L_{p1} = 1 - e^{-L_p} \tag{61}$$

$$L_{p2} = L_p - L_{p1} \tag{62}$$

Relying on the projected canopy area index of both layers, the elemental areas (L_1 and L_2) can be split between them:

$$L_1 = \frac{L_{p1}}{L_p}\frac{C_{max}}{v_{e0}} \tag{63}$$

$$L_2 = \frac{L_{p2}}{L_p}\frac{C_{max}}{v_{e0}} \tag{64}$$

Finally, rainfall can be portioned between the top and the ground (since direct rainfall does not reach the bottom layer). The shedding water from the top layer can be portioned between the bottom layer and the ground. The same idea of the projected canopy area index is applied to the gross rainfall amount (Equation 65) and the input of water into the bottom layer is a fraction of the shed water (Equation 66):

$$GP_1 = f_1 GP = L_{p1} GP \tag{65}$$

$$GP_2 = f_2 Sh = 1 - e^{-L_{p2}} Sh \quad (66)$$

where f_1 and f_2 are the fractions of the gross rainfall and shed water (Sh), respectively.

Overall, strengths and weaknesses could be drawn from Calder's model (MUZYLO et al., 2009). First, Calder (1996) proved that by increasing rainfall intensity and raindrop size, the canopy storage capacity decreases proportionally, i.e., the Calder model advanced the knowledge of the physical processes encompassing rainfall canopy interception. These essential characteristics are not accounted for in Rutter, Gash, and Liu models, which consider that canopy storage capacity is a function of canopy structure regardless of the weather condition. Although the stochastic approach is an interesting way to look at interception modeling, its application is complex, time-consuming, and without any significant improvement regarding the physical models (MUZYLO et al., 2009). Furthermore, physical models are more appropriate to deal with different weather and climate conditions than stochastic models. Therefore can be applied to forecast rainfall canopy interception outside the range within with they were calibrated (RODRIGUES et al., 2021).

2.5 Parameters retrieving

2.5.1 Weather parameters

2.5.1.1 Rainfall

The Gash and Liu models rely on the mean rainfall rate for canopy saturation conditions (CARLYLE-MOSES; PARK; CAMERON, 2010; GASH, 1979; GASH; LLOYD; LACHAUD, 1995). Gash (1979) defined that canopy is saturated when rainfall intensity ≥ 0.5 mm h^{-1}. The mean rainfall intensity considers all rainfall events throughout the study period ($\bar{R} \geq 0.5$ mm h^{-1}). Using the average, some studies observed an overestimation of $\bar{R}$ because of its non-normal distribution (GHIMIRE et al., 2017a; RODRIGUES et al., 2021). In this regard, the median is a better approach for determining $\overline{R}$.

2.5.1.2 Evaporation

The Penman-Monteith was the first method applied to define evaporation from a saturated canopy condition (RUTTER et al., 1971). When canopy is saturated,

transpiration can be neglected and, hence, the roughness resistance can be neglected (MONTEITH, 1965)

$$E_{PM} = \frac{\Delta R_n + \rho_a c_p g_a (e_s - e_a)}{\lambda(\Delta + \gamma)} \quad (67)$$

where Δ is the slope of the saturation vapor pressure curve; R_n is the net radiation; ρ_a is the mean air density at constant pressure; c_p is the specific heat of the air; g_a is the aerodynamic conductance; e_s is the saturation vapor pressure; e_a is the actual vapor pressure; $(e_s - e_a)$ is known as the vapor pressure deficit; λ is the latent heat for water vaporization; and γ is the psychrometric constant.

The success of the modeling depends on the correct determination of the aerodynamic conductance (g_a). Such a conductance differs among the elements being transferred, i.e., the transfer of heat, vapor, and momentum in the canopy-atmosphere turbulent zone is different. However, the original studies (GASH, 1979; GASH; LLOYD; LACHAUD, 1995; LIU, 1997; RUTTER et al., 1971; RUTTER; MORTON; ROBINS, 1975; VALENTE; DAVID; GASH, 1997) did not considered these differences, and therefore computed evapotranspiration using the aerodynamic conductance for momentum ($g_{a,M}$):

$$g_{a,M} = \left\{\frac{k}{\ln[(z-d)/z_0]}\right\}^2 * u \quad (68)$$

where k is the von Kármáns's constant velocity (0.41); u is the wind velocity (m s^{-1}) measured at the MOT; z is the height of wind speed measurement; d is the zero plane displacement height (m); and z_0 is the roughness length governing transfer of momentum, heat, and vapor (m).

Although suitable performance of the models had been attained, Lankreijer, Hendriks, and Klaassen (1993) argued for the need to include the different mechanisms for vapor and heat transfer. Gash, Valente, and David (1999) performed a thoroughly investigation to point out the most suitable approach to compute aerodynamic computation for modeling rainfall canopy interception. Taking into account all the transfer mechanisms (heat, vapor, and momentum), the aerodynamic conductance can be written as:

$$g_{a,V} = \frac{k^2 u}{ln[(z-d)/z_{0,M}] ln[(z-d)/z_{0,H}]} \quad (69)$$

where $z_{0,M}$ is the roughness length for momentum; and $z_{0,H}$ is the roughness length for vapor and heat. The additional complexity of $g_{a,V}$ did not improve the results of $g_{a,M}$ because $z_{0,M}/z_{0,H} \sim 1$, which reduces Equation 69 into 68 (GASH; VALENTE; DAVID, 1999). Therefore, $g_{a,M}$ can be applied to estimate evaporation under wet canopy condition without significant errors. FAO-56 (ALLEN et al., 1996) also recommend the use of $g_{a,M}$, reinforcing it suitability. Even though substantial improvement has not been observed when considering atmosphere instability (GASH; VALENTE; DAVID, 1999), its effects can also be added to the aerodynamic conductance equation.

Gash (1979) proposed an indirect determination of the mean evaporation rate ($\overline{E}$) based on the regression between canopy interception (CI) and gross rainfall (GP) for rainfalls that saturate the canopy ($CI = aGP + b$). According to Gash (1979), the slope (a) is $\overline{E}/\overline{R}$ and a previous determination of the mean rainfall rate for wet canopy condition is necessary. The methods for determining $\overline{R}$ are described in the proper section.

2.6 Structural parameters

2.6.1 Canopy parameters

Jackson (1975) proposed that the free throughfall coefficient (p) is the slope of the linear regression between TF and GP for small events (where canopy are still unsaturated). GP values between 1.0 and 2.0 mm have been considered as the threshold for this methodology (LEYTON; REYNOLDS; THOMPSON, 1967; GASH; MORTON, 1978). Leyton, Reynolds, and Thompson (1967) proposed an envelopment of the throughfall variation. The upper part of the envelope regards the conditions of minimum evaporation rate and canopy saturation (RUTTER et al., 1971). If a regression line is fit to the bottom part considering only events < 1 mm, the p value is the slope of the regression. Then, the canopy cover fraction can be determined as $c = 1 - p$.

The mean method was proposed by Klaassen, Bosveld, and Water (1998) and relies on the water-box concept, i.e., drainage only happens when C > S. Based on this concept, the rainfall events can be split into two parts: (i) a wetting part, where canopy is unsaturated ($GP < P'_G$) and (ii) a saturated part ($GP \geq P'_G$). Considering that for C > S the excess is quickly drained, the mean method by Klassen et al. (1998) is:

$$CI = \left(1 - p - \frac{\overline{E}}{\overline{R}}\right) P'_G + \frac{\overline{E}}{\overline{R}} GP \qquad (70)$$

Canopy interception and gross rainfall are plotted and linear regression ($CI = \alpha GP + \beta$) is fit. α is the $\bar{E}/\bar{R}$ ratio and $\beta = S = (1 - p - \bar{E}/\bar{R})P'_G$. Both free throughfall coefficient (p) and canopy storage capacity (S) can be retrieved from this approach.

Instruments can also be applied to observe canopy gaps, and therefore define canopy cover fractions. Gash and Morton (1978) carried out a measurement of the canopy cover fraction over the rain gauge through an anascope. On the other hand, Carlyle-Moses, Park, and Cameron (2010) analyzed four digital fisheye photographs taken around the threes studied using a Gap Light Analyzer (GLA). Junqueira Junior et al. (2019) used the Leaf Area Index (LAI) measured at 32 inventory parcels within an Atlantic forest to determine the canopy cover fraction (c). These are some examples of retrieving canopy cover fraction from the direct measurement of the canopy structure.

Because of the upper envelope of Leyton, Reynolds, and Thompson (1967) encompasses only events with minimum evaporation and canopy saturation, the interception of the linear regression is theoretically the canopy saturation capacity (S) since it is expected that the linear regression has unit slope (i.e. $TF = GP - S$). Gash and Morton (1978) and Rutter et al. (1971) used this methodology. The Rutter model can also be applied to define S in a canopy water balance approach. A water balance is performed when drainage (D) becomes 0.002 mm/min, which is the threshold when the actual canopy storage (C) equals S (RUTTER et al., 1971). From the rainfall onset until S equals C, the water balance can be written as:

$$\sum R - \sum TF = \sum E - S \tag{71}$$

Since in the Rutter model the evaporation is a function of S, a running water balance with an initial value of S is necessary. Rutter et al. (1971) used a computer program and a 5-minute time-step to define S. This method is laborious and time demanding, and therefore has been poorly applied.

Valente et al. (1997) proposed a methodology to retrieve the canopy storage capacity per unit area (S) based on the envelope of Leyton, Reynolds, and Thompson (1967) and the sparse Rutter equations. By considering individual storms, drainage can be disregarded and Equations 12 and 13 can be rewritten (Valente et al., 1997):

$$TF = (1 - cp_d)GP - (1 - p_d)S - (1 - p_d)c \int E_c dt \tag{72}$$

$$SF = p_d/(1 - p_d)[TF - (1 - c)GP] - S_t - c\int E_{t,c}dt \quad (73)$$

The evaporation term of Equation 72 can be set to zero by fitting a linear regression in the upper envelope. S is the negative interception divided by $(1 - p_d)$ of the envelope regression with a pre-established slope of $(1 - cp_d)$. From Equation 73, the evaporation from the trunks can also be neglected for some selected rainfall events (VALENTE; DAVID; GASH, 1997). By fitting a regression line between SF and TF – (1 – c)GP, S_t is the negative value of the interception whereas p_d = slope/(1+slope).

2.6.2 Trunk parameters

The regression approach is the widespread method applied to retrieve trunk storage capacity (S_t) and trunk portioning (p_t) (GASH; MORTON, 1978). It relies on fitting a linear regression to the stemflow (SF) versus gross rainfall (GP) plot. The negative of the interception is S_t, and the slope is p_t.

Carlyle-Moses, Park, and Cameron (2010) proposed a methodology to determine S_t based on the funneling ratio concept. The funneling ratio measures the amount of water reaching the ground as SF about the water that would be caught by a hypothetical rain gauge with an open area equal to the basal area of the studied tree. These authors suggested that the amount of rainfall that produced the maximum funneling ratio (GP_F) is the amount of water needed to saturate the canopy and trunk (P''_G). Then, $S_{t,c}$ can be determined using a water balance:

$$S_{t,c} = GP_{F,c} - TF_d - S_c - \frac{\bar{E}_c}{\bar{R}}GP - SF_c \quad (74)$$

where the subscribed c means that the variables are considered per unit canopy area and TF_d is the throughfall draining as drip.

2.7 Problems in canopy interception modeling: Extra sources of energy

Rainfall interception modeling has been spreading worldwide in a broad range of forest types since the development of the preceding models (Muzylo et al., 2009). Although it improved the understanding of the rainfall redistribution within a forest

considerably, deadlocks arose, and advances toward the physics of the atmosphere-canopy relationship were deemed necessary (DIJK et al., 2015). Penman-Monteith theory was the first proposed methodology to determine canopy evaporation under rainfall conditions (RUTTER et al., 1971) because it relies on the energy balance (MONTEITH, 1965)

Some assumptions were adopted when developing the Penman-Monteith theory and should be minutely analyzed (DIJK et al., 2015): (i) all ways of energy and water exchange are accounted for; (ii) the vegetation is homogeneous and horizontally distributed; (iii) the flow reaches the vegetation horizontally and is stationary. The Penman-Monteith approach had been such a notorious advance in evapotranspiration prediction that the Food and Agriculture Organization (FAO) standardized the parameters to its widespread use in irrigation and water management planning (ALLEN et al., 1998). However, other methodologies have been applied to appraisal the most suitable parameters to model rainfall interception. These methodologies are indirect and based on both linear regressions and canopy water balance (GASH, 1979; GASH; LLOYD; LACHAUD, 1995; GHIMIRE et al., 2017a; JUNQUEIRA JUNIOR et al., 2019; RODRIGUES et al., 2021)

By comparing them all, an underestimation of the Penman-Montieh approach raised concerns against the energy balance theory (DIJK et al., 2015). The energy balance of a forest can be described as:

$$R_n = H + \lambda E + Q_a + Q_l + Q_b + Q_G + Q_P + X \quad (75)$$

where R_n is the net radiation flux; H and λE are the sensible and latent heat fluxes, respectively; Q_a and Q_l are the energy stored (as sensible and latent heat, respectively) in the air inside the forest; Q_b is the energy stored in the forest biomass; Q_G is the energy stored in the soil; Q_P is the energy consumed by plants for photosynthesis; and X is the advection energy. Regarding the energy balance that based the Penman-Monteith theory, the only accounted sources of energy are H, λE, and R_n. Many studies did not observe an energy balance closure by considering only these three forms of energy (CAMPOS et al., 2019; KILINC et al., 2012; MICHILES; GIELOW, 2008). Dijk et al. (2015) called attention to the unaccounted energy stored inside the forest and their relevance for supporting wet canopy evaporation, which the greatest contribution of those stored as sensible heat (in the air and biomass). However, studies joining rainfall interception modeling and energy balance are still lacking. Furthermore, the importance

of extra sources of energy for evaporation is expected to be more highlighted in extreme weather conditions (as drought periods) since a more unstable atmosphere enhances evaporation (NÁVAR, 2019).

Dijk et al. (2015) also described the importance of energy reaching the forest by advection. Drier and hotter surrounding areas can provide substantial energy by advection (KOCHENDORFER; PAW U, 2011). Návar (2019) observed the importance of energy advection to wet canopy evaporation due to temperature gradient to the atmosphere and surrounding areas. The strong updraft of bulk air also contributes to energy advection during convective rainfalls (DIJK et al., 2015). It is worth mentioning that changes in wind flow turbulence improve heat and momentum transport. Holwerda et al. (2012) attached the increase in evaporation to the steep topography in mountainous terrains. Complex terrains increase turbulence and, therefore, heat and momentum transport. Moreover, energy advection is also expected to increase in such circumstances (DIJK et al., 2015).

In this context, studies that couple energy balance and rainfall interception modeling are urgent to better frame the complex process evolving the atmosphere-canopy environment. Even more in the expected extreme weather conditions (OLIVEIRA et al., 2017).

2.8 Throughfall

2.8.1 The spatial variability

The spatial distribution of throughfall controls soil moisture dynamics (JUNQUEIRA et al., 2017; OLIVEIRA et al., 2021), nutrient redistribution (MANTOVANI et al., 2021; TONELLO et al., 2021), the formation of preferential pathways and hotspots for groundwater recharge (BIALKOWSKI; BUTTLE, 2015; GUSWA; SPENCE, 2011), evapotranspiration (GUSWA; SPENCE, 2011; RODRIGUES et al., 2021b), root growth, and the distribution of tree species according to soil water availability (PRESSLAND, 1976; TERRA et al., 2018b). There are many ways to characterize the spatial variability of throughfall. One of the most applied is the coefficient of variation (CV), which can be related to the amount, duration, and intensity of rainfall events (LIU et al., 2019; SHENG; CAI, 2021; SU et al., 2019; ZHANG et al., 2019; ZHU et al., 2021).

As long as rainfall amount, intensity, and duration increases, the spatial variability of throughfall decreases, indicating a more significant influence of the canopy in small events (SHENG AND CAI, 2;021; STAELENS et al., 2006; SU et al., 2019; ZHU et al., 2021). For instance, Fan et al. (2015) observed a stable CV of 16.5% in a pine forest as long as the rainfall event proceeded. In a mixed deciduous forest, Staelens et al. (2006) observed 19% and 11% CV for the leafed and leafless periods, respectively. Sheng and Cai (2021), Zhu et al. (2021), and Su et al. (2019) observed a stable CV of ~ 20% in boreal, semiarid mountain forests, and mixed evergreen-deciduous broadleaved forests, respectively.

Although the coefficient of variation can describe the spatial variability of throughfall, it fails to characterize the spatial structure. In this sense, geostatistics has been considered to model the spatial structure of eco-hydrological variables (RODRIGUES et al., 2021b; VOSS; ZIMMERMANN; ZIMMERMANN). The first step is the calculation of the experimental semivariogram proposed by Matheron (1962). Matheron's equation is widely applied because it is asymptotically unbiased and efficient (LARK, 2000).

$$\hat{\gamma}_M(\boldsymbol{h}) = \frac{1}{2 * N(\boldsymbol{h})} \sum_{i=1}^{N(\boldsymbol{h})} \{z(\boldsymbol{x}_i) - z(\boldsymbol{x}_i + \boldsymbol{h})\}^2 \quad (76)$$

where $z(\mathbf{x}_i)$ is the observed value at location $\mathbf{x}_i$, $N(\mathbf{h})$ are the pairs of observations that are separated by each lag $\mathbf{h}$. Some theoretical models (e.g., exponential, Gaussian, and spherical) are fitted to the experimental semivariograms using the ordinary least squares, weighted least square, or maximum likelihood to minimize the objective function. By carrying out a leave-one-out cross-validation, the best model can be selected and applied for forecasting the spatial variability of the target variable using kriging approaches (WEBSTER; OLIVER, 2007). The fitted model can also be used to optimize the monitoring set to better characterize the spatial variability of throughfall in forests (ZIMMERMAN; ZIMMERMAN, 2014). Further importance should be given to the drivers of the spatial distribution of throughfall to enhance the understanding of the

rainfall-forest-hydrology connections because a variety of internal and external factors are believed to influence the spatial patterns.

2.8.2 The time stability

Time stability has been used in a broad range of forests to assess the spatial variability of throughfall behavior over time (KEIM; LINK, 2018; VAN STAN et al., 2020). This approach highlights the most time stable locations and is persistently wetter and drier than the spatial average. Therefore, this methodology enables defining time stable positions to decrease the monitoring effort since a few positions can be used to determine the spatial average of throughfall (VACHAUD et al., 1985). This approach has already been applied in a montane rainforest (WUALLERT et al., 2009), in a tropical forest (ZIMMERMANN et al., 2008), in a dominant beech tree (STAELENS et al., 2006), in xerophytic shrubs (ZHANG et al., 2016), in a semi-arid mountain forest (ZHU et al., 2021), in a boreal forest (SHENG; CAI, 2021), in young, deciduous, and old conifers (KEIM; SKAUGSET; WEILER., 2005), in a rubber plantation (LIU et al., 2019), in a eucalyptus plantation (SATO et al., 2011), and a pine plantation (FAN et al., 2015).

In all these studies, the spatial variability of throughfall was classified as time stable. However, Zimmermann, Zimmermann, and Elsenbeer (2009) observed that the temporal persistence of throughfall at individual plots disappeared after one year in a tropical semideciduous moist forest. Assessing long periods is needed to observe patterns in the spatial distribution of throughfall (LEVIA; FROST, 2006) because weather and forest dynamics are likely to affect the time stability of throughfall. Intense droughts change forest dynamics and the biogeochemistry cycles, increasing biomass loss due to tree mortality (mainly the large ones) (RYAN, 2015). The duration and aggressiveness of such events influence water and soil nutrient availability and consequently change the structure and composition of the forest (HE; DIJKSTRA, 2014). These conditions also modify the carbon balance and favor drought-tolerant tree species (CHOAT et al., 2018; ESQUIVEL-MUELBERT et al., 2018; SCHLESINGER et al., 2016).

Such changes are likely to affect the spatial distribution of throughfall over time (STOGSDILL et al., 1989). However, only a few studies considered forest traits as drivers of throughfall time stability, mainly focusing on trees' traits as opposed to forest

traits (e.g., canopy thickness, LAI, leaf characteristics, and stem architecture) (SHENG; CAI, 2021; STAELENS et al., 2006). The importance of forest structure (e.g., basal area) was highlighted in a Pinus plantation by Stogsdill et al. (1986), who assessed the relationship between thinning and throughfall input to improve soil water. However, this evaluation is still lacking in tropical forests, where canopies are more complex and heterogeneous (AUBRY-KIENTZ et al., 2019; GUAN et al., 2013). Therefore, it is crucial to appraise the consequences of changes in forest structure on the spatial dynamics of throughfall. Without accounting for structural changes, misinterpretation of time stability of throughfall may occur.

2.8.3 Measuring time stability

The first step relies on computing the relative differences ($RD_{i,j}$), which measure the differences of monitoring locations to the site's average. The relative difference describes whether a location *j* is wetter, dryer, or close to the site's average for each time interval *i* considered. The time average of the relative difference (MRD_j) of throughfall is then calculated for each location *j*. MRD_j is a description of the overall pattern of the spatial distribution over time (VACHAUD et al., 1985).

$$RD_{i,j} = \frac{TF_{i,j} - \overline{TF_i}}{\overline{TF_i}} \tag{76}$$

$$MRD_j = \frac{1}{n}\sum_{i=1}^{n} RD_{ij} \tag{77}$$

where *n* is the monitoring length and $\overline{TF_i}$ is the spatial average of throughfall at each time *i*. $MRD_j > 0$ represents wetter locations, $MRD_j < 0$ drier locations, and $MRD_j \sim 0$ locations with TF amount close to the forest average. MRD_j represents the plots of the Atlantic Forest remnant that are wetter, dryer, or closer to the spatial average TF. However, MRD_j only describe the expected throughfall for each location regarding the site's average nothing accounting for the variability of the spatial variability throughout the time. In this sense, the standard deviation of the relative positions (σ_{RD_j}) should be

considered to highlight how much the TF spatial pattern varies between events (VACHAUD et al., 1985).

$$\sigma_{RD_j} = \sqrt{\frac{1}{n-1}\sum_{i=1}^{n}\left(RD_{i,j} - MRD_j\right)^2} \tag{78}$$

It is not appropriate to rely only on MRD_j to define time stability because its variability ($\sigma_{RD_{ij}}$) is also important. Therefore, the Time Stability Indicator (TSI) was developed (JACOBS et al., 2004) to integrate the effects of MRD_j and σ_{RD_j}. TSI is applied to identify the most time stable positions to describe the spatial average of throughfall (MINET et al., 2013).

$$TSI = \sqrt{\left(MRD_j\right)^2 + \left(\sigma_{RD_j}\right)^2} \tag{79}$$

The lower the TSI value, the more time stable is the location. Assessing TSI differs from MRD because it describes the persistence of the spatial distribution, i.e., the TF time stability, whereas MRD describes the expected spatial distribution of TF throughout the study period.

The nonparametric Spearman's test has also been applied to assess time stability (VACHAUD et al., 1985). The throughfall observed at location j is ranked (R_{ij}) for every time interval i. For each location j, the same variable is ranked in the time i'. Then, the Spearman rank can be calculated as:

$$r_s = 1 - \frac{6\sum_{i=1}^{n}\left(R_{i,j} - R_{i\prime,j}\right)^2}{n(n^2-1)} \tag{80}$$

where n is the number of observations. For $r_s = 1$ the rank positions are kept over time with a perfect time stability. Therefore, the closer r_s is to the unity, the more time stable the spatial variability will be (VACHAUD et al., 1985).

Temporal semivariance is another possibility to assess the time stability of throughfall (ZIMMERMANN; ZIMMERMANN; ELSENBEER, 2009). This approach will highlight the maximum period length in which time stability of throughfall could be considered without the risk of misinterpretation (ZIMMERMANN; ZIMMERMANN;

ELSENBEER, 2009). It relies on the calculation of the experimental semivariogram proposed by Matheron (1962):

$$\hat{\gamma}_M(\boldsymbol{h}) = \frac{1}{2 * N(\boldsymbol{h})} \sum_{i=1}^{N(\boldsymbol{h})} \{z(\boldsymbol{x}_i) - z(\boldsymbol{x}_i + \boldsymbol{h})\}^2 \quad (81)$$

where $z(\mathbf{x}_i)$ is the observed value at time $\mathbf{x}_i$, $N(\mathbf{h})$ are the pairs of observations that are separated by each time lag **h**. The time lag is defined according to the monitoring schedule (and data availability). Theoretical semivariograms (e.g., exponential, Gaussian, and spherical) are fitted to the experimental semivariograms minimizing the objective function by means of: (i) ordinary least squares; (ii) weighted least square; or (iii) maximum likelihood.

The advantages of temporal semivariograms over time stability indexes are the differentiation in temporal lags and the definition of the maximum period length, in which the spatial variability still holds (ZIMMERMANN; ZIMMERMANN; ELSENBEER, 2009). However, this method demands longer monitoring periods, which is not easily available in most forests worldwide. Therefore, this methodology is not widespread yet, which precludes comparison with the studies that used the time stability index.

2.9 Drought characterization

2.9.1 Drought assessment

A shortage of water characterizes drought over time (QUIRING, 2009). The drought can be classified as meteorological, agricultural, hydrological, and socioeconomic, depending on where the shortage occurred and which affected systems (VICENTE-SERRANO et al., 2020). Meteorological drought occurs due to a precipitation deficit throughout a period. Hydrological drought is usually followed by a meteorological drought (JUNQUEIRA et al., 2020) in a delayed process and is related to the lower availability of surface and groundwater. The decrease in soil water availability may be classified as agricultural drought as long as it affects the growth and yield of agricultural fields. Socioeconomic drought is the most difficult to observe because it depends on the social and economic sector and how they were affected (e.g.,

beef, dairy, crop production, unemployment, increased risk to fire rages) (WILHITE; GLANTZ, 1985).

However, these definitions are not enough to assess whether a drought is occurring or not (WILHITE; GLANTZ, 1985). In this regard, drought indexes were developed to characterize the intensity, frequency, and duration of droughts and enable comparison among different climate conditions (QUIRING, 2009). Overall, these indexes quantify how much a period (e.g., day, week, season, and year) departure from the long-term average (or "normal" condition) (WILHITE; GLANTZ, 1985). One of the first and widely applied drought indexes was developed by Palmer (1965). The Palmer Drought Severity Index (PDSI) relies on daily precipitation, air temperature, and soil water availability. By running a daily water balance, the PDSI value is compared to the "normal" (or climatically expected) moisture conditions (QUIRING, 2009). However, some drawbacks limit the use of PDSI. The potential evapotranspiration is calculated using Thornthwaite's method, relying only on the air temperature (QUIRING, 2009). Moreover, the runoff is only generated when soil is saturated, and plant growth (and root dynamics) is not considered between seasons (QUIRING, 2009). Therefore, other indexes were developed to solve drawbacks, such as the Standardized Precipitation Index (SPI).

The SPI is a probabilistic approach idealized by McKee, Doesken, and Kliest (1993) to characterize drought occurrence, frequency, and duration based on precipitation time series. Interestingly, this index is that rainfall deficit, or surplus can be highlighted together with its return period. Moreover, it is spatially invariant and can compare droughts among different regions (and climates) (QUIRING, 2009). Because of its characteristics, this index is recommended by the World Meteorological Organization (WMO) as a standard index.

The steps for computing SPI are: (i) a time series of rainfall accumulated on the scale of interest, such as daily, weekly, monthly, and yearly. The time series length strongly influences SPI, and more than 50 years is recommended to avoid distortions and 80 years to be more accurate (QUIRING, 2009). (ii) A theoretical probability function (e.g., two-parameter gamma, three-parameter Pearson type III, three-parameter generalized extreme value, four-parameter kappa) is fitted to the time series, and its adequacy should be assessed using the Anderson-Darling test (ANDERSON; DARLING, 1952, 1954) because this approach assesses the behavior at the distribution

tail, where the extreme events are; (iii) the respective probability is then applied to an inverse standard normal distribution ($\mu = 0$; $\sigma = 1$) (MCKEE et al., 1993). The positive and negative deviations are the SPI and indicate rainfall surplus and deficit, respectively. This index has been widely applied in Brazil's Brazilian Savanna (JUNQUEIRA et al., 2020) and Atlantic Forest biomes (SILVA; MELLO, 2021) for water resources management.

2.9.2 Droughts and forests

The effects of droughts on forests have been the subject of many studies and can be classified as an environmental effect (i.e., environmental drought), which can be highlighted by the observed increased wildfires, drought-driven tree mortality, and decreased forest growth (VICENTE-SERRANO et al., 2020). Long-term meteorological droughts can affect forest structure, function, and ecosystem services by leading to higher tree individuals loss and lower tree growth, ultimately reducing forest productivity (ANDEREGG; KANE; ANDEREGG, 2013) The duration and aggressiveness of such events influence water and soil nutrient availability and consequently change structure and composition of the forest (HE; DIJKSTRA, 2014). Because trees are long-lived organisms, they are expected to be more vulnerable to rapid changes in climate (BRODRIBB et al., 2020).

Deciduous and semi-deciduous forests (such as the Atlantic Forest) are adapted to climate seasonality and to a certain degree of periodic drought (SOUZA et al., 2021). However, the intensification of droughts changes the forest structure with an observed loss of trees along with basal area (negative net change) (BERENGUER et al., 2021; PHILLIPS et al., 2009). Climate scenarios indicate that extreme weather events will increase in the future, making longer dry periods more likely (NEHREN et al. 2019). In such condition, more forests will dry up and likely accelerate climate change due to increased carbon losses and changing surface energy balances (PHILLIPS et al., 2009). Moreover, paleoenvironmental studies show that changes in precipitation patterns during the Late Quaternary have repeatedly led to shifts in the transition zone between the Cerrado and the Atlantic Forest biomes, and that even small changes in water balance affect the fragile ecological balance (KIRCHNER et al. 2015).

The water balance is directly related to disturbances in forests due to changes in evapotranspiration and soil water availability (RODRIGUES et al., 2021b). Preserved and well-managed Atlantic Forest remnants increased water yield in southeastern Brazil (TEIXEIRA et al., 2021) as well as improved groundwater recharge (MELLO et al., 2019). These hydrological responses are due to small scale processes (e.g. the canopy water balance), which drive the rainfall redistribution (PAGE et al., 2020). This redistribution is the driving force of the subsequent hydrological processes (e.g., streamflow, groundwater recharge, evapotranspiration, and soil moisture dynamics). Although the recognized importance of canopy interception and rainfall redistribution, these processes are still poorly evaluated, and therefore further studies on this subject are required.

References

ALLEN, S.T. et al. The role of pre-event canopy storage in throughfall and stemflow by using isotopic tracers. **Ecohydrology**, v. 7, p. 858–868, 2013.

ALVARENGA, L. A. et al. Impacts of Climate Change on the Hydrology of a Small Brazilian Headwater Catchment Using the Distributed Hydrology-Soil-Vegetation Model. **American Journal of Climate Change**, v. 7, p. 355–366, 2018.

ANDEREGG, W. R. L.; KANE, J. M.; ANDEREGG, D. L. Consequences of widespread tree mortality triggered by drought and temperature stress. **Nature Climate Change**, v. 3, p. 30–36, 2013.

ANDERSON, T. W.; DARLING, D. A. Asymptotic theory of certain "goodness of fit" criteria based on stochastic processes. **The Annals of Mathematical Statistics**, v. 23, n. 2, p. 193–212, 1952.

ANDERSON, T. W.; DARLING, D. A. A Test of Goodness of Fit. **Journal of the American Statistical Association**, v. 49, n. 268, p. 765–769, 1954.

ARCOVA, F. C. S.; CICCO, V. DE; ROCHA, P. A. B. Precipitação efetiva e interceptação das chuvas por floresta de Mata Atlântica em uma microbacia experimental em Cunha - São Paulo. **Revista Árvore**, v. 27, n. 2, p. 257–262, 2003.

AUBRY-KIENTZ, M. et al. A comparative assessment of the performance of individual tree crowns delineation algorithms from ALS data in tropical forests. **Remote Sensing**, v. 11, p. 1–21, 2019.

BERENGUER, E. et al. Tracking the impacts of El Niño drought and fire in human-

modified Amazonian forests. **PNAS**, v. 119, p. 1–8, 2021.

BIALKOWSKI, R.; BUTTLE, J. M. Stemflow and throughfall contributions to soil water recharge under trees with differing branch architectures. **Hydrological Processes**, v. 29, p. 4068–4082, 2015.

BONAL, D. et al. The response of tropical rainforests to drought-lessons from recent research and future prospects. **Annals of Forest Science**, v. 73, p. 27–44, 2016.

BRODRIBB, T. J. et al. Hanging by a thread? Forests and drought. **Science**, v. 368, p. 261–266, 2020.

CALDER, I. A. N. R. A STOCHASTIC MODEL OF RAINFALL INTERCEPTION. **Journal of Hydrology**, v. 89, p. 65–71, 1986.

CALDER, I. R. 1 . Development of the two-layer stochastic model. v. 185, p. 363–378, 1996.

CALDER, I. R. et al. Dependence of rainfall interception on drop size: 2. Experimental determination of the wetting functions and two-layer stochastic model parameters for five tropical tree species. **Journal of Hydrology**, v. 185, n. 1–4, p. 379–388, 1996.

CAMPOS, S. et al. Closure and partitioning of the energy balance in a preserved area of a Brazilian seasonally dry tropical forest. **Agricultural and Forest Meteorology**, v. 271, p. 398–412, 2019.

CARLYLE-MOSES, D. E.; PARK, A. D.; CAMERON, J. L. Modelling rainfall interception loss in forest restoration trials in Panama. **Ecohydrology**, v. 3, p. 272–283, 2010.

CARLYLE-MOSES, D. E.; PRICE, A. G. Modelling canopy interception loss from a Madrean pine-oak stand, Northeastern Mexico. **Hydrological Processes**, v. 21, p. 2572–2580, 2007.

CHAVE, J. et al. Improved allometric models to estimate the aboveground biomass of tropical trees. **Global Change Biology**, v. 20, p. 1–14, 2014.

CHOAT, B. et al. Triggers of tree mortality under drought. Nature, v. 538, p. 531-539, 2018.

CORLETT, R. T. The Impacts of Droughts in Tropical Forests. **Trends in Plant Science**, v. 21, n. 7, p. 584–593, 2016.

CROCKFORD, R. H.; RICHARDSON, D. P. Partitioning of rainfall into throughfall, stemflow and interception: effect of forest type, ground cover and climate. **Hydrological Processes**, v. 14, n. 16–17, p. 2903–2920, 2000.

CUARTAS, L. A. et al. Interception water-partitioning dynamics for a pristine rainforest in Central Amazonia: Marked differences between normal and dry years. **Agricultural and Forest Meteorology**, v. 145, p. 69–83, 2007.

DEAN, W. **A Ferro e Fogo**: a história e a devastação da Mata Atlântica brasileira. 1ª edição. São Paulo: Companhia das Letras, 1995.

DIJK, A. I. J. M. VAN et al. Rainfall interception and the coupled surface water and energy balance. **Agricultural and Forest Meteorology**, v. 214–215, p. 402–415, 2015.

DYKES, A. P. Rainfall interception from a lowland tropical rainforest in Brunei. **Journal of Hydrology**, v. 200, p. 260–279, 1997.

ESQUIVEL-MUELBERT, A. et al. Compositional response of Amazon forests to climate change. **Global Change Biology**, v. 25, p. 39–56, 2018.

FAN, J. et al. Measuring and modeling rainfall interception losses by a native Banksia woodland and an exotic pine plantation in subtropical coastal Australia. **Journal of Hydrology**, v. 515, p. 156–165, 2014.

FAN, J. et al. Spatial variability of throughfall and stemflow in an exotic pine plantation of subtropical coastal Australia. **Hydrological Processes**, v. 29, n. 5, p. 793–804, 2015.

GASH, J. H. C. An analytical model of rainfall interception by forests. **Quartely Journal of the Royal Meteorological Society**, v. 105, p. 43–55, 1979.

GASH, J. H. C.; LLOYD, C. R.; LACHAUD, G. Estimating sparse forest rainfall interception with an analytical model. **Journal of Hydrology**, v. 170, p. 79–86, 1995.

GASH, J. H. C.; MORTON, A. J. An application of the Rutter model to the estimation of the interception loss from thetford forest. **Journal of Hydrology**, v. 38, p. 49–58, 1978.

GASH, J. H. C.; VALENTE, F.; DAVID, J. S. Estimates and measurements of evaporation from wet, sparse pine forest in Portugal. **Agricultural and Forest Meteorology**, v. 94, p. 149–158, 1999.

GERMER, S.; WERTHER, L.; ELSENBEER, H. Have we underestimated stemflow? Lessons from an open tropical rainforest. **Journal of Hydrology**, v. 395, p. 169–179, 2010.

GERMER, S.; ELSENBEER, H; MORAES, J.M. Throughfall and temporal temporal trends of rainfall redistribution in an open tropical rainforest, south-western Amazonia (Rondônia, Brazil). **Hydrology and Earth System Science**, v. 10, p. 383–393, 2006.

GHIMIRE, C. P. et al. Measurement and modeling of rainfall interception by two differently aged secondary forests in upland eastern Madagascar. **Journal of Hydrology**, v. 545, p. 212–225, 2017a.

GUAN, K. et al. Seasonal coupling of canopy structure and function in African tropical forests and its environmental controls. **Ecosphere**, v. 4, p. 1–21, 2013.

GUSWA, A. J.; SPENCE, C. M. Effect of throughfall variability on recharge : application to hemlock and deciduous forests in western Massachusetts. **Ecohydrology**, v. 5, p. 563-574, 2011.

HAVERD, V. et al. Air and biomass heat storage fluxes in a forest canopy: Calculation within a soil vegetation atmosphere transfer model. **Agricultural and Forest Meteorology**, v. 147, p. 125–139, 2007.

HE, M.; DIJKSTRA, F. A. Drought effect on plant nitrogen and phosphorus: a meta-

analysis. **New Phytologist**, v. 204, p. 924–931, 2014.

HOLWERDA, F. et al. Rainfall and cloud water interception in mature and secondary lower montane cloud forests of central Veracruz , Mexico. **Journal of Hydrology**, v. 384, p. 84–96, 2010.

HOLWERDA, F. et al. Wet canopy evaporation from a Puerto Rican lower montane rain forest: The importance of realistically estimated aerodynamic conductance. **Journal of Hydrology**, v. 414–415, p. 1–15, 2012a.

HOLWERDA, F. et al. Wet canopy evaporation from a Puerto Rican lower montane rain forest: The importance of realistically estimated aerodynamic conductance. **Journal of Hydrology**, v. 414–415, p. 1–15, 2012b.

JACKSON, I. J. Relationships between rainfall parameters and interception by Tropical forest. **Journal of Hydrology**, v. 24, p. 215–238, 1975.

JACOBS, J. M. et al. SMEX02: Field scale variability, time stability and similarity of soil moisture. **Remote Sensing of Environment**, v. 92, p. 436-446, 2004.

JUNQUEIRA JUNIOR, J. A. et al. Time-stability of soil water content (SWC) in an Atlantic Forest - Latosol site. **Geoderma**, v. 288, p. 64–78, 2017.

JUNQUEIRA JUNIOR, J. A. et al. Rainfall partitioning measurement and rainfall interception modelling in a tropical semi-deciduous Atlantic forest remnant. **Agricultural and Forest Meteorology**, v. 275, p. 170–183, 2019.

JUNQUEIRA, R. et al. Drought severity indexes for the Tocantins River Basin, Brazil. **Theoretical and Applied Climatology**, v. 141, p. 465–481, 2020.

JOLY, C. A.; METZGER, J. P.; TABARELLI, M. Experiences from the Brazilian Atlantic Forest: ecological findings and conservation initiatives. **New Phytologist**, v. 204, p. 459–473, 2014.

KEIM, R. F.; LINK, T. E. Linked spatial variability of throughfall amount and intensity during rainfall in a coniferous forest. **Agricultural and Forest Meteorology**, v. 248, p. 15–21, 2018.

KEIM, R. F.; SKAUGSET, A. E.; WEILER, M. Temporal persistence of spatial patterns in throughfall. **Journal of Hydrology**, v. 314, p. 263–274, 2005.

KILINC, M. et al. An analysis of the surface energy budget above the world's tallest angiosperm forest. **Agricultural and Forest Meteorology**, v. 167, p. 23–31, 2012.

KLAASSEN, W.; BOSVELD, F.; WATER, E. Water storage and evaporation as constituents of rainfall interception. **Journal of Hydrology**, v. 212–213, p. 36–50, 1998.

KOCHENDORFER, J.; PAW U, K. T. Field estimates of scalar advection across a canopy edge. **Agricultural and Forest Meteorology**, v. 151, p. 585–594, 2011.

LARK, R. M. A comparison of some robust estimators of the variogram for use in soil survey, **European Journal of Soil Science**, v. 51, p; 137–157, 2000

LEVIA, D. F. et al. Throughfall partitioning by trees. **Hydrological Processes**, v. 33, p. 1698–1708, 2019.

LEVIA, D. F.; FROST, E. E. Variability of throughfall volume and solute inputs in wooded ecosystems. **Progress in Physical Geography**, v. 30, n. 5, p. 605–632, 2006.

LINHOSS, A. C.; SIEGERT, C. M. A comparison of five forest interception models using global sensitivity and uncertainty analysis. **JOURNAL OF HYDROLOGY**, v. 538, p. 109–116, 2016a.

LINHOSS, A. C.; SIEGERT, C. M. A comparison of five forest interception models using global sensitivity and uncertainty analysis. **Journal of Hydrology**, v. 538, p. 109–116, 2016b.

LIU, J.; ZHANG, Z.; ZHANG, M. Impacts of forest structure on precipitation interception and run-off generation in a semiarid region in northern China. **Hydrological Processes**, v. 32, n. 15, p. 2362–2376, 2018.

LIU, S. A new model for the prediction of rainfall interception in forest canopies. **Ecological modelling**, v. 99, p. 151–159, 1997.

LIU, S. Evaluation of the Liu model for predicting rainfall interception in forests world-wide. **Hydrological Processes**, v. 15, n. 12, p. 2341–2360, 2001.

LIU, J. et al. How does a rubber plantation affect the spatial variability and temporal stability of throughfall?, **Hydrology Research**, v. 50, 60-74, 2019

MACINNIS-NG, C. M. O. et al. Throughfall and stemflow vary seasonally in different land-use types in a lower montane tropical region of Panama. **Hydrological Processes**, v. 28, p. 2174–2184, 2014.

MANTOVANI, V. A. et al. Spatial and Temporal Patterns in Carbon and Nitrogen Inputs by Net Precipitation in Atlantic Forest, Brazil. **Forest Science**, v. 68, n. 1, p. 113–124, 2021.

MARQUES, V. A. et al. Rainfall water quality under different forest stand. **CERNE**, v. 25, n. 1, p. 8–17, 2019.

MATHERON, G. (1962), Traité de Géostatistique Appliqué, Tome 1, Memoires du Bureau de Recherches Géologiques et Miniéres, Paris.

MARTINS, S. V. et al. Colonization of gaps produced by death of bamboo clumps in a semideciduous mesophytic forest in south-eastern Brazil. **Plant Ecology**, v. 172, p. 121–131, 2004.

MCKEE, T. B.; DOESKEN, N. J.; KLIEST, J. The relationship of drought frequency and duration to time scales. *In*: Proceedings of the 8th Conference of Applied Climatology, 1993, Anaheim, CA. **Preprints, Eighth Conference on Applied Climatology**. American Meteorological Society. p. 17–22.

MELLO, C. R. et al. Water balance in a neotropical forest catchment of southeastern Brazil. **Catena**, v. 173, n. September 2018, p. 9–21, 2019.

METZGER, J. C. et al. Stemflow infiltration hotspots create soil microsites near tree

stems in an unmanaged mixed beech. **Frontiers in Forest and Global Change**, v. 4, p. 9–21, 2021.

MICHILES, A. A. S.; GIELOW, R. Above-ground thermal energy storage rates, trunk heat fluxes and surface energy balance in a central Amazonian rainforest. **Agricultural and Forest Meteorology**, v. 148, p. 917–930, 2008.

MINET, J. et al. Temporal stability of soil moisture patterns measured by proximal ground-penetrating radar. **Hydrology and Earth System Sciences Discussions**, v. 10, n. 4, p. 4063–4097, 2013.

MUZYLO, A. et al. A review of rainfall interception modelling. **Journal of Hydrology**, v. 370, p. 191–206, 2009.

MYERS, N. et al. Biodiversity hotspots for conservation priorities. **Nature**, v. 403, p. 853–858, 2000.

NANKO, K. et al. Spatial variability of throughfall under a single tree: Experimental study of rainfall amount, raindrops, and kinetic energy. **Agricultural and Forest Meteorology**, v. 151, p. 1173–1182, 2011.

NÁVAR, J. Fitting rainfall interception models to forest ecosystems of Mexico. **Journal of Hydrology**, v. 548, p. 458–470, 2017.

NÁVAR, J. Modeling rainfall interception components of forests: Extending drip equations. **Agricultural and Forest Meteorology**, v. 279, p. 1–12, 2019.

NEHREN, U. et al. Natural hazards and climate change Impacts in the state of Rio de Janeiro: A landscape historical analysis. In: NEHREN, U. et al. **Strategies and tools for a sustainable rural Rio de Janeiro**. 1ª edição. Switzerland: Springer, 2019. E-book.

NOBRE, C. A. et al. Some Characteristics and Impacts of the Drought and Water Crisis in Southeastern Brazil during 2014 and 2015. **Journal of Water Resources and Protection**, v. 8, p. 252–262, 2016.

OLIPHANT, A. J. et al. Heat storage and energy balance fluxes for a temperate deciduous forest. **Agricultural and Forest Meteorology**, v. 126, p. 185–201, 2004.

OLIVEIRA-FILHO, A. T. et al. Comparison of the woody flora and soils of six areas of montane semideciduous forest in southern Minas Gerais, Brazil. **Edinburgh Journal of Botany**, v. 51, n. 3, p. 355–389, 1994.

OLIVEIRA, V. A. et al. Assessment of climate change impacts on streamflow and hydropower potential in the headwater region of the Grande river basin , Southeastern Brazil. **International Journal of Climatology**, v. 37, n. 15, p. 1–19, 2017.

OLIVEIRA, V. A. et al. Modeling the effects of climate change on hydrology and sediment load in a headwater basin in the Brazilian Cerrado biome. **Ecological Engineering**, v. 133, p. 20–31, 2019.

OLIVEIRA, V. A. et al. Spatiotemporal modelling of soil moisture in an Atlantic forest through machine learning algorithms. **European Journal of Soil Science**, p. 1–19, 2021.

PAGE, T. et al. Assessing the significance of wet-canopy evaporation from forests during extreme rainfall events for flood mitigation in mountainous regions of the United Kingdom. **Hydrological Processes**, v. 34, p. 4740–4754, 2020.

PALMER, W. C. Meteorological drought. Reseach Paper No. 45. Washington, DC : US Weather Bureau.

PEREIRA, F. L. et al. Rainfall interception modelling: Is the wet bulb approach adequate to estimate mean evaporation rate from wet/saturated canopies in all forest types? **Journal of Hydrology**, v. 534, p. 606–615, 2016.

PHILLIPS, O. L. et al. Drought sensitivity of the Amazon Rainforest. **Science**, v. 323, n. March, p. 1344–1347, 2009.

POORTER, L.; BONGERS, L.; BONGERS, F. Architecture of 54 moist-forest tree species: traits, trade-offs, and functional groups. **Ecology**, v. 87, p. 1289–1301, 2006.

PRESSLAND, A. J. Soil moisture redistribution as affected by throughfall and stemflow in an arid zone shrub community. **Australian Journal of Botany**, v. 24, n. 5, p. 641–649, 1976.

QUIRING, S. M. Monitoring drought: An evaluation of meteorological drought indices. **Geography Compass**, v. 3, n. 1, p. 64–88, 2009.

RIBEIRO, M. C. et al. The Brazilian Atlantic Forest: How much is left and is the remaining forest distributed? Implications for conservation. **Biological Conservation**, v. 142, p. 1141–1153, 2009.

RODRIGUES, A. F. et al. Soil water content and net precipitation spatial variability in an Atlantic forest remnant. **Acta Scientiarum-Agronomy**, v. 42, p. 1–13, 2020.

RODRIGUES, A. F. et al. Modeling canopy interception under drought conditions: The relevance of evaporation and extra sources of energy. **Journal of Environmental Management**, v. 292, p. 1–14, 2021a.

RODRIGUES, A. F. et al. Water balance of an Atlantic forest remnant under a prolonged drought period. **Ciencia e Agrotecnologia**, v. 45, p. 1–13, 2021b.

RODRIGUES, A. F. et al. Throughfall spatial variability in a Neotropical forest: Have we correctly accounted for time stability? **Journal of Hydrology**, in press, 2022.

RODRIGUES, J. A. M. et al. Climate change impacts under RCP scenarios on streamflow and droughts of basins in the Brazilian Cerrado Biome. **International Journal of Climatology**, v. 40, p. 2511–2526, 2019.

RUTTER, A. J. et al. A predictive model of rainfall interception in forests, 1. Derivation of the model from observations in a plantation of Corsican Pine. **Agricultural Meteorology**, v. 9, p. 367–384, 1971.

RUTTER, A. J.; MORTON, A. J. A Predictive Model of Rainfall Interception in Forests. III. Sensitivity of The Model to Stand Parameters and Meteorological Variables. **Journal of Applied Ecology**, v. 14, n. 2, p. 567–588, 1977.

RUTTER, A. J.; MORTON, A. J.; ROBINS, P. C. A Predictive Model of Rainfall

Interception in Forests . II. Generalization of the Model and Comparison with Observations in Some Coniferous and Hardwood Stands. **Journal of Applied Ecology**, v. 12, p. 367–380, 1975.

RYAN, M. G. Tree mortality: Large trees losing out to drought. **Nature Plants**, v. 1, n. 10, p. 1–3, 2015.

SADEGHI, S. et al. Agricultural and Forest Meteorology Efficiency of the reformulated Gash's interception model in semiarid afforestations. **Agricultural and Forest Meteorology**, v. 201, p. 76–85, 2015.

SALEMI, L. F. et al. Land-use change in the Atlantic rainforest region : Consequences for the hydrology of small catchments. **Journal of Hydrology**, v. 499, p. 100–109, 2013.

SATO, A. M.; AVELAR, A. DE S.; NETTO, A. L. C. Spatial variability and temporal stability of throughfall in a eucalyptus plantation in the hilly lowlands of southeastern Brazil. **Hydrological Processes**, v. 25, p. 1910–1923, 2011.

SCHLESINGER, W. H. et al. Forest biogeochemistry in response to drought. **Global change biology**, v. 22, n. 7, p. 2318–2328, 2016.

SHENG, H.; CAI, T. Spatial Variability of Throughfall in a Larch (Larix gmelinii) Forest in Great Kingan Mountain , Northeastern China. **Forests**, v. 12, p. 1–13, 2021.

SILVA, V. O., MELLO, C. R. Meteorological droughts in part of southeastern Brazil : Understanding the last 100 years. **Anais da Academia Brasileira de Ciência**, e20201130, p.1-17, 2021.

SOUZA, C. R. et al. Long-term ecological trends of small secondary forests of the atlantic forest hotspot: A 30-year study case. **Forest Ecology and Management**, v. 489, n. November 2020, 2021.

STAELENS, J. et al. Spatial variability and temporal stability of throughfall water under a dominant beech (Fagus sylvatica L.) tree in relationship to canopy cover. **Journal of Hydrology**, v. 330, n. 3–4, p. 651–662, 2006.

STOGSDILL, W. R. et al. Relationship between throughfall and stand density in a Pinus taeda plantation. **Forest Ecology and Management**, v. 29, p. 105–113, 1989.

SU, L. et al. Variability of throughfall quantity in a mixed evergreen-deciduous broadleaved forest in central China. **Journal of Hydrology and Hydromechanics**, v. 67, p. 225–231, 2019

TEIXEIRA, G. M. et al. Regeneration of tropical montane cloud forests increases water yield in the Brazilian Atlantic Forest. **Ecohydrology**, v. 15, n. 4, p. 1–11, 2021.

TERRA, M. DE C. N. S. et al. Stemflow in a neotropical forest remnant : vegetative determinants, spatial distribution and correlation with soil moisture. **Trees**, v. 32, p. 323–335, 2018a.

TERRA, M. C. S. N. et al. Water availability drives gradients of tree diversity, structure and functional traits in the Atlantic-Cerrado-Caatinga transition, Brazil. **Journal of Plant Ecology**, v. 11, n. 6, p. 803–814, 2018b.

TONELLO, K., et al. Rainfall partitioning in the Cerrado and its influence on net rainfall nutrient fluxes. **Agricultural and Forest Meteorology**, v. 303, p. 1-12, 2021

VACHAUD, G. et al. Temporal stability of spatially measured soil water probability density function. **Soil Science Society of America Journal**, v. 49, p. 822–828, 1985.

VALENTE, F.; DAVID, J. S.; GASH, J. H. C. Modelling interception loss for two sparse eucalypt and pine forests in central Portugal using reformulated Rutter and Gash analytical models. **Journal of Hydrology**, v. 190, p. 141–162, 1997.

VAN STAN J. T. et al. Spatial variability and temporal stability of local net precipitation patterns. In: VAN STAN, II J. T., GUTMANN E., FRIESEN J. (eds) **Precipitation partitioning by vegetation**. 1ª edição. Springer, Cham, 2020.

VICENTE-SERRANO, S. M. et al. A review of environmental droughts: Increased risk under global warming?. **Earth-Science Reviews**, v. 201, 102953, 2020.
VOSS, S.; ZIMMERMANN, B.; ZIMMERMANN, A. Detecting spatial structures in throughfall data: The effect of extent, sample size, sampling design, and variogram estimation method. **Journal of Hydrology**, v. 540, p. 527-537, 2016.

WALLACE, J.; MCJANNET, D. Modelling interception in coastal and montane rainforests in northern Queensland, Australia. **Journal of Hydrology**, v. 348, p. 480–495, 2008.

WANG, Z. et al. Climate change enhances the severity and variability of drought in the Pearl River Basin in South China in the 21st century. **Agricultural and Forest Meteorology**, v. 249, p. 149–162, 2018.

WEBSTER, R.; OLIVER, M. A. **Geostatistics for Environmental Scientists**. 2° Edition. John Wiley & Sons, 2007.

WILHITE, D. A., GLANTZ, M. H. Understanding the drought phenomenon: The role of definitions. **Water Int**, v. 10, p. 111-120, 1985.

WULLAERT, H. et al. Spatial throughfall heterogeneity in a montane rain forest in Ecuador: extent, temporal stability and drivers. **Journal of Hydrology**, v. 377, p. 71–79, 2009

YAN, T. et al. Effects of the morphological characteristics of plants on rainfall interception and kinetic energy. **Journal of Hydrology**, v. 592, p. 1–15, 2021.

ZHANG, H. et al. Spatial-temporal variability of throughfall in a subtropical deciduous forest from the hilly regions of eastern China. **Journal of Mountain Science**, v. 16, n. 8, p. 1788–1801, 2019.

ZHANG, Y. et al. Throughfall and its spatial variability beneath xerophytic shrub canopies within water-limited arid desert ecosystems. **Journal of Hydrology**, v. 539, p. 406–416, 2016.

ZHANG, Y. et al. Rainfall partitioning into throughfall, stemflow and interception loss by two xerophytic shrubs within a rain-fed re-vegetated desert ecosystem, northwestern China. **Journal of Hydrology**, v. 527, p. 1084–1095, 2015.

ZHU, X. et al. Spatial heterogeneity of throughfall and its contributions to the

variability in near-surface soil water-content in semiarid mountains of China. **Forest Ecology and Management**, v. 488, p. 1–12, 2021.

ZIMMERMANN, A.; ZIMMERMANN, B. Requirements for throughfall monitoring: The roles of temporal scale and canopy complexity. **Agricultural and Forest Meteorology**, v. 189–190, p. 125–139, 2014.

ZIMMERMANN, A.; ZIMMERMANN, B.; ELSENBEER, H. Rainfall redistribution in a tropical forest: Spatial and temporal patterns. **Water Resources Research**, v. 45, n. 11, p. 1–18, 2009.

ZIMMERMANN, A. et al. Spatio-temporal patterns of throughfall and solute deposition in an open tropical rain forest. **Journal of Hydrology**, v. 360, p. 87–102, 2008.

ARTICLE 1 – MODELING CANOPY INTERCEPTION UNDER DROUGHT CONDITIONS: THE RELEVANCE OF EVAPORATION AND EXTRA SOURCES OF ENERGY

André Ferreira Rodrigues[a*], Carlos Rogério de Mello[a], Udo Nehren[b], João Pedro de Coimbra Ribeiro[a], Vanessa Alves Mantovani[a], José Marcio de Mello[c].

[a] *Water Resources and Sanitation Department, Federal University of Lavras, MG. Brazil.*

[b] *Institute for Technology and Resources Management in the Tropics and Subtropics, TH Köln – University of Applied Sciences, Köln, Germany.*

[c] *Forest Science Department, Federal University of Lavras, MG. Brazil.*

[*]Corresponding author: André F. Rodrigues (afrodrigues09@gmail.com)

Address: Universidade Federal de Lavras, Departamento de Engenharia – Laboratório de Hidráulica. C.P. 3037, CEP 37200-900, Lavras, MG. Brazil.

Artigo publicado no periódico "Journal of Environmental Management" – ISSN: 0301-4797, sendo apresentado segundo normas de publicação do mesmo.

DOI: https://doi.org/10.1016/j.jenvman.2021.112710

Abstract: Modeling canopy interception is fundamental for understanding the forests' role in local and regional hydrology. In this study, canopy interception (CI), throughfall (TF), and stemflow (SF) were evaluated for a semi-deciduous Atlantic Forest (AFR) from 2013 to 2019, where a prolonged dry period occurred. The Gash and Liu models were analyzed in detail to determine the most appropriate for modeling CI throughout drought conditions. Thus, the climatic parameters were retrieved annually by a modified TF-based method ($E_{I\%}$), whereas the structural parameters represented the entire period. The contribution of the energy stored in the forest (i.e. air and biomass; Q) to CI was also assessed in the AFR stand. Both models performed well when using $E_{I\%}$, as the Gash model overestimated CI by 71 mm (4.6%), whereas the Liu model underestimated it by only 13 mm (0.85%). This performance is due to an increased Q and turbulent mechanisms (such as advection and strong updrafts) that occur in drought conditions and are indirectly accounted for in $E_{I\%}$. However, the Liu model stood out for modeling CI under a prolonged dry period, as the exponential wetting approach better represents the complex canopies of the semi-deciduous forests. Thus, we recommend the Liu model and additional energy sources when dealing with prolonged droughts, as in the case of climate change scenarios projected to the studied region.

Keywords: Tropical forest; Liu model; Energy stored rate (ESR); Energy advection; Biomass energy; Gash model.

1. Introduction

The Atlantic Forest biome is one of the most diverse tropical/subtropical ecosystems in the world, being classified as a biodiversity hotspot due to its high level of plant endemism and at the same time high losses of primary vegetation (Myers et al., 2000). Despite its fragmentation and degradation, Atlantic Forest remnants provide

numerous important ecosystem functions and services, including hydrological cycle regulation (Mello et al., 2019) and hazard mitigation among them (Nehren et al. 2019). Groundwater recharge is of particular importance in order to maintain the water regime, especially during dry periods (Mello et al., 2019).

Another hydrologically important factor of the Atlantic Forest is the rainfall canopy interception which can achieve up to 32.4% of gross precipitation (Salemi et al., 2013). It can reduce the water availability and impair the subsequent processes in the watershed, primarily during drought conditions when evaporation tends to increase. Canopy evaporation represents a considerable amount of water that is released into the atmosphere and should be thoroughly investigated. Thus, understanding the dynamics of canopy interception under a changing climate situation is fundamental to overcome the unavoidable water scarcity which threatens southeastern Brazil (Oliveira et al, 2019; Oliveira et al., 2017).

The canopy water balance (CWB) is initiated by attaining the gross precipitation and partitioning it into throughfall, stemflow, and canopy interception. Throughfall and stemflow are routed toward the forest floor, whereas the intercepted water returns to the atmosphere by evaporation (Macinnis-ng et al., 2014; Salemi et al., 2013). Weather and forest traits interact to drive CWB, which occurs in unique responses in the Atlantic Forest (Junqueira Junior et al., 2019; Rodrigues et al., 2020) and other tropical forests worldwide (Ghimire et al., 2017; Holwerda et al., 2012).

The best way to tackle the intrinsic responses of CWB is by means of canopy interception modeling. In an initial approach, Rutter et al. (1971) proposed a physical-based model which required hourly meteorological information to run a simulation. Since then, this model has been used worldwide and has demonstrated satisfactory results (Muzylo et al., 2009). However, the Rutter model is discouraged for developing

countries which have limited hydrological instrumentation (Muzylo et al., 2009). Thus, the analytical model proposed by Gash (1979) and further expanded for sparse canopies (Gash et al., 1995) has been preferred, as it enables simulation on a per-day basis.

The Gash model is based on six parameters, which can be divided into weather ($\overline{E}$ and $\overline{R}$) and structural (S, p, S_t, and p_t) parameters. $\overline{E}$ and $\overline{R}$ describe the evaporation and rainfall rates for the wet canopy condition (during rainfall), whereas S and S_t represent the minimum water depth to saturate the canopy and trunks, respectively. Lastly, p and p_t are the free throughfall coefficient and the water partition derived to the trunks after canopy saturation, respectively. The Gash model performed properly over the entire period for an Atlantic Forest remnant in Brazil (Junqueira Junior et al., 2019), two rainforests with different recovery stages in Madagascar (Ghimire et al., 2017), and a montane rainforest in Puerto Rico (Holwerda et al., 2012), resulting in relative errors below 12%. These studies showed some differences in the structural parameters; however, the main condition for improving the model performance was correct assessment of the weather parameters, primarily $\overline{E}$ (Carlyle-Moses et al., 2010; Linhoss and Siegert, 2016). Retrieving the evaporation parameter by Gash's methodology (E_{TF}; Gash, 1979) was preferred to the Penman-Monteith approach (E_{PM}), as the latter usually underestimated evaporation (Dijk et al., 2015).

Many reasons for such discrepancies between $\overline{E}$ determinations have been studied by Dijk et al. (2015). However, the most intriguing concept is the additional energy sources which are those stored within the forest (in the air and biomass) and arriving by advection from surrounding areas (Kochendorfer and Paw, 2011; Návar, 2019; Ringgaard et al., 2014). The energy budget has been studied for forest closure (Kilinc et al., 2012; Michiles and Gielow, 2008), but has not been accounted for supplying canopy evaporation. This is of even greater concern for prolonged dry

periods, as the atmospheric stress imposed on the Atlantic Forest is expected to increase canopy evaporation. Thus, we hypothesize that atmospheric dynamics during drought periods may increase the difference between E_{TF} and E_{PM} as a consequence of additional energy sources (Dijk et al., 2015) taking place in rainless periods between events.

Furthermore, the Gash model assumes that canopy drainage does not start until saturation, which configures a water-box approach. This has likely led to an overestimation of canopy interception (Carlyle-Moses and Price, 2007; Cuartas et al., 2007), as drainage begins prior to saturation in complex canopies (as will be further demonstrated in this paper). In this sense, Liu (1997) proposed a new model based on exponential canopy wetting which enables drainage to start before canopy saturation. This exponential approach resembles the actual wetting of a stratified canopy, where upper layers are filled before bottom leaves (Carlyle-Moses et al., 2010) due to the sheltering effect. In addition, the Liu model also differs from the Gash model by (i) accounting together for canopy and trunk storages; and (ii) eliminating empirical issues (Carlyle-Moses et al., 2010). Since the original Liu model (Liu, 1997) does not account for canopy sparseness, Carlyle-Moses and Price (2007) proposed its analytical form for sparse canopies. The Liu model relies on the same set of parameters as the Gash model.

Although Junqueira Junior et al. (2019) investigated both the Gash and Liu models for the Atlantic Forest biome in a dry year (2014), there is a lack of understanding how to model canopy interception during prolonged drought periods (successive dry years). Tropical forests are well-known to change their structure in a delayed process after drought conditions (Rowland et al., 2018). Thus, a prolonged monitoring period is crucial to address this behavior. For addressing the above knowledge gaps, we aim to answer the following questions: (i) Is there a better approach for retrieving $\overline{E}$ for drought periods?; (ii) Are additional energy sources

important for canopy evaporation? In the positive case, are they increased under prolonged droughts?; (iii) Is the Gash or the Liu model better for simulating canopy interception under drought conditions? The canopy interception modeling for a prolonged drought period is a novel approach in tropical regions. Thus, with these results, we want to support decision-making of the international community based on climate change scenarios.

2. Study area

This study was conducted in a semi-deciduous Atlantic Forest remnant (AFR) in southeastern Brazil. The AFR covers an area of 6.35 ha with an Oxisols soil type (USDA Soil Taxonomy) (Figure 1). The topography is mostly undulating with slopes from 5 to 15% (Junqueira Junior et al., 2017). The forest stand is surrounded by dry areas mostly consisting of cropland, urban areas, and bare soils (Figure 1a). As a consequence of uneven heating of the surfaces, such a configuration can affect the micrometeorology of the forest, since the surrounding environment may provide an additional energy source (Kochendorfer and Paw, 2011).

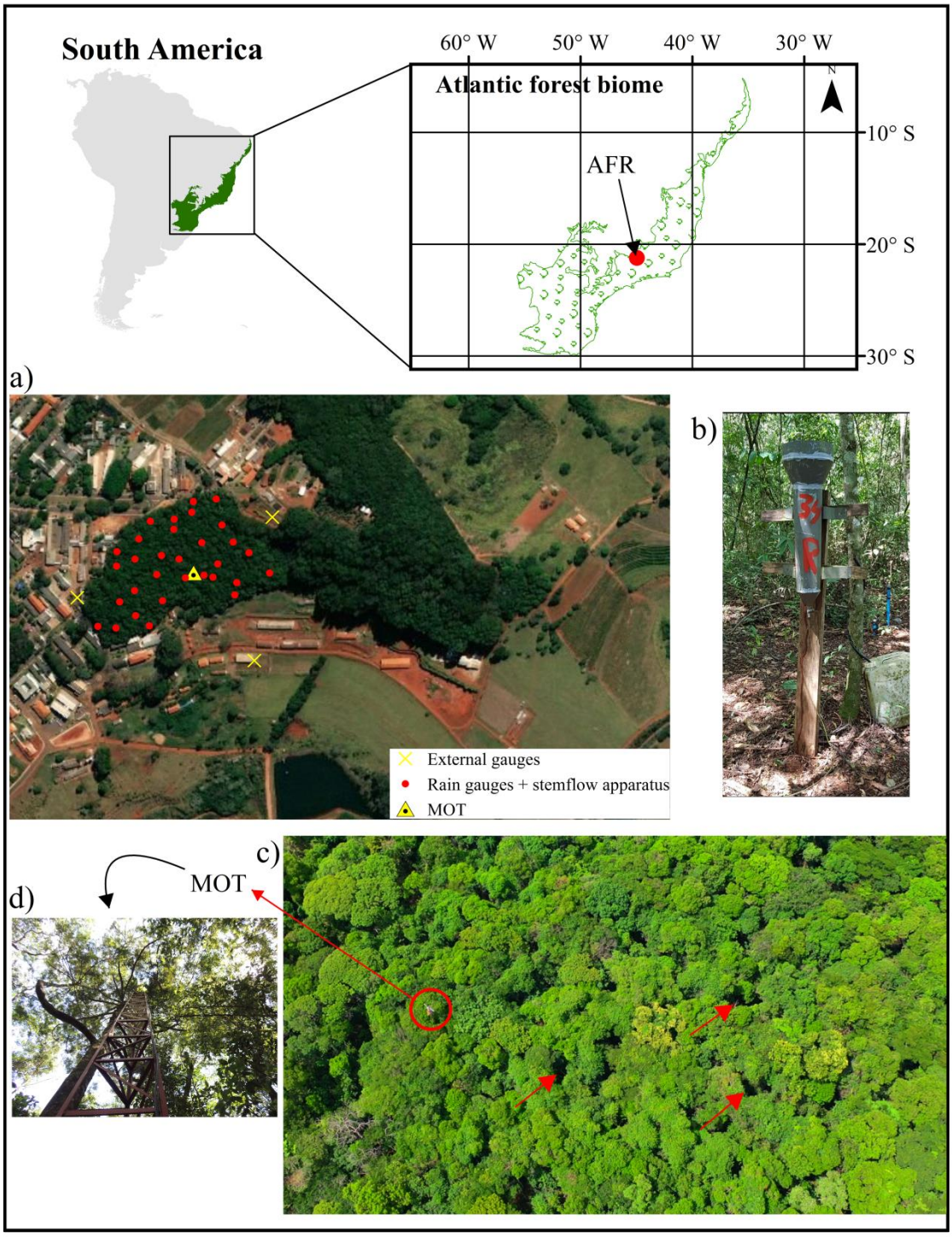

Figure 1. The location of the AFR: (a) spatial distribution of the monitoring sets and surrounding areas; (b) rain gauge and stemflow apparatus; (c) drone image highlighting the AFR canopy gaps (red arrows) and the Meteorological Tower (MOT); and (d) the bottom view of the MOT.

One of the primordial characteristics of AFR is its semi-deciduousness, in which up to 50% of the species lose their leaves in response to water deficiency. This shedding can be tracked by the leaf area index (LAI) fluctuation, which ranged from 3.7 m^2 m^{-2} to 5.0 m^2 m^{-2} throughout the study period (2013/2019). The AFR is composed of 136 different species (DBH > 5 cm) with a density of 2,036 individuals ha^{-1}. According to Oliveira-Filho et al. (1994), the most abundant species are *Xylopia brasiliensis, Copaifera langdorffii, Ocotea odorifera, Sclerolobium rugosum, Amaioua guianensis, and Tapiria obtusa*. Most of these species are within the 5 – 15 cm (67%) and 15 – 25 cm (25%) DBH ranges (Junqueira Junior et al., 2019).

The forest canopy consists of a scattered upper layer of emergent trees (~ 20 m height), a main layer (10 – 15 m height), and an under-layer mostly composed of shrubs and seedlings. Canopy gaps are observed throughout the area due to falling trees, resulting in a degree of sparseness to the AFR (Figure 1c).

The Köppen climate classification is Cwa, which means a seasonal precipitation pattern that splits the hydrological year into a wet (October to March) and a dry (April to September) period. The long-term annual precipitation is 1,462 mm, of which 81% falls in the wet season (Instituto Nacional de Meteorologia – INMET; access link: *http://www.inmet.gov.br/portal/index.php?r=clima/normaisClimatologicas*). January, February, and December are the wettest months, together accounting for 53% of the average annual precipitation. The maximum and minimum average temperatures are 22.8 °C (February) and 16.9 °C (June and July), respectively. The average relative humidity ranges from 62.3% in August to 79.8% in December. Furthermore, an average wind velocity of 2.5 m s^{-1} (± 0.25) is expected to hit the forest canopy in either an easterly or northeasterly direction.

The analyzed period spanned from 2013 to 2019 and included one meteorological year with slightly below-average precipitation (2013), followed by six years with precipitation well below the long-term average (Figure 2). Such climate anomalies are the consequence of changes in the regional atmospheric circulation and an associated blockage of cold fronts from the south and moisture from the Amazon (Nobre et al., 2016), impairing the action of the South Atlantic Convergence Zone (SACZ), which brings significant amounts of rainfall in summer.

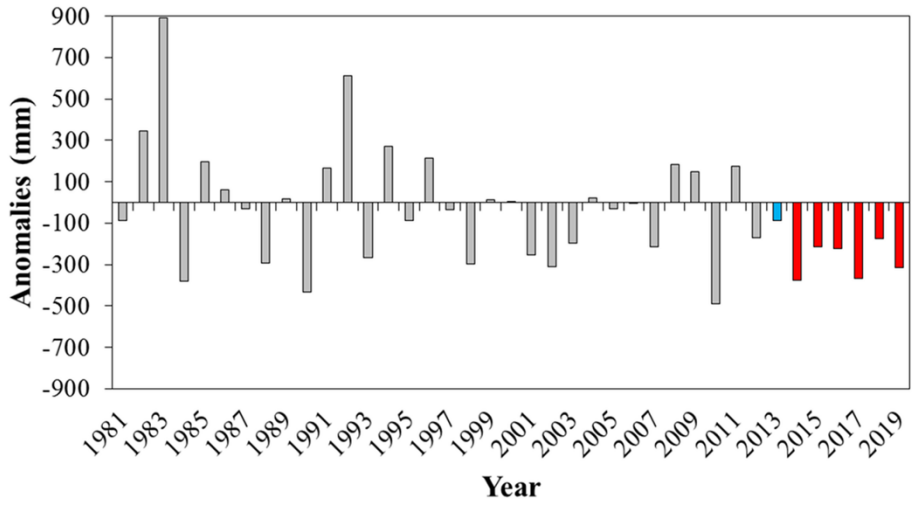

Figure 2. Precipitation anomalies from 1981 to 2019 according to INMET's data highlighting the study period (2013: blue; 2014 to 2019: red).

3. Material and Methods

3.1 Experimental design and monitoring strategies

The present study was conducted with the objective of monitoring a broad period from January 2013 to December 2019, encompassing seven years of measurements. This is a novelty in terms of canopy interception modeling, as most of the studies have been carried out for two years or less (Cuartas et al., 2007; Fan et al., 2014; Ghimire et al., 2017; Holwerda et al., 2012; Sadeghi et al., 2015). Gross

precipitation (GP) was measured using a tipping bucket rain gauge with 0.20 mm resolution (Campbell Scientific CR10X) installed at the top of a 22-meter meteorological tower (MOT) in a 10-minute-time-step configuration (upscale to one hour). The MOT was placed inside the AFR and was equipped with meteorological instruments and a totalizing rain gauge.

GP for both the bucket tipping and the totalizing gauge agreed well (*rain gauge = 1.047 * tipping bucket*, $r^2 = 0.95$) according to Junqueira Junior et al. (2019) (from September 2012 to March 2015). Three external rain gauges were installed around the AFR to obtain improved data from 2016. Their measurement reliability was assessed by comparing the daily average of the external gauges (y, mm) with a gauge operated by INMET (x, mm) located 2 km from the forest. The measurements matched with good agreement ($y = 1.019 * x$, $r^2 = 0.98$).

Throughfall (TF) was measured using 32 Ville de Paris-type rain gauges (Figure 1). Junqueira Junior et al. (2019) observed low standard errors for this configuration, implying high spatial representativeness. These gauges were built with an open area of 378.5 cm^2 and installed 150 cm above the ground to avoid splash-in. TF measurements were carried out at least four hours after the end of a rainfall event, except for those that occurred in the late afternoon, in which readings were taken the next morning.

A stemflow (SF) apparatus with a total of 32 measuring points was installed in the tree shading the rain gauges. This apparatus consists of a hose slit to the length and nailed to the trunk in a spiral configuration. The SF drained into a vessel and was collected at the same moment as TF. Trees were selected based on both abundance and DBH to represent the forest structure as close as possible.

Meteorological variables were monitored above the forest canopy in a 10-minute time step and included as an l-hour average. Wind velocity (m s^{-1}) and direction (°)

were measured by the Wind Speed and Direction Set Smart Sensor (S-WSET-A). The incoming and outgoing radiation (W m^{-2}) was measured by a Solar Radiation Smart Sensor – Silicon Pyranometer (S-LIB-M003). Air temperature (°C) and relative humidity (%) were measured using a 12-bit Temperature/Relative Humidity Smart Sensor (S-THB-M002).

3.2 Interception measurement

The preceding measurement provided a daily dataset in which the canopy interception (CI) was determined by canopy water balance. Since TF + SF is the net precipitation (NP) (i.e. the parcel of GP which reaches the forest floor), CI can be obtained as follows:

$$\mathrm{CI} = \mathrm{GP} - (\mathrm{TF} + \mathrm{SF}) \quad (1)$$

3.3 Canopy interception modeling

3.3.1 Gash model for sparse canopy (Gash et al., 1995; Gash, 1979)

The Gash revised analytical model (Gash et al., 1995) replaced the original version (Gash, 1979) to correct some physical inconsistences and to account for forest sparseness. Two major changes were made: first, the parameter pertaining to evaporation rate per unit area basis ($\overline{E}$, mm h^{-1}) was replaced by evaporation originating exclusively from the canopy ($\overline{E}_c$, mm h^{-1}). Evaporation for the entire area can be scaled to the canopy area as:

$$\overline{E}_c = \frac{\overline{E}}{c} \quad (2)$$

where c is the canopy cover fraction (c = 1 – p); and p is the free throughfall coefficient.

The second modification was related to the fact that the rainfall fraction directed to the trunks (p_t) only occurs after canopy saturation (Gash et al., 1999). In this regard, the sparse model is compound by climate and structural parameters. The structural

parameters describe the canopy excluding the stems. S_c (mm) is the canopy saturation capacity relative to the canopy cover fraction (c), while stems are represented by the trunk saturation capacity (S_t, mm) and p_t. For the climate parameters, $\overline{E}_c$ (mm h^{-1}) and the rainfall rate ($\overline{R}$, mm h^{-1}) describe the weather influence on evaporation for saturated canopy conditions throughout the entire period. A rainfall rate $\geq$ 0.5 mm h^{-1} was adopted as the threshold for canopy saturation (Gash, 1979).

Overall, the Gash sparse model is based on three phases: (i) the wetting phase, in which GP is lower than necessary for canopy saturation (P'_G, mm); (ii) the saturation phase, in which rainfall surpasses P'_G; and (iii) the drying phase, in which no more precipitation occurs (Table 1). In addition, this model considers that these phases occur separately for each rainfall event, and therefore an adequate time for complete canopy dryness must be defined. This was accomplished using the daily interception database.

Table 1. The revised analytical model of Gash.

Interception loss components	Gash sparse model	
Small storms insufficient to saturate the canopy (m).	$c\sum_{j=1}^{m} GP_j$	(3)
Wetting phase for n rainfalls that saturate the canopy (> P'_G).	$ncP'_G - ncS_c$	(4)
Saturated phase where evaporation happens until rainfall ceases.	$\left(\frac{c\overline{E}_c}{\overline{R}}\right)\sum_{j=1}^{n}\left(GP_j - P'_G\right)$	(5)
Drying phase	ncS_c	(6)
Evaporation from trunks, for q storms (> S_t/p_t) saturating the stems and the n – q that do not saturate.	$qS_t + p_t\sum_{j=1}^{n-q} GP_j$	(7)
Rainfall amount necessary to saturate the canopy.	$P'_G = -\frac{\overline{R}S_c}{\overline{E}_c}\ln\left[1 - \frac{\overline{E}_c}{\overline{R}}\right]$	(8)

3.3.2 Liu model (Liu, 1997)

The Liu model (Liu, 1997) considers exponential wetting of the canopy instead of a water-box approach. This gradual storage resembles the wetting on a stratified canopy, where the bottom leaves only receive rainfall after it has been stored on the upper layers (Carlyle-Moses et al., 2010). This model is also applied to individual events that reach a completely dry canopy. The single storm analytical form for sparse canopy was proposed by Carlyle-Moses and Price (2007):

$$CI = c\left[C_{mc}\left[1 - \exp\left[\left(-\frac{1}{C_{mc}}\right)GP\right]\right] \times \left[1 - \frac{\overline{E}_c}{\overline{R}}\right] + \frac{\overline{E}_c}{\overline{R}}GP\right] \quad (9)$$

where C_{mc} is the canopy plus trunk storage capacity (i.e. S_c + S_{tc}); and S_{tc} is the trunk saturation capacity scaled to the canopy as $S_{tc} = \frac{S_t}{c}$.

Further assumptions include (Carlyle-Moses et al., 2010): (i) storage capacity is reached exponentially; (ii) exponential wetting differs from the water-box approach because drainage starts before canopy saturation; (iii) canopy and trunk storages are accounted together; (iv) there is no empirical parameter.

3.4 Retrieving the model parameters

3.4.1 Structural parameters

The p coefficient was derived as the angular coefficient of the linear regression between TF and GP for events below 1.9 mm (Jackson, 1975). This value ensures that the canopy is still unsaturated. Hence, $c = 1 - p$. Canopy storage capacity per unit area (S) follows Valente et al. (1997), and it is scaled to the canopy area as $S_c = S/c$. For the stems, S_t and p_t were derived from the relationship between SF and TF (Valente et al., 1997).

Canopy interception modeling has demonstrated some sensitivity to canopy storage capacity (S) (Linhoss and Siegert, 2016) and it has been suggested that its seasonality should be considered (Wallace and Mcjannet, 2008). This is of concern in the AFR due to its semi-deciduousness, and therefore a sensitivity analysis was performed to track its seasonal relevance. Sensitivity was assessed by varying the S value in 10%, as this range encompasses most of the S in tropical forests worldwide (Cuartas et al., 2007; Dykes, 1997; Ghimire et al., 2017; Junqueira Junior et al., 2019). The other structural parameters were not evaluated as they have previously demonstrated low sensitivity to different forest stands (Pereira et al., 2016).

3.4.2 Climate parameters

Two methods were applied to derive evaporation from a saturated canopy ($\overline{E}$). The first regards the Penman-Monteith (E_{PM}) method defined for a wet-canopy condition ($\overline{R}$ > 0.5 mm h^{-1}), where the roughness resistance (r_s) can be neglected (Monteith, 1965):

$$E_{PM} = \frac{\Delta R_n + \rho_a c_p g_a (e_s - e_a)}{\lambda(\Delta + \gamma)} \quad (10)$$

where Δ is the slope of the saturation vapor pressure curve (kPa $°C^{-1}$); R_n is the net radiation (MJ m^{-2} h^{-1}); ρ_a is the mean air density at constant pressure (kg m^{-3}); c_p is the specific heat of the air (MJ kg^{-1} $°C^{-1}$); g_a is the aerodynamic conductance (m s^{-1}); e_s is the saturation vapor pressure (kPa); e_a is the actual vapor pressure (kPa); ($e_s - e_a$) is known as the vapor pressure deficit (kPa); λ is the latent heat for water vaporization (MJ kg^{-1}); and γ is the psychrometric constant (kPa $°C^{-1}$).

Aerodynamic conductance (g_a) was determined following the FAO-56 (Allen et al., 1998) recommendation for a nearly neutral condition:

$$g_a = \left\{\frac{k}{\ln[(z-d)/z_o]}\right\}^2 * u \quad (11)$$

where k is the von Kármáns's constant velocity (0.41); u is the wind velocity (m s^{-1}) measured at the MOT; z is the height of wind speed measurement (22.0 m); d is the zero plane displacement height (m); and z_o is the roughness length governing transfer of momentum, heat, and vapor (m). The parameters d and z_o can be defined by:

$$d = \frac{2h}{3} \quad (12)$$

$$z_o = h * 0.123 \quad (13)$$

where h is the mean tree height of the AFR (10.2 m).

The second method was proposed by Gash (1979) as the linear relationship between GP and CI, whose slope is $\overline{E}/\overline{R}$. This methodology is known as the TF-based evaporation from saturated canopy conditions (E_{TF}). Such an approach demands previous determination of the rainfall rate parameter ($\overline{R}$), which is the median from all hourly events greater than 0.5 mm. $\overline{R}$ and E_{PM} are usually averaged for saturated canopy conditions (Fan et al., 2014; Sadeghi et al., 2015), however, the median was firstly preferred since these parameters showed a non-normal distribution (Shapiro-Wilk test; p-value < 0.05).

Both $\overline{E}$ and $\overline{R}$ were retrieved from the entire period (Gash et al., 1995; Gash, 1979). However, as our study period encompasses dry years (Figure 2), it is different from the previous ones, and therefore a different canopy-atmosphere relationship can be expected. Thus, these parameters were also determined annually to detect the effects of dry weather conditions on canopy interception. Figure 3 clarifies the methodology.

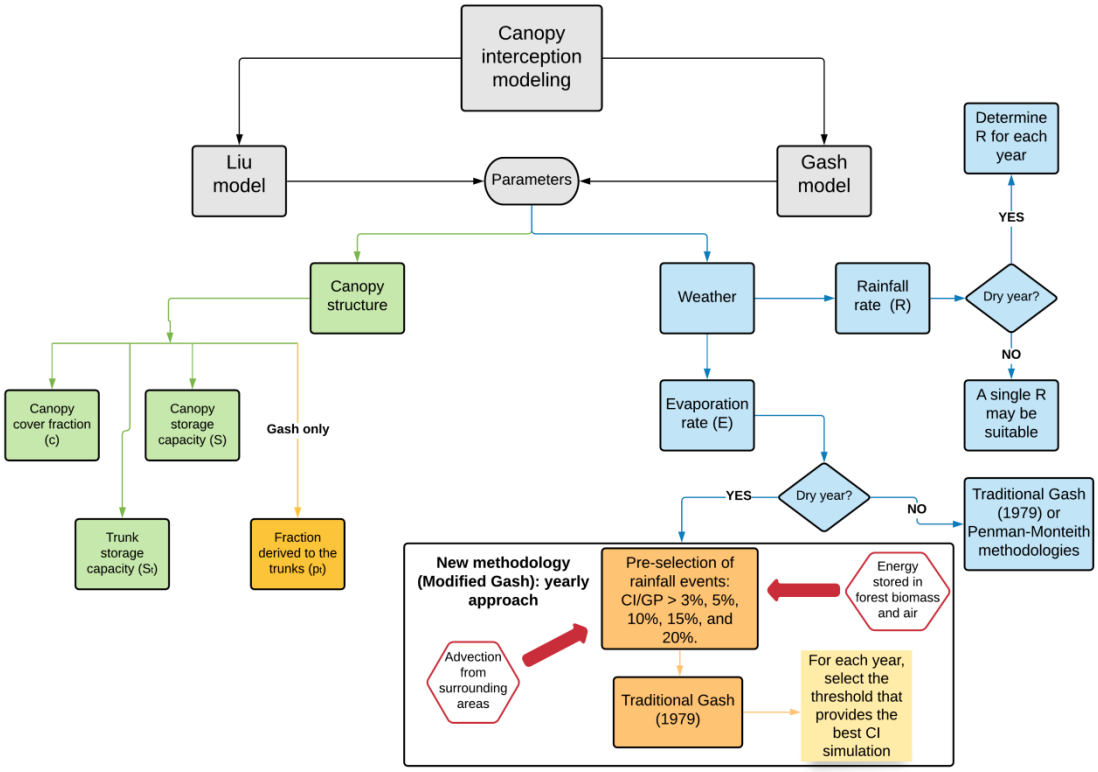

Figure 3. Methodological flowchart for canopy interception modeling.

3.5 Performance of the models

The bootstrap approach was carried out in the R language to create samples with the same dataset size (473 events) in order to validate the Liu and Gash models. Ten samples with replacement were created to address the variability in the canopy interception in prolonged drought periods. The models' performance for both calibration and validation was assessed through the mean relative error (MRE):

$$\mathrm{MRE} = \frac{1}{n}\sum_{i=1}^{n}\frac{|O_i - E_i|}{O_i} \qquad (14)$$

where O_i is the observed canopy interception (mm); E_i is the simulated canopy interception (mm); and n is the number of events.

3.6 Energy balance

Although minor energy sources and sinks have been evaluated to improve forest energy balance (Kilinc et al., 2012), the vertical balance described by E_{PM} was preferred in canopy interception modeling. The energy balance of a forest can be described as follows:

$$R_n = H + \lambda E + Q \quad (15)$$

where H is the sensible heat flux (W m^{-2}); λE is the latent heat flux (W m^{-2}); and Q is the minor energy contribution (W m^{-2}). Q can also be defined as the energy storage rate (ESR) which is the rate of energy leaving a given forest component as heat flux per unit ground area:

$$Q = Q_a + Q_l + Q_b + Q_G + Q_P \quad (16)$$

where Q_a and Q_l are the energy rates (as sensible and latent heat, respectively) stored in the air column between the MOT instrumentation and the forest floor (W m^{-2}); Q_b is the rate of energy stored in the forest biomass (W m^{-2}); Q_G is the rate of energy stored in the soil (W m^{-2}); and Q_P is the rate of energy consumed by the plants for photosynthesis (W m^{-2}). Q_G and Q_P are not considered in this study as they represent a small fraction of ESR for tall forests with complex canopies (Dijk et al., 2015; Kilinc et al., 2012).

In aiming to overcome the robust instrumentations (such as eddy-covariance flux tower) and measurement configurations (temperature and humidity profile of trees and air) demanded to study ESR, Michiles and Gielow (2008) proposed an analytical approach that requires less information about the forest:

$$Q_a = \rho_a c_p \Delta T_a \frac{\Delta z}{\Delta t} \quad (17)$$

$$Q_l = \rho_a \lambda \Delta q \frac{\Delta z}{\Delta t} \quad (18)$$

$$Q_b = m_b c_b \frac{\Delta T_b}{\Delta t} \quad (19)$$

where ΔT_a (°C) and Δq (kg m^{-2}) are the variation in temperature and humidity of the air column, respectively; Δz is the height of the air column (22.0 m); m_b (kg m^{-2}) and c_b (J kg^{-1} $°C^{-1}$) are the aboveground biomass per unit area and the specific biomass heat, respectively; Δt (s) is the interval between two measurements; and ΔT_b (°C) is the variation in the biomass temperature.

T_a and T_b were considered the same for intervals without rainfall. The variation in air temperature (ΔT_a) was that from one hour before the onset of the rainfall to the lowest temperature during the event. The air humidity (q) values followed the hours considered for T_a. Regarding the fresh biomass, T_b is a well-known lagged temperature expected to differ from that of the air (Haverd et al., 2007) once rainfall begins. However, Dijk et al. (2015) suggested the wet-bulb temperature (T_w) to represent the rapid drop of T_b as a consequence of the evaporative cooling. T_w was determined following Stull (2011).

The AFR aboveground biomass was firstly determined for each species through a pantropical allometric model proposed by Chave et al. (2014) for tropical forests worldwide. The fresh biomass of 5,142 individuals totaled 918.8 Mg, occurring in an m_b of 14.5 kg m^{-2}. Determining the specific heat of biomass (c_b) is challenging since it demands knowledge of the moisture content and the temperature of tree traits (Michiles and Gielow, 2008). Furthermore, it varies among species, thus configuring as a costly and time-consuming endeavor. In this sense, the proposed value of 2407 J kg^{-1} $°C^{-1}$ for the Amazon forest (Michiles and Gielow, 2008) was applied in this study.

4. Results

4.1 Gross precipitation, throughfall, stemflow, and canopy interception

Gross precipitation (GP) for the entire period (2013-2019) was 7,303 mm, varying from 894 mm (2016) to 1,178 mm (2019) (Table S1). An average rainfall rate of 15.4 mm d^{-1} (ranging from 0.33 mm d^{-1} to 93.6 mm d^{-1}) was observed on a daily basis for a total of 473 events, with the highest average observed in 2017 (18.9 mm d^{-1}; 57 events) and the lowest in 2015 (13.1 mm d^{-1}; 81 events).

A remarkable seasonality was observed, since at least 75% of the GP (Figure 4) occurred in the wet period (October to March). These events showed intensities which ranged from 14.1 mm d^{-1} to 18.5 mm d^{-1} and from 8.1 mm d^{-1} to 18.8 mm d^{-1} for the wet and dry periods, respectively.

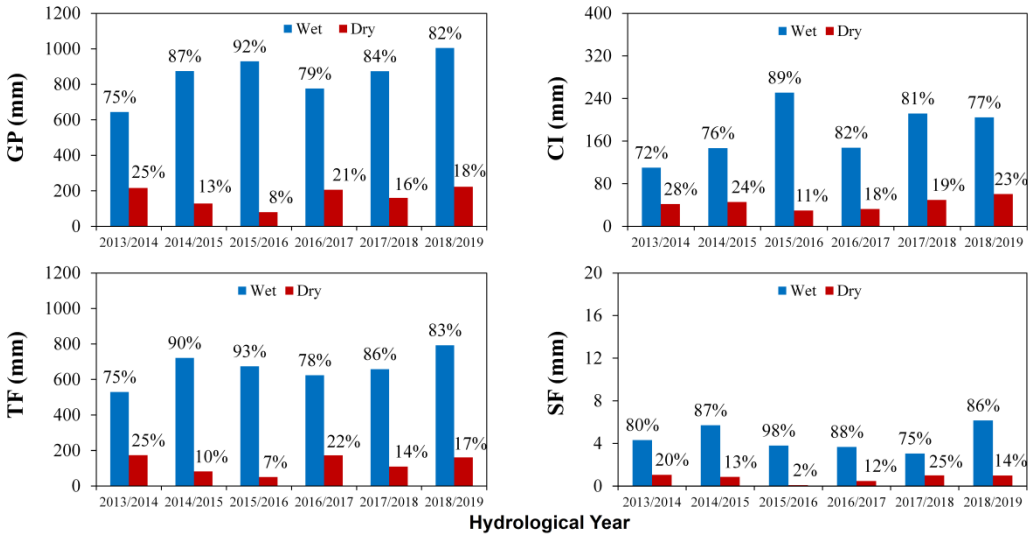

Figure 4. Seasonality of the gross precipitation (GP), canopy interception (CI), throughfall (TF), and stemflow (SF).

Throughfall (TF) accounted for 5,716 mm, representing the greatest parcel of the rainfall portion (78%). There is a decrease in TF contribution in the dry years (Table S1) as the study period encompasses one "normal" year (2013) and six years with precipitation below the long-term average (dry years). The lowest TF/GP was observed

for 2015 and 2018, coinciding with the lowest daily rainfall intensities (i.e. the meteorological conditions in these years seemed to provide greater evaporation). Furthermore, TF followed the seasonality of the region, in which 84% occurred during the wet period (Figure 4).

Stemflow (SF) was the minor contribution of rainfall reaching the forest floor. Only 0.5% of GP was derived to SF on average, which is a similar value to those found by Junqueira Junior et al. (2019) and Terra et al. (2018).

Canopy interception (CI) accumulated to 1,548 mm (21% of GP) and ranged from 16% in 2013 to 24% in 2015. Interception was greater in all dry years when compared to 2013 (Table S1). Moreover, up to 89% of the water returning to the atmosphere occurred during the wet period which follows GP seasonality (Figure 4).

4.2 Simulation results and model performance

Canopy interception modeling was performed in two ways: (i) a single calibration for the entire period; and (ii) calibration of a set of parameters for each year separately. Both approaches were tested using the Liu and Gash models.

The canopy (S = 1.22 mm, p = 0.28, S_t = 0.029 mm, p_t = 0.01) and weather (E_{TF} = 0.16 mm h^{-1}, E_{PM} = 0.11 mm h^{-1}, $\bar{R}$ = 1.78 mm h^{-1}) parameters were the same for both models for the entire period. Regardless of applying E_{TF} or E_{PM}, the models had a poor performance, underestimating CI. In applying E_{TF}, Gash and Liu estimated a CI of 1,192 mm and 1,132 mm, respectively.

A modification regarding the yearly approach was proposed to estimate E_{TF} (hereafter $E_{I\%}$). Following Gash (1979), the slope of the linear regression between CI and GP for the events that saturate the canopy (GP > 1.9 mm in the present case) is $\bar{E}/\bar{R}$. However, some events with small CI/GP seemed interfere with the linear regression

throughout the drier years (Table 2), and hence underestimated evaporation. Therefore, five CI/GP ratios were tested (3%, 5%, 10%, 15%, and 20%) as thresholds for discarding rainfall events in order to improve E_{TF}. The best estimates are presented in Table 2 together with the linear regression coefficients. Despite the natural variability of the phenomenon (CV ~ 76%), the linear model generally showed superior performance as the simulated CI approached the observed values (Figure 5).

Table 2. Yearly evaporation parameter (Gash 1979) and the proposed methodology ($E_{I\%}$) with the slope parameter (a) of the linear regressions and the respective R^2.

	All events			Event elimination					§	
Year	**E_{TF}†**	**a**	**R^2**	**$E_{I\%}$**	**a**	**R^2**	**Threshold (%)**	**Events ‡**	**E_{PM}**	**$\bar{R}$**
2013	0.06	0.0501	0.1574	0.13	0.1059	0.4914	5	7	0.11	1.27
2014	0.19	0.0837	0.2206	0.29	0.1247	0.3925	3	3	0.12	2.29
2015	0.29	0.1611	0.324	0.29	0.1657	0.3662	3	4	0.09	1.78
2016	0.25	0.1650	0.4318	0.26	0.1735	0.4851	5	4	0.10	1.52
2017	0.18	0.0863	0.2981	0.35	0.1708	0.5981	15	10	0.13	2.03
2018	0.21	0.1379	0.733	0.27	0.1785	0.6588	5	1	0.09	1.52
2019	0.14	0.1079	0.5647	0.18	0.1427	0.6655	15	8	0.11	1.27

† Considering all events.

‡ Number of eliminated events.

§ Applied for all simulations.

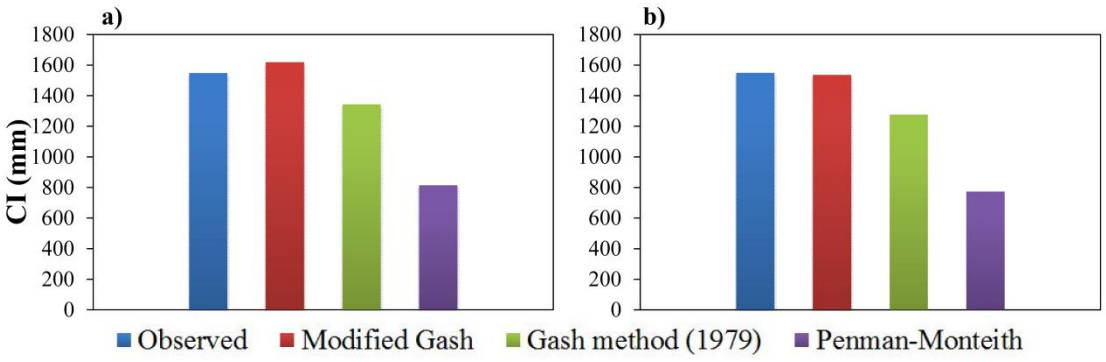

Figure 5. Total observed and simulated canopy interception (CI) based on three different methodologies for retrieving $\overline{E}$, two models (a: Gash; b: Liu), and the yearly approach (Modified Gash).

At this point, one can notice the increase in evaporation for 2014 and 2017 (> 0.1 mm h^{-1}), which is even greater than most of the values retrieved by the E_{PM}, with the exception of 2013. This increase corresponds to the largest precipitation deficit of our study period confirming previous concerns regarding canopy interception dynamics throughout drier years (Figure 6).

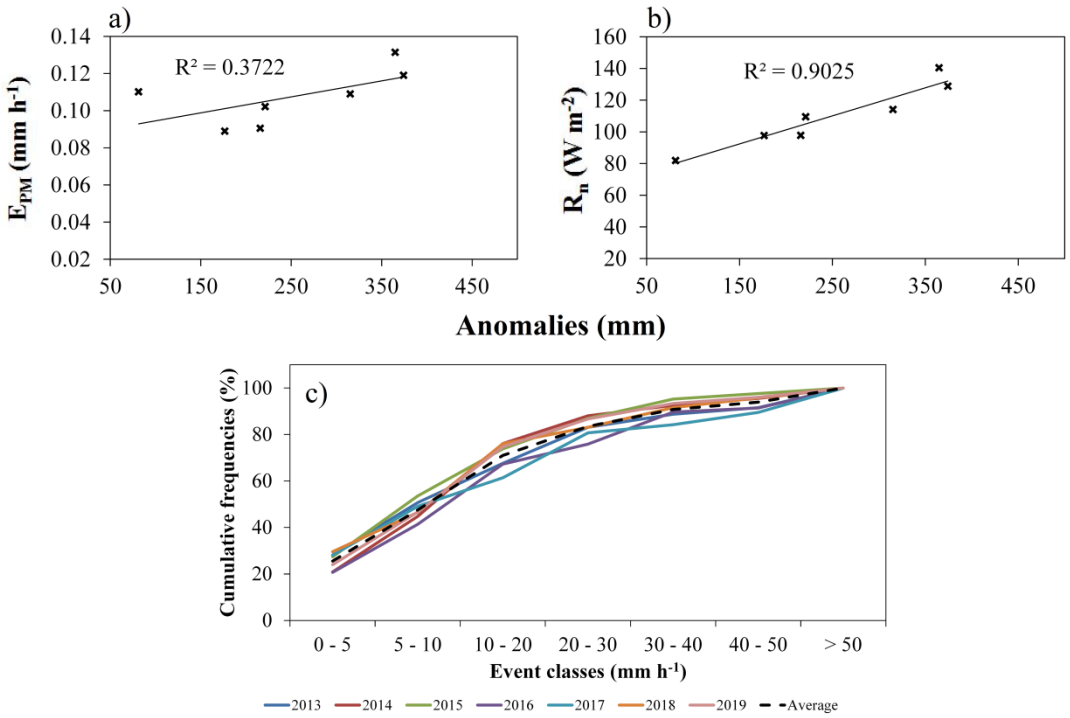

Figure 6. Relationship of the precipitation anomalies with: (a) the Penman-Monteith evaporation (E_{PM}) and (b) net radiation (R_n); and (c) the yearly cumulative frequencies of rainfall rate.

In addition, the inter-annual variability of the canopy parameters was also tested, as the forest could respond differently under drought conditions (Corlett, 2016). Therefore, a sensitivity analysis was performed to assess the impact of S in the

modeling. For this purpose, S was varied by ± 10% (i.e. 1.10 mm and 1.34 mm). The results did not differ by more than 4% and were in agreement with Carlyle-Moses and Price (2007). In this sense, the S determined for the entire period is suitable for the yearly approach without having significant impact on the simulation.

Next, the yearly approach was further explored in this study as it showed the best results (Figure 5). Both the Gash and Liu models enhanced their performance regarding E_{PM} by applying this methodology (Figure 7). The CI for E_{PM} was underestimated by 734 mm and 775 mm for the Gash and Liu models, respectively. Otherwise, in considering $E_{I\%}$ the Gash model overestimated CI by 71 mm, whereas the Liu model underestimated it by 13 mm. The Liu model underestimated CI by only 0.85%, and provided a yearly simulation which was closer to the observations (Table 3). Furthermore, despite the fact that the Gash and Liu models were developed to simulate long-term CI, their performance on an event basis was also satisfactory, with MRE of 0.48 and 1.23, respectively.

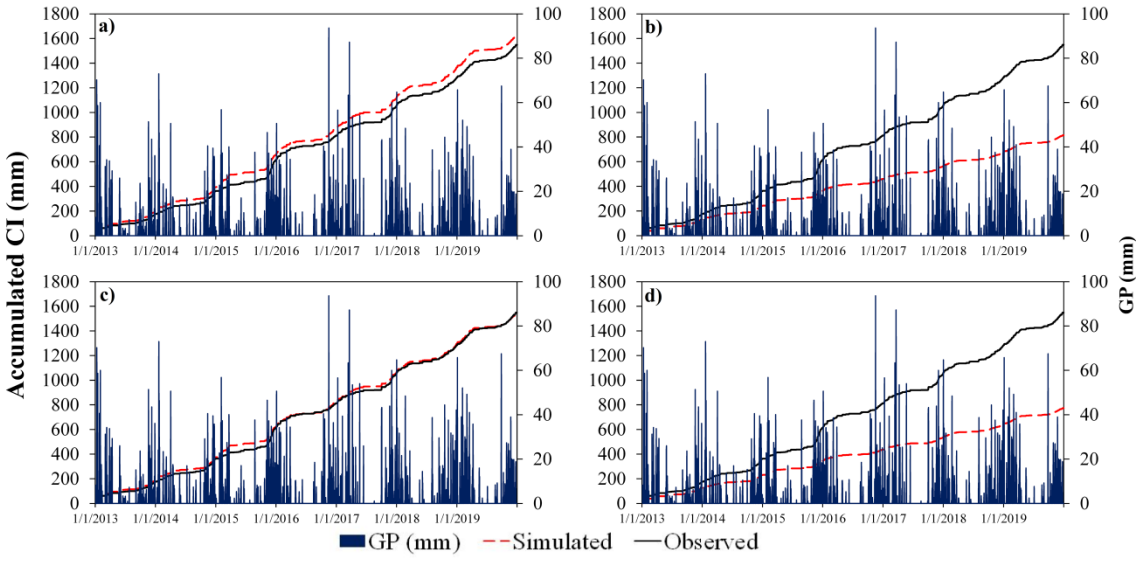

Figure 7. Observed and simulated cumulative canopy interception (CI) by both Gash (a, b) and Liu models (c, d) applying $E_{I\%}$ (a, c) and E_{PM} (b, d).

Table 3. Yearly canopy interception with E_{PM} and $E_{I\%}$, using both the Gash and Liu models.

Year	Observed (mm)	$E_{I\%}$		E_{PM}	
		Gash (mm)	Liu (mm)	Gash (mm)	Liu (mm)
2013	177	199	189	132	126
2014	186	195	185	110	105
2015	251	262	246	121	113
2016	199	214	204	97	93
2017	238	245	234	103	98
2018	231	251	237	115	109
2019	266	253	240	135	129
Entire Period	1548	1619	1535	814	773

The Liu model overcame the Gash model when applying $E_{I\%}$ in the validation. The Liu model presented MRE ranging from 0.39 to 0.56 and differences in total CI of -0.57 ± 63 mm for ten bootstrap samples, whereas the Gash model presented MRE ranging from 0.40 to 0.53 and differences in total CI of 45.5 ± 172.6.

4.3 Forest energy budget

The colored areas displayed in Figure 8 represent each parcel of minor energy sources' and sinks' contribution to Q. As expected, Q_a and Q_b were the greatest fractions regardless of the year analyzed (together accounting for up to 94% in 2013), attaining the maximum significance of -96.4 W m^{-2} and -108.8 W m^{-2}, respectively. Q_l became more negative toward 2019, reaching 26% of Q. Although 2017 presented the highest contribution (-58.6±52.5), there was no clear trend in Q (Table S2), revealing that minor energy sources are important for canopy evaporation, regardless of climatic conditions.

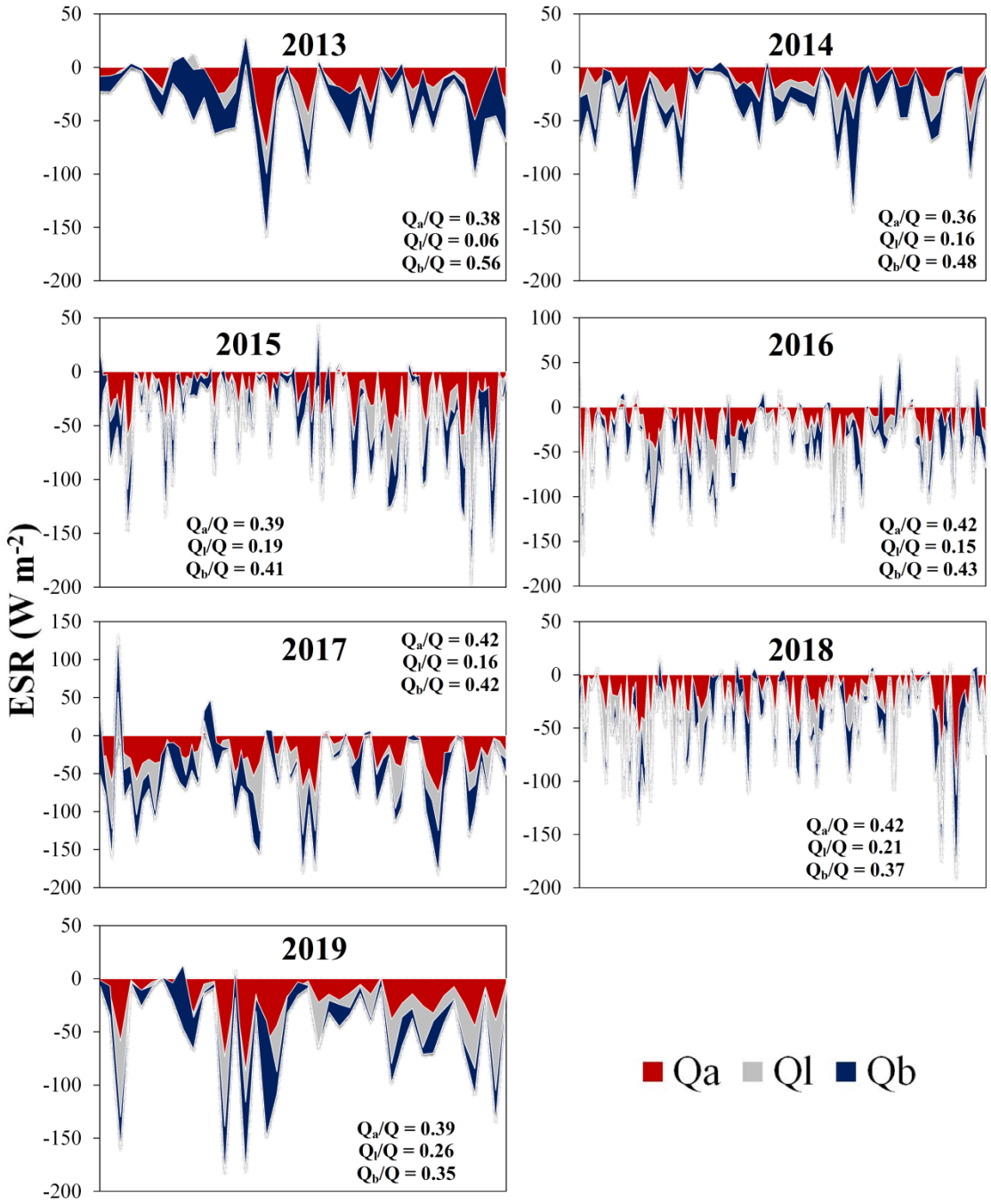

Figure 8. Individual importance of the energy stored in the forest. Q_a: sensible heat; Q_l: latent heat; Q_b: energy stored in biomass; Q: energy stored in the AFR.

Supposing that Q is fully converted to latent flux, we can add it to the vertical energy balance described by E_{PM}. Figure 9 highlights the importance of Q in the "normal" year (2013) as E_{PM} + Q approached $E_{I\%}$ when scaled to the canopy ($Ec_{I\%}$). However, this was not observed in the dry years. This evidences that unaccounted energy sources are likely occurring, which demands evaluation.

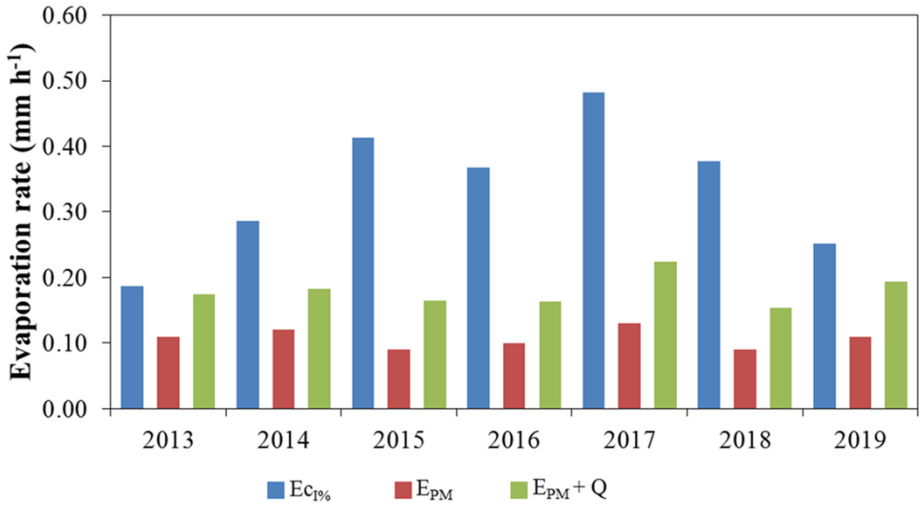

Figure 9. Comparison of the evaporation parameters (E_{PM} and $Ec_{I\%}$) by accounting for Q as a potential source for evaporation (E_{PM} + Q). E_{PM} is the evaporation rate from Penman-Monteith; $Ec_{I\%}$ is the evaporation rate from the new methodology scaled to the canopy; Q is the energy stored within the forest.

5. Discussion

5.1 Canopy water balance

Canopy interception and water partitioning are driven by both weather and forest structure (Zheng and Jia, 2020). In this study, a TF/GP of 78.3% was obtained over an observation period of seven years. This value is lower than those observed by Junqueira Junior et al. (2019), who obtained 87% in the AFR (2012/2015). This period encompassed a close to average hydrological year (2012/2013) which resulted in a

greater TF. The same was reported for a lower montane tropical forest in Panama (82%; Macinnis-ng et al., 2014), a rainforest in Brunei (81.2%; Dykes, 1997), and an Atlantic Forest in the Mantiqueira mountain range in Brazil (81.2%; Arcova et al., 2003), where precipitation was close to or above average. Two main characteristics were considered to explain increased TF in wet years (Junqueira Junior et al., 2019; Ghimire et al., 2017): (i) rainfall amount and intensity; and (ii) consecutive rainy days.

Despite the importance of rainfall characteristics on canopy partitioning, they did not seem to be the primary cause of decreasing TF in drier years, since the cumulative frequencies of the event classes (Figure 6c) were not statistically different (ANOVA 5% of significance). However, a significant decrease in TF/GP was observed (Table S1) along with an increment in evaporation demand (Table 2). This means that evaporation is the leading cause of the canopy water balance in the AFR.

The increased CI/GP ratio (21.2%) in the dry years is similar to that observed by Holwerda et al. (2012) for a lower montane forest in Panama (21.6%), where more intense atmospheric dynamics occurred. E_{PM} increased with precipitation anomalies, indicating that the drier the year, the higher the atmospheric demand during rainfall events (Figure 6a). Although Rn is the main driving force for evaporation (Figure 6b), this is not sufficient to explain the observed evaporated water, since CI tended to be underestimated when applying E_{PM}. The Penman-Monteith evaporation calculation requires hours of meteorological data when rainfall intensity (R) is greater than 0.5 mm h^{-1}, which guarantees the models' evaporation condition during rainfall. Instead, atmospheric conditions of the canopy during the rainless periods are also accounted for when determining the evaporation rate from daily events (i.e. $E_{i\%}$). The significant improvement of CI simulation applying $E_{i\%}$ stresses that the meteorological conditions of rainless periods (intra and inter-events) are crucial for modeling canopy interception.

This increment can be attached to additional energy sources (Dijk et al., 2015; Kochendorfer and Paw, 2011; Michiles and Gielow, 2008), which are further discussed in this paper.

The increase in CI was not followed by a significant change in the forest canopy structure, as the LAI showed little fluctuation between the years, ranging from 3.7 m^2 m^{-2} to 5.0 m^2 m^{-2}. CI was also not sensitive to S, one of the main parameters driving canopy interception. This behavior demonstrates that semi-deciduous Atlantic Forests may be adapted to drier years (Bonal et al., 2016), at least for shorter periods. In a climate change scenario in which drought may be more intense, prolonged, and frequent (Corlett, 2016), a drier and warmer atmosphere and higher incoming radiation (more cloudless days) will lead to an environment with higher evaporation. The increase in evaporation in such a scenario will exacerbate water scarcity in Southeastern Brazil, primarily in the watersheds dominated by Atlantic Forests (Mello et al., 2019).

SF had the lowest contribution to canopy water balance (Table S1), accounting for only 0.5% of GP. Terra et al. (2018) related the low SF to the canopy architecture of main species which favor evaporation. Our findings support this assumption, as SF decreases as $E_{i\%}$ increases. In comparing 2013 (a "normal" meteorological year) and 2017 (the driest studied year), SF was greater in the first year (9 mm), matching with the extremes of canopy evaporation (0.13 mm h^{-1} and 0.35 mm h^{-1}, respectively). A greater SF/GP ratio has been reported for tropical forests with a significant presence of palms and small trees (Germer et al., 2010; Holwerda et al., 2012; Macinnis-ng et al., 2014), as they present an array of branches which favors the funneling ratio. SF contribution in the AFR is of minor relevance due to the predominant horizontal position of leaves on the upper trees (Terra et al., 2018) and the high observed evaporation.

5.2 Modeling canopy interception

The canopy interception modeling will focus on the yearly approach, as it demonstrated the best results in simulating CI over continuous dry years. The application of $E_{I\%}$ improved the simulation (Table 3) for both models, and provided similar to or even better results than other studies (Cuartas et al., 2007; Ghimire et al., 2017; Holwerda et al., 2012). These results are even more satisfactory due to the extension of the study period (most of the related studies spanned up to 2 years) and the unusual weather condition faced in those years. Furthermore, one can realize how the Liu model matched CI for the driest years of 2014 and 2017 when performed with $E_{I\%}$ (Table 3), indicating that this array is the best choice when dealing with CI for a tropical forest under drought conditions. The validation reinforces these results, where the Liu model showed the best performance in bootstrap samples. The modeled CI was within the standardized error of the observations on the event scale, confirming the spatial representativeness of the arrangement (Junqueira Junior et al., 2019) and the suitability of the proposed methodology.

The Liu model performed best in the AFR (Figure 7), indicating an exponential wetting of the canopy in which the upper leaves are become wet faster than the sheltered ones. This approach better represents the dynamics of canopy interception, as the closer the storage gets to saturation, the lower the storage is, since a fuller reservoir drains more water toward the forest floor. The Liu model underestimated CI by 1.9 mm for the AFR, whereas the Gash model overestimated it by 4.5 mm when only considering events lower than 1.9 mm. This difference may be significant for periods when low rainfall is prevalent, making the former model preferable. However, this is not sufficient to explain the notoriously superior performance of the Liu model. Overall,

CI was greater for the Gash than the Liu model (Table 3). This difference goes beyond small events and is mostly related to how the canopy stores water (either the water-box or exponential approach).

Although the exponential wetting has been highlighted as the better approach for tropical forests (Holwerda et al., 2010; Junqueira Junior et al., 2019), an analytical analysis of both models is fundamental to resolve their conceptual discrepancies. After some algebraic manipulation, the models can be rewritten as follows:

$$\mathrm{CI_{GASH}} = \left\{ \mathrm{cP'_G}\left(1 - \frac{\overline{\mathrm{E}}_c}{\overline{\mathrm{R}}}\right) + \mathrm{S_t} + \mathrm{p_t GP} + \mathrm{cGP} \right\} + \mathrm{c}\frac{\overline{\mathrm{E}}_c}{\overline{\mathrm{R}}}\mathrm{GP} \tag{20}$$

$$\mathrm{CI_{LIU}} = \left\{ \mathrm{cC_{mc}}\left[1 - \exp\left[\left(-\frac{1}{\mathrm{C_{mc}}}\right)\mathrm{GP}\right]\right] \times \left[1 - \frac{\overline{\mathrm{E}}_c}{\overline{\mathrm{R}}}\right] \right\} + \mathrm{c}\frac{\overline{\mathrm{E}}_c}{\overline{\mathrm{R}}}\mathrm{GP} \tag{21}$$

where for CI_{GASH}, the p_tGP and cGP terms take place for the non-saturating events (stems and canopy, respectively).

It can be seen that the second member on the right-hand side is the same for both models. Thus, the discrepancies between them are in the first member, which describes the storing process. Thus, we applied a set of parameters obtained for tropical forests (Table 4), in addition to the ones with the lowest and the highest $\overline{\mathrm{E}}/\overline{\mathrm{R}}$ determined in this study (2013 and 2018, respectively) to understand their differences. The analysis demonstrates that the Gash model simulates greater CI than the Liu model with an increasing difference up to P'_G (dashed line) and a tendency to stabilize thereafter (Figure 10). This may not be a concern for short time periods (up to one year) where the Gash model slightly overestimated the observed CI (Ghimire et al., 2017; Holwerda et al., 2012). In addition, both models are likely to provide satisfactory results for regions with low $\overline{\mathrm{E}}/\overline{\mathrm{R}}$ and a closed canopy (i.e. Cuartas et al., 2007). On the other hand, larger time periods are problematic as the discrepancies accumulate throughout the years, especially under extreme weather, as differences between simulated CI were greater for

2018 than for 2013 (Figure 10). These aspects highlight the shortcomings of the Gash model.

Table 4. Canopy interception parameters for different tropical forests worldwide.

Study	**Forest biome**	**Parameters**						
		$\overline{E}/\overline{R}$	P'_G	c	S_c	S_{tc}	C_{mc}	p_t
Junqueira Jr et al. (2019)	Semi-deciduous Atlantic Forest	0.02	1.58	0.83	1.56	0.76	2.32	0.01
Holwerda et al. (2012)	Tabonuco-type rainforest	0.20	0.54	0.77	0.48	0.18	0.66	0.05
Ghimire et al. (2017)	Semi-mature rainforest	0.17	1.96	0.70	1.71	0.10	1.81	0.03
Dykes (1997)	Low land tropical forest	0.13	1.13	0.95	1.05	0.11	1.16	0.03
Cuartas et al. (2007)	Amazon Forest	0.04	1.11	0.97	1.08	0.06	1.14	0.01
This study (2013)	Semi-deciduous Atlantic Forest	0.10	1.79	0.72	1.70	0.04	1.74	0.01
This study (2018)	Semi-deciduous Atlantic Forest	0.18	1.87	0.72	1.70	0.04	1.74	0.01

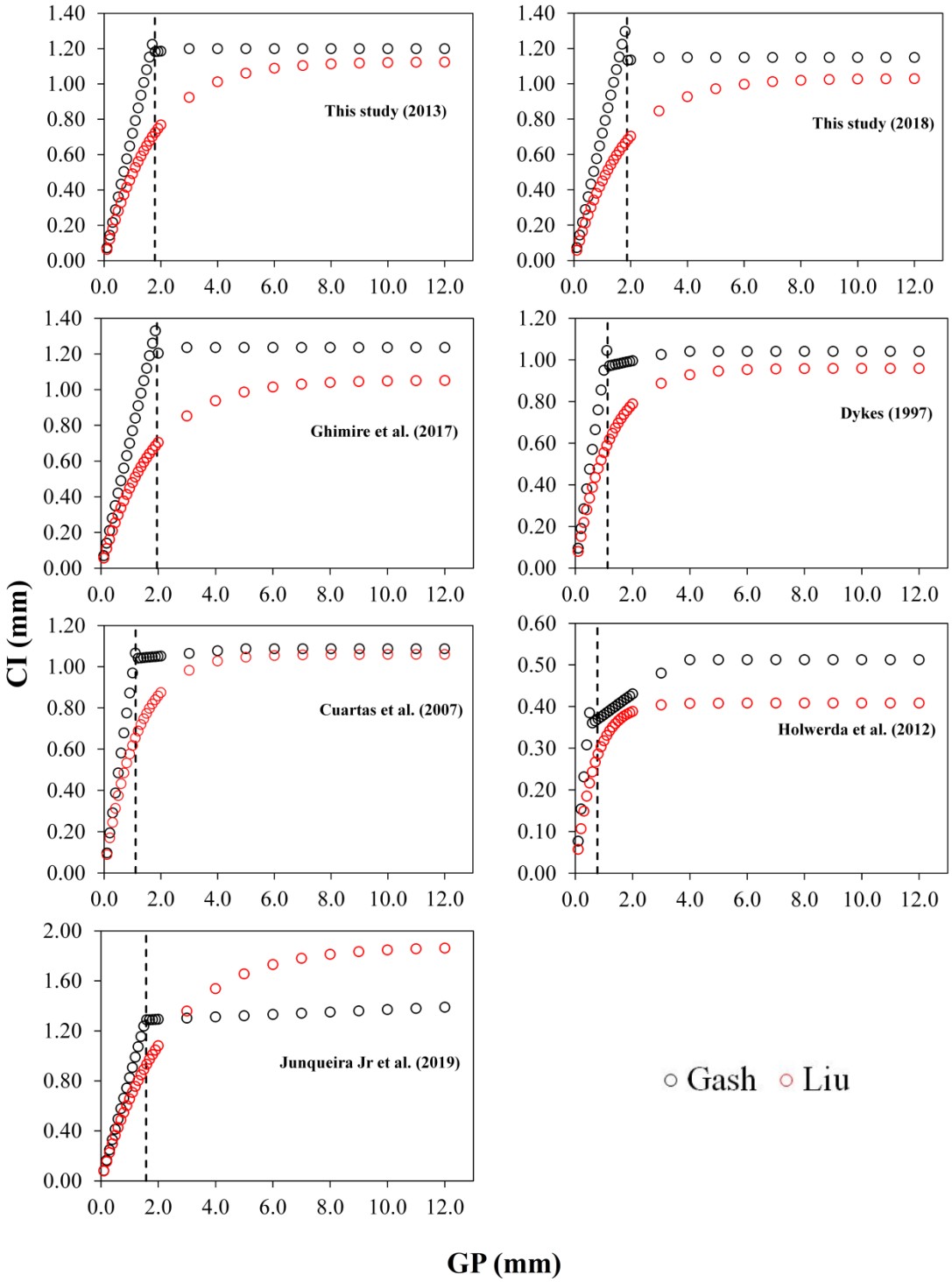

Figure 10. The behavior of the storing process of the Gash and Liu models regarding different sets of parameters from tropical forests worldwide. The dashed line represents the minimum rainfall to saturate the canopy (P'_G).

Moreover, another caution is required before selecting the best model. From the range of parameters encompassing tropical forests worldwide, Gash overestimates CI with regard to Liu saving the set of parameters from Junqueira Junior et al. (2019). The variation of c, p_t, S_c, and $\overline{E}/\overline{R}$ for other studies only influenced the discrepancies between the models without reversing the trend (Figure 10). The reversion occurs as a consequence of the greatest S_{tc} determined by Junqueira Junior et al. (2019). Unlike Gash, the Liu model does not split the storage between S_{tc} and S_c; however, it does account for a total storage (C_{mc}) which is filled at the onset of the rainfall. As S_{tc} was almost 50% of S_c, either an overestimation of C_{mc} or an underestimation of P'g (since it only considers S_c) seems to be the reason for the poorer simulation provided by the Gash model in Junqueira Junior et al. (2019). The above S_{tc} demands a rainfall amount > 78 mm to saturate the entire canopy, which is not feasible even for studies that have considered the funneling ratio for determining the capacity of trunks to store water (Carlyle-Moses et al., 2010). Thus, future studies dealing with significantly greater values of S_{tc} should consider adding it at least on the determination of P'g for proper application of the Gash model. Given the shortcomings of the Gash model as presented, we recommend the Liu model for studying the canopy water balance in tropical forests, particularly when dealing with prolonged dry periods.

For different climate zones (where tree species, architecture, age, leaf density, canopy sparseness, leaf shedding patterns, rainfall intensity, atmospheric demand, and wind velocity might vary), the use of the proposed methodology is encouraged if drought conditions are expected. However, some cautions should be taken. First, the CI/GP ratio varies according to the vegetation and weather characteristics (Zheng and Jia, 2020), and therefore other thresholds for pre-selecting rainfall events should be evaluated. Second, since canopy structure may change significantly in different climate

zones, we recommend future studies to assess the models' sensitivity to the canopy parameters before modeling interception (Linhoss and Siegert, 2016).

5.3 Potential energy sources in AFR

The individual contribution of Q_a, Q_b, and Q_l can be better understood when analyzed on an event basis. Overall, Q was negative (Figure 8), indicating a release of energy after the onset of rainfall which contributes to evaporation. The Q for the AFR reached a value of -196 W m^{-2}, which is similar to that observed in the Amazon forest (-200 W m^{-2}) (Michiles and Gielow, 2008). Kilinc et al. (2012) observed that 78% of energy was stored in both air and biomass, which is close to the dry years of this study. Furthermore, the few positive cases are due to rapid events with a small amount of water, where the energy for evaporation was entirely supplied by R_n.

Q_l increased from 2013 and reached its maximum contribution in 2019 (all years were greater than 2013; Figure 8). The contribution of Q_l increased with the duration of the drought, with a maximum energy release of -91.1 W m^{-2}. Although Michiles and Gielow (2008) observed a release of up to -140 W m^{-2}, this amount accounted for Q_a and Q_l together, precluding an evaluation of their individual contributions. The negative value of Q_l indicates that water vapor condenses, favoring TF. This seems paradoxical since CI/GP increased in the drier years. In this sense, upward flux of bulk air is likely occurring to provide the observed evaporation, as hypothesized by Dijk et al. (2015). This mechanism would carry the condensed drops away from the forest environment, providing another opportunity for it to evaporate in the upper atmosphere. The sudden and strong vertical updrafts are common during convective rainfall, which partially explains the amount of evaporated water, as convective storms are more common in dry years.

In Figure 9, we can see that E_{PM} was virtually $E_{I\%}$ (scaled up to the canopy area; $Ec_{I\%}$) for 2013 considering the minor energy sources. Although the contribution of Q may be linked to the onset of the rainfall, the terms described in Equation (15) seem to be the main energy sources expected in average rainfall years. However, only adding Q to E_{PM} was not enough to explain the dimension of $Ec_{I\%}$ in the drier years. Therefore, an advection of energy from the surrounding dry areas, which adds up to a strong updraft, is likely the cause of the greater evaporation in drought conditions. In agreement with our findings, Kochendorfer and Paw (2011) observed that horizontal and vertical advection of latent and sensible heat play a significant role in the energy balance in a field with an abrupt change from dryland to cropland. Furthermore, Návar (2019) highlighted the importance of advection on CI during convective rainfall as a consequence of the temperature gradient to the atmosphere and surrounding areas. Based on these results, we recommend that future studies consider forest energy balance and the abovementioned turbulent mechanisms when forecasting CI for tropical forests, primarily when drier years are expected.

6. Conclusions

Canopy evaporation increases in drier years as a consequence of a more turbulent environment associated with additional energy sources. Q_a, Q_l, and Q_b play an important role in the available energy, as E_{PM} approaches the observed evaporation rate ($E_{I\%}$) when added to the minor energy sources in normal meteorological years. However, these extra sources are not enough to explain the canopy evaporation in drier years. This highlights the importance of advection.

The modified approach proposed ($E_{I\%}$) is recommended for prolonged drought as it satisfactorily describes the evaporating process, provided that external energy sources are indirectly considered.

Both the Gash and Liu models satisfactorily simulated canopy interception in the AFR when $E_{I\%}$ was applied. However, the Liu model stood out in both calibration and validation, representing the exponential wetting of the canopy.

Acknowledgments: We acknowledge the Improvement of Higher Educational Personnel – CAPES [grant number 88882.306661/2018-01]; the National Council for Scientific and Technological Development – CNPQ [grant number 401760/2016-2]; and FAPEMIG [grant number PPMX-545/18] for supporting and funding this work.

7. References

Allen, R.G., Pereira, L.S., Raes, D., & Smith M. (1998). Crop evapotranspiration - guidelines for computing crop water requirements: *FAO Irrigation and drainage paper 56.* Food and Agriculture Organization, Rome.

Arcova, F. C. S., Cicco, V., & Rocha, P. A. B. (2003). Precipitação efetiva e interceptação das chuvas por floresta de Mata Atlântica em uma microbacia experimental em Cunha - São Paulo. *Revista Árvore*, *27*(2), pp. 257–262. https://doi.org/10.1590/S0100-67622003000200014

Bonal, D., Burban, B., Stahl, C., Wagner, F., & Hérault, B. (2016). The response of tropical rainforests to drought-lessons from recent research and future prospects. *Annals of Forest Science*, *73*, pp. 27–44. https://doi.org/10.1007/s13595-015-0522-5

Carlyle-Moses, D. E., Park, A. D., & Cameron, J. L. (2010). Modelling rainfall interception loss in forest restoration trials in Panama. *Ecohydrology*, *3*, pp. 272–283. https://doi.org/10.1002/eco

Carlyle-Moses, D. E., & Price, A. G. (2007). Modelling canopy interception loss from a Madrean pine-oak stand, Northeastern Mexico. *Hydrological Processes*, *21*, pp. 2572–2580. https://doi.org/10.1002/hyp

Chave, J., Réjou-Méchain, M., Búrquez, A., Chidumayo, E., Colgan, M. S., Delliti, W. B. C., Duque, A., …, & Vieilledent, G. (2014). Improved allometric models to estimate the aboveground biomass of tropical trees. *Global Change Biology*, *20*, pp. 1–14. https://doi.org/10.1111/gcb.12629

Corlett, R. T. (2016). The impacts of droughts in tropical forests. *Trends in Plant Science*, *21*(7), pp. 584–593. https://doi.org/10.1016/j.tplants.2016.02.003

Cuartas, L. A., Tomasella, J., Nobre, A. D., Hodnett, M. G., Waterloo, M. J., & Múnera, J. C. (2007). Interception water-partitioning dynamics for a pristine rainforest in central Amazonia: Marked differences between normal and dry years. *Agricultural and Forest Meteorology*, *145*, pp. 69–83. https://doi.org/10.1016/j.agrformet.2007.04.008

Dijk, A. I. J. M., Gash, J. H., Gorsel, E., Blanken, P. D., Cescatti, A., Emmel, C., Gielen, B., ..., & Wohlfahrt, G. (2015). Rainfall interception and the coupled surface water and energy balance. *Agricultural and Forest Meteorology*, *214–215*, pp. 402–415. https://doi.org/10.1016/j.agrformet.2015.09.006

Dykes, A. P. (1997). Rainfall interception from a lowland tropical rainforest in Brunei. *Journal of Hydrology*, *200*, pp. 260–279. https://doi.org/10.1016/S0022-

1694(97)00023-1

Fan, J., Oestergaard, K. T., Guyot, A., & Lockington, D. A. (2014). Measuring and modeling rainfall interception losses by a native Banksia woodland and an exotic pine plantation in subtropical coastal Australia. *Journal of Hydrology*, *515*, pp. 156–165. https://doi.org/10.1016/j.jhydrol.2014.04.066

Gash, J. H. C., Valente, F., & David, J. S. (1999). Estimates and measurements of evaporation from wet, sparse pine forest in Portugal. *Agricultural and Forest Meteorology*, *94*, pp. 149–158. https://doi.org/10.1016/S0168-1923(99)00008-8

Gash, J. H. C., Lloyd, C. R., & Lachaud, G. (1995). Estimating sparse forest rainfall interception with an analytical model. *Journal of Hydrology*, *170*, pp. 79–86. https://doi.org/10.1016/0022-1694(95)02697-N

Gash, J. H. C. (1979). An analytical model of rainfall interception by forests. *Quartely Journal of the Royal Meteorological Society*, *105*, pp. 43–55. https://doi.org/10.1002/qj.49710544304

Germer, S., Werther, L., & Elsenbeer, H. (2010). Have we underestimated stemflow? Lessons from an open tropical rainforest. *Journal of Hydrology*, *395*, pp. 169–179. https://doi.org/10.1016/j.jhydrol.2010.10.022

Ghimire, C. P., Bruijnzeel, L. A., Lubczynski, M. W., Ravelona, M., Zwartendijk, B. W., & Meerveld, H. J. I. Van. (2017). Measurement and modeling of rainfall interception by two differently aged secondary forests in upland eastern Madagascar. *Journal of Hydrology*, *545*, pp. 212–225. https://doi.org/10.1016/j.jhydrol.2016.10.032

Haverd, V., Cuntz, M., Leuning, R., & Keith, H. (2007). Air and biomass heat storage

fluxes in a forest canopy: Calculation within a soil vegetation atmosphere transfer model. *Agricultural and Forest Meteorology*, *147*, pp. 125–139. https://doi.org/10.1016/j.agrformet.2007.07.006

Holwerda, F., Bruijnzeel, L. A., Scatena, F. N., Vugts, H. F., & Meesters, A. G. C. A. (2012). Wet canopy evaporation from a Puerto Rican lower montane rain forest: The importance of realistically estimated aerodynamic conductance. *Journal of Hydrology*, *414–415*, pp. 1–15. https://doi.org/10.1016/j.jhydrol.2011.07.033

Holwerda, F., Bruijnzeel, L. A., Muñoz-villers, L. E., Equihua, M., & Asbjornsen, H. (2010). Rainfall and cloud water interception in mature and secondary lower montane cloud forests of central Veracruz, Mexico. *Journal of Hydrology*, *384*, pp. 84–96. https://doi.org/10.1016/j.jhydrol.2010.01.012

Jackson, I. J. (1975). Relationships between rainfall parameters and interception by Tropical forest. *Journal of Hydrology*, *24*, pp. 215–238. https://doi.org/10.1016/0022-1694(75)90082-7

Junqueira Junior, J. A., Mello, C. R., Mello, J. M., Scolforo, H. F., Beskow, S., & McCartes, J. (2019). Rainfall partitioning measurement and rainfall interception modelling in a tropical semi-deciduous Atlantic forest remnant. *Agricultural and Forest Meteorology*, *275*, pp. 170–183. https://doi.org/10.1016/j.agrformet.2019.05.016

Junqueira Junior, J. A., Mello, C. R., Owens, P. R., Mello, J. M., Curi, N., & Alves, G. J. (2017). Time-stability of soil water content (SWC) in an Atlantic Forest - Latosol site. *Geoderma*, *288*, pp. 64–78. https://doi.org/10.1016/j.geoderma.2016.10.034

Kilinc, M., Beringer, J., Hutley, L. B., Haverd, V., & Tapper, N. (2012). An analysis of the surface energy budget above the world's tallest angiosperm forest. *Agricultural and Forest Meteorology*, *167*, pp. 23–31. https://doi.org/10.1016/j.agrformet.2012.05.014

Kochendorfer, J., & Paw, K. T. (2011). Field estimates of scalar advection across a canopy edge. *Agricultural and Forest Meteorology*, *151*, pp. 585–594. https://doi.org/10.1016/j.agrformet.2011.01.003

Linhoss, A. C., & Siegert, C. M. (2016). A comparison of five forest interception models using global sensitivity and uncertainty analysis. *Journal of Hydrology*, *538*, pp. 109–116. https://doi.org/10.1016/j.jhydrol.2016.04.011

Liu, S. (1997). A new model for the prediction of rainfall interception in forest canopies. *Ecological Modelling*, *99*, pp. 151–159. https://doi.org/10.1016/S0304-3800(97)01948-0

Macinnis-ng, C. M. O., Flores, E. E., Müller, H., & Schwendenmann, L. (2014). Throughfall and stemflow vary seasonally in different land-use types in a lower montane tropical region of Panama. *Hydrological Processes*, *28*, pp. 2174–2184. https://doi.org/10.1002/hyp.9754

Mello, C. R., Ávila, L. F., Lin, H., Terra, M. C. N. S., & Chappell, N. A. (2019). Water balance in a neotropical forest catchment of southeastern Brazil. *Catena*, *173*, pp. 9–21. https://doi.org/10.1016/j.catena.2018.09.046

Michiles, A. A. S., & Gielow, R. (2008). Above-ground thermal energy storage rates, trunk heat fluxes and surface energy balance in a central Amazonian rainforest. *Agricultural and Forest Meteorology*, *148*, pp. 917–930.

https://doi.org/10.1016/j.agrformet.2008.01.001

Monteith, J.L., 1965. Evaporation and the environment. In: *19th Symposium of the Society for Experimental Biology, 19*, pp. 205-234.

Muzylo, A., Llorens, P., Valente, F., Keizer, J. J., Domingo, F., & Gash, J. H. C. (2009). A review of rainfall interception modelling. *Journal of Hydrology*, *370*, pp. 191–206. https://doi.org/10.1016/j.jhydrol.2009.02.058

Myers, N., Mittermeier, R. A., Mittermeier, C. G., Fonseca, G. A. B., & Kent, J. (2000). Biodiversity hotspots for conservation priorities. *Nature*, *403*, pp. 853–858. https://doi.org/10.1038/35002501

Návar, J. (2019). Modeling rainfall interception components of forests: Extending drip equations. *Agricultural and Forest Meteorology*, *279*, pp. 1–12. https://doi.org/10.1016/j.agrformet.2019.107704

Nehren, U., A. Kirchner, W. Lange, M. Follador & D. Anhuf (2019): Natural hazards and climate change Impacts in the state of Rio de Janeiro: A landscape historical analysis. In: Nehren, U., et al. (Hrsg.): Strategies and tools for a sustainable rural Rio de Janeiro, Chapter 20, Springer Series on Environmental Management, 313-330.

Nobre, C. A., Marengo, J. A., Seluchi, M. E., Cuartas, L. A., & Alves, L. M. (2016). Some characteristics and impacts of the drought and water crisis in southeastern Brazil during 2014 and 2015. *Journal of Water Resources and Protection, 8*, pp. 252–262. https://doi.org/10.4236/jwarp.2016.82022

Oliveira-Filho, A. T., Vilela, E. A., Gavilanes, M. L., & Carvalho, D. A. (1994). Comparison of the woody flora and soils of six areas of montane semideciduous

forest in southern Minas Gerais, Brazil. *Edinburgh Journal of Botany*, *51(3)*, pp. 355–389. https://doi.org/10.1017/S0960428600001839

Oliveira, V. A., Mello, C. R., Beskow, S., Viola, M. R., & Srinivasan, R. (2019). Modeling the effects of climate change on hydrology and sediment load in a headwater basin in the Brazilian Cerrado biome. *Ecological Engineering*, *133*, pp. 20–31. https://doi.org/10.1016/j.ecoleng.2019.04.021

Oliveira, V. A., Mello, C. R. De, Viola, M. R., & Srinivasan, R. (2017). Assessment of climate change impacts on streamflow and hydropower potential in the headwater region of the Grande river basin, Southeastern Brazil. *International Journal of Climatology*, *37*(15), pp. 1–19. https://doi.org/10.1002/joc.5138

Pereira, F. L., Valente, F., David, J. S., Jackson, N., Minunno, F., & Gash, J. H. (2016). Rainfall interception modelling: Is the wet bulb approach adequate to estimate mean evaporation rate from wet/saturated canopies in all forest types? *Journal of Hydrology*, *534*, pp. 606–615. https://doi.org/10.1016/j.jhydrol.2016.01.035

Ringgaard, R., Herbst, M., & Friborg, T. (2014). Partitioning forest evapotranspiration: Interception evaporation and the impact of canopy structure, local and regional advection. *Journal of Hydrology*, *517*, pp. 677–690. https://doi.org/10.1016/j.jhydrol.2014.06.007

Rodrigues, A. F., Mello, C. R., Terra, M. D. C. N. S., Silva, V. O., Pereira, G. A., & Antônio, R. (2020). Soil water content and net precipitation spatial variability in an Atlantic forest remnant. *Acta Scientiarum-Agronomy*, *42*, pp. 1–13. https://doi.org/10.4025/actasciagron.v42i1.43518

Rowland, L., Antonio, C.L., Alex, C., Samuel, A.R.O., Ferreira, L.V., Malhi, Y.,

Metcalfe, D.B., Mencuccini, M., Grace, J., & Meir, P. (2018). Shock and stabilization following long-term drought in tropical forest from 15 years of litterfall dynamics. *Journal of Ecology*, 106, pp. 1673-1682. https://doi.org/10.1111/1365-2745.12931

Rutter, A. J., Kershaw, K. A., Robins, P. C., & Morton, A. J. (1971). A predictive model of rainfall interception in forests, 1. Derivation of the model from observations in a plantation of Corsican Pine. *Agricultural Meteorology*, *9*, pp. 367–384. https://doi.org/10.1016/0002-1571(71)90034-3

Sadeghi, S., Attarod, P., Stan II, J., Pypker, T., & Dunkerley, D. (2015). Agricultural and forest meteorology efficiency of the reformulated Gash's interception model in semiarid afforestations. *Agricultural and Forest Meteorology*, *201*, pp. 76–85. https://doi.org/10.1016/j.agrformet.2014.10.006

Salemi, L. F., Groppo, J. D., Trevisan, R., Moraes, J. M. de, Ferraz, S. F. de B., Villani, J. P., Duarte-Neto, P. J., & Martinelli, L. A. (2013). Land-use change in the Atlantic rainforest region: Consequences for the hydrology of small catchments. *Journal of Hydrology*, *499*, pp. 100–109. https://doi.org/10.1016/j.jhydrol.2013.06.049

Soil Survey Staff. 1999. Soil taxonomy: A basic system of soil classification for making and interpreting soil surveys. 2nd edition. Natural Resources Conservation Service. U.S. Department of Agriculture, Handbook 436.

Stull, R. (2011). Wet-bulb temperature from relative humidity and air temperature. *Journal of Appllied Meteorology and Climatology, 50 (11)*, pp. 2257-2269. https://doi.org/10.1175/JAMC-D-11-0143.1

Terra, M. C. N. S., Mello, C. R., Mello, J. M., Oliveira, V. A., Nunes, M. H., Silva, V. O., Rodrigues, A. F., & Alves, G. J. (2018). Stemflow in a neotropical forest remnant : vegetative determinants, spatial distribution and correlation with soil moisture. *Trees*, *32*, pp. 323–335. https://doi.org/10.1007/s00468-017-1634-3

Valente, F., David, J. S., & Gash, J. H. C. (1997). Modelling interception loss for two sparse eucalypt and pine forests in central Portugal using reformulated Rutter and Gash analytical models. *Journal of Hydrology*, *190*, pp. 141–162. https://doi.org/10.1016/S0022-1694(96)03066-1

Wallace, J., & Mcjannet, D. (2008). Modelling interception in coastal and montane rainforests in northern Queensland, Australia. *Journal of Hydrology*, *348*, pp. 480–495. https://doi.org/10.1016/j.jhydrol.2007.10.019

Zheng, C., & Jia, L. (2020). Global canopy rainfall interception loss derived from satellite earth observations. *Ecohydrology*, 13, pp. 1–13. https://doi.org/10.1002/eco.2186

8. Supplementary Material

Table S1. The contributions of canopy interception (CI), throughfall (TF), and stemflow (SF) to gross precipitation (GP) and the number of rainfall events for the study period.

Year	GP† (mm)	GP‡ (mm)	CI (mm)	TF (mm)	SF (mm)	I/GP (%)	TF/GP (%)	SF/GP (%)	N° of events	Events with SF
2013	1,381	1,128	177	943	9	15.7	83.6	0.8	70	48
2014	1,088	977	186	785	6	19.0	80.3	0.7	66	46
2015	1,246	1,060	251	804	5	23.7	75.8	0.5	81	49
2016	1,241	894	199	690	5	22.2	77.2	0.6	55	36
2017	1,097	1,078	238	837	2	22.1	77.7	0.2	57	28
2018	1,285	987	231	750	6	23.4	76.0	0.6	69	47
2019	1,147	1,178	266	907	6	22.6	76.9	0.5	75	50
Entire period	8,484	7,303	1,548	5,716	39	21.2	78.3	0.5	473	304

†From INMET.

‡From MOT after discarding inconsistent events.

Table S2. Yearly average rate and standard deviation of the energy stored in the AFR (Q) and its components in the air, sensible (Q_a) and latent heat (Q_l), in biomass (Q_b), and net radiation (R_n).

Year	R_n† (W m^{-2})	Q_a (W m^{-2})	Q_l (W m^{-2})	Q_b (W m^{-2})	Q (W m^{-2})
2013	123.2±182.6	-14.9±17.1	-2.6±11.9	-22.1±14.7	-39.5±33.0
2014	128.9±120.1	-14.1±13.2	-6.2±10.8	-18.8±15.4	-39.1±32.2
2015	97.7±105.4	-18.4±18.7	-9.0±19.3	-19.2±17.0	-46.7±43.5
2016	109.5±116.2	-16.6±16.6	-6.0±23.0	-16.9±16.2	-39.5±39.8
2017	140.5±132.0	-24.8±20.7	-9.4±32.2	-24.4±20.8	-58.6±52.5
2018	97.7±78.4	-16.6±17.3	-8.3±18.5	-14.6±15.2	-39.4±39.7
2019	114.1±169.7	-20.6±20.9	-13.4±22.7	-18.3±21.1	-52.4±58.3

†For rainfall conditions on the daytime.

ARTICLE 2 – THROUGHFALL SPATIAL VARIABILITY IN A NEOTROPICAL FOREST: HAVE WE CORRECTLY ACCOUNTED FOR TIME STABILITY?

André F. Rodrigues[a*], Marcela C.N.S. Terra[b], Vanessa A. Mantovani[a], Natielle G. Cordeiro[b], João P.C. Ribeiro[a], Li Guo[c], Udo Nehren[d], José M. Mello[b], Carlos R. Mello[a]

[a]*Universidade Federal de Lavras, Water Resources Department, CP 3037, Lavras, MG, 37200-900, Brazil*

[b]*Universidade Federal de Lavras, Forest Science Department, CP 3037, Lavras, MG, 37200-900, Brazil*

[c]*State Key Laboratory of Hydraulics and Mountain River Engineering, College of Water Resource and Hydropower, Sichuan University, Chengdu, 610065, China*

[d]*Institute for Technology and Resources Management in the Tropics and Subtropics, TH Köln, University of Applied Sciences, Köln, Germany.*

*Corresponding author, *email: andre.rodrigues3@estudante.ufla.br*

Artigo publicado no periódico "Journal of Hydrology" – ISSN: 0022-1694, sendo apresentado segundo normas de publicação do mesmo.

DOI: https://doi.org/10.1016/j.jhydrol.2022.127632

Abstract: The complexity of rainfall-canopy interactions is likely to increase under extreme weather events. Extreme conditions may affect forest structure and change the throughfall (TF) spatial distribution over time. Mistakenly claiming the time stability of TF spatial variability can lead to misunderstanding the rainfall-canopy interactions, obscuring the relationships between weather, forests, and hydrology. Herein we rely on an unprecedented six-hydrological-year event-based dataset from the Brazilian Atlantic Forest, spanning from 2013 to 2019 (summing up 427 rainfall events) to assess: (i) the effects of a prolonged drought period on the TF time stability; and (ii) the importance of forest structure for the TF time stability. The mean relative difference and time stability index were applied for different period lengths and related to forest structure, gross rainfall amount (GR), maximum rainfall intensity, and drought occurrence to assess whether they affect the TF spatial variability. The results indicated that the throughfall spatial variability is less time stable during droughts due to a combination of more light intensity events with some extreme intensities (> 20 mm h^{-1}), which were not observed in the non-drought period. Changes in forest structure became evident after drought conditions and could not be tracked in studies with short monitoring periods. Since throughfall spatial distribution is driven by forest structure (e.g., tree density, species dominance, and biomass), such dynamics affected the time stability of the spatial variability. The time instability was even greater for GR < 10 mm because of the greater rainfall-canopy interactions prior to canopy saturation. Therefore, not accounting for forest dynamics and drought effects on the TF spatial variability lead to misinterpreting time stability.

Keywords: Ecohydrology, rainfall partitioning, canopy traits, spatial variability, drought, Atlantic Forest

1. Introduction

Forest ecosystems are recognized for their fundamental role in climate regulation, water yield, carbon uptake and storage, as well as biochemical dynamics at local, regional, and even continental scales (Zhang et al., 2017). However, specific hydrological-forest studies are needed to better understand these important ecosystem services. These studies can enhance knowledge on water regulation and thereby contribute to improve management and conservation policies. This could lead to more sustainable practices to mitigate the negative impacts of extreme weather events, such as those caused by prolonged droughts which affect people's livelihood and ecosystem health (Coelho et al., 2016; Ellison et al., 2017). This is critical since anomalously dry years entail more intense droughts in tropical regions (Nobre et al., 2016), expanding their effects over the wet period, and modifying the water budget in many forested catchments (Helman et al., 2017).

Precipitation falling on a forest canopy takes different pathways on its way to the forest floor. The incident (or gross) rainfall is routed to the subcanopy by throughfall and stemflow (Crockford and Richardson, 2000; Guo et al., 2020). Throughfall (TF) is defined as the largest fraction of gross rainfall (GR) which directly passes through the canopy along with the portions that drip and splash from it. Stemflow is the minor GR fraction which drains from outlying leaves and branches and is channeled to the bole (or stem) of plants (Levia and Germer, 2015; Liu et al., 2018; Llorens and Domingo, 2007). Such rainfall redistribution is driven by both weather and forest characteristics (Van Stan et al., 2020, Yan et al., 2021; Zhang et al., 2015). Rainfall intensity, duration, and amount under different wind speeds and directions have been recognized as the main meteorological drivers of rainfall redistribution in forests (e.g., Nanko et al., 2011). On the other hand, the structure and architecture of the forest canopy are generally

considered the most critical biotic features controlling rainfall redistribution in forests (Staelens et al., 2006; Terra et al., 2018a).

Such redistribution entails different spatial and temporal dynamics of TF, being an important element of forest hydrology and biogeochemistry dynamics (Metzger et al., 2021), as it controls soil moisture patterns (Junqueira Junior et al., 2017; Oliveira et al., 2021), nutrient input and redistribution (Mantovani et al., 2021; Tonello et al., 2021), preferential pathway formation and groundwater recharge (Bialkowski and Buttle, 2015; Guswa and Spence, 2011), forest transpiration (Guswa and Spence, 2011; Rodrigues et al., 2021b), root growth, and the distribution of tree species according to soil water availability (Pressland, 1976; Terra et al., 2018b). Although many studies have addressed the connections between TF and soil moisture in both time and space (Junqueira Junior et al., 2017; Molina et al., 2019; Oliveira et al., 2021; Rodrigues et al., 2020; Zhu et al., 2021), further importance should be given to TF spatial variability and its drivers to enhance understanding of the rainfall-forest-hydrology connections. A variety of internal and external factors are believed to influence TF spatial patterns, but the methods for testing them are still in their infancy. This is particularly the case for tropical forests. Therefore, there is a great need for studies that address the physical relationships related to the influence of canopy properties on forest hydrological variables.

One approach used worldwide in various forest ecosystems is that of time stability to assess the dynamics of TF spatial variability over time (Keim and Link, 2018; Van Stan et al., 2020). This approach highlights the most time stable locations as well as those which are persistently wetter and/or drier than the TF spatial average, regardless of the time. Keim and Link (2018) studied the temporal persistence of TF spatial patterns in forest stands in the US Pacific Northwest region, linking time

stability with geostatistical properties. Staelens et al. (2006) analyzed the TF spatial variability and temporal stability under a dominant beech tree in relation to the canopy cover and found that the TF spatial variability was significantly higher during the leafed season than during the leafless season at different time scales. Zhang et al. (2016) found that TF spatial variability in xerophytic shrub canopies is temporally stable. Zhu et al. (2021) also studied TF time stability in a semi-arid mountain range in China and related the stability to the spatial dynamics of soil moisture. Wullaert et al. (2009) classified the TF spatial variability in a montane rainforest as "extremely" stable over time regardless of the time period analyzed. Therefore, the TF spatial variability seems to be time stable in most of the ecosystems around the world.

However, Zimmermann et al. (2009) observed that the temporal persistence of throughfall at individual plots disappeared after one year in a tropical semi-deciduous moist forest. The need for longer event-based sample periods to better characterize patterns in throughfall distribution was highlighted by Levia and Frost (2006) in a broad review about the spatial and temporal variability of throughfall. Long sample periods enable observing forest and weather dynamics and how these dynamics affect TF variability. None of the abovementioned studies performed an assessment based on more than four years of observation and/or included extreme weather conditions, such as prolonged droughts. A knowledge gap arises as the time stability of TF spatial variability may be affected by intense droughts, which in turn would lead to: (i) greater impacts on forest dynamics and biogeochemistry cycles, such as biomass loss due to tree mortality, especially for large ones (Ryan, 2015); (ii) favoring of drought-tolerant tree species (Esquivel-Muelbert et al., 2018); and (iii) change in carbon balance (Choat et al., 2018; Schlesinger et al., 2016).

Although several studies have evaluated the temporal persistence of throughfall spatial patterns in temperate forests (i.e. Staelens et al., 2006), semi-arid mountain forests (i.e. Zhu et al., 2021), and tropical forests (i.e. Wullaert et al., 2009), only a few studies considered forest traits as drivers of throughfall time stability, mostly focusing on individual tree traits as opposed to forest traits (e.g., canopy thickness, LAI, leaf characteristics, and stem architecture) (Sheng and Cai, 2021; Staelens et al., 2006). Aware of this importance, Stogsdill et al. (1986) assessed the relationship between thinning and throughfall input to improve soil water availability in a Pinus plantation. However, the TF observed in tropical forests where canopies are closed, stratified, and complex (Aubry-kientz et al., 2019; Guan et al., 2013) has probably interacted and responded to the traits of several trees. Therefore, it is crucial to appraise the consequences of changes in forest structure (as a consequence of droughts) on the TF dynamics. As further highlighted in this study, the usually short monitoring period has blurred the real dynamics of TF spatial distribution, which in turn has led to misinterpretation of TF time stability. Tropical forests are dynamic ecosystems that respond to soil moisture and nutrient availability, and are therefore subject to constant modification (Souza et al., 2021; Terra et al., 2018b). As the spatiotemporal distribution of soil moisture and nutrient availablitiy is partly determined by TF (Metzger et al., 2021; Oliveira et al., 2021), misunderstanding the TF spatiotemporal distribution precludes correctly assessing forest growth and dynamics under a changing climate with more likely stressful conditions (Anderegg et al., 2020). A better understanding of forest resilience therefore depends on a proper assessment of the temporal evolution of TF spatial distribution.

Southeastern Brazil harbors part of the Brazilian Atlantic Forest, one of the world's most biodiverse areas (Myers et al., 2000), with remarkable endemism and a

strong hydrological role (Mello et al., 2019; Rodrigues et al., 2021b). However, this biome has been highly degraded by the historical expansion of both urban and agricultural activities (Dean, 1995; Joly et al., 2014; Ribeiro et al., 2009). There is currently ca. 12.4% of the original extent when considering remnants larger than 3 hectares (SOS Mata Atlântica, access link: https://www.sosma.org.br/), which points out the biome devastation degree. Fortunately, the largest remaining Atlantic Forest patches are located in mountain ranges, which are advantageous environments from a hydrological perspective (i.e. water yield) (Mello et al., 2019; Teixeira et al., 2021). This reinforces the importance of the Atlantic Forest for water management due to its close relationship with water availability (Terra et al., 2018b). However, long-term field data for hydrology and water management are scarce in Brazil since collecting long-term field data is extremely time and resource consuming. However, such datasets are essential for better resource planning and enable evaluating hydrological behavior at different temporal and spatial scales. In brief, they provide a better understanding of complex hydrological processes, notably in relation to tropical forest environments.

Against this background, our study relies on an unprecedented six-hydrological-year event-based dataset spanning from 2013 to 2019 to track the temporal and spatial variability of throughfall in an Atlantic Forest remnant in Southeastern Brazil. The study was carried out per hydrological year (October to September) to answer the following questions: (i) Do dry conditions affect the time stability of throughfall patterns?; (ii) What are the effects of forest structure on throughfall spatial variability and time stability under different drought conditions?; and (iii) Have previous studies mistakenly suggested throughfall time stability? Considering that the Atlantic Forest is a fundamental biome for water resources in Brazil (Mello et al., 2019; Teixeira et al., 2021), answering these questions can help the eco-hydrological stakeholders address

adaptations to adverse conditions and improve strategies to maintain ecosystem services. Moreover, this study aims to stimulate reflection on the suggested throughfall time stability in a dynamic environment, as misinterpretation can lead to erroneously understanding the rainfall-forest-hydrology connections in a climate change scenario.

2. Material and Methods

2.1 Study site

The study site (44°58'15'' W and 21°13'42' S) is a 6.35 ha Atlantic Forest remnant (Figure 1) in an advanced successional stage after full protection in 1986 (Souza et al., 2021). The forest is classified as semi-deciduous since up to 50% of its trees lose their leaves during the dry season, which is an adaptation to rainfall seasonality (Oliveira-Filho and Fontes, 2000). The canopy is stratified, and three tree layers can be identified. The main layer consists of trees ranging from 10 m to 15 m in height and forms the remnant body. Emergent trees scatter across the main layer with ~20 m in height (upper layer), whereas small trees, seedlings, and bushes compose the understory layer (Junqueira Junior et al., 2019; Terra et al., 2018a). There are canopy gaps distributed across the remnant formed by fallen trees (Rodrigues et al., 2021a). The position and openness of such gaps are random and mainly depend on the size of the felled trees which caused the openness. The study area is upon a gneiss geological formation from the Archean period (access link: http://www.portalgeologia.com.br/index.php/mapa/#col-form-download-tab). The soil is a red Oxisol, with slopes ranging from 5% to 15% in an undulating topography (Junqueira Junior et al., 2017), forming a common landscape in Southeast Brazil (Atlantic Forest – Oxisol site).

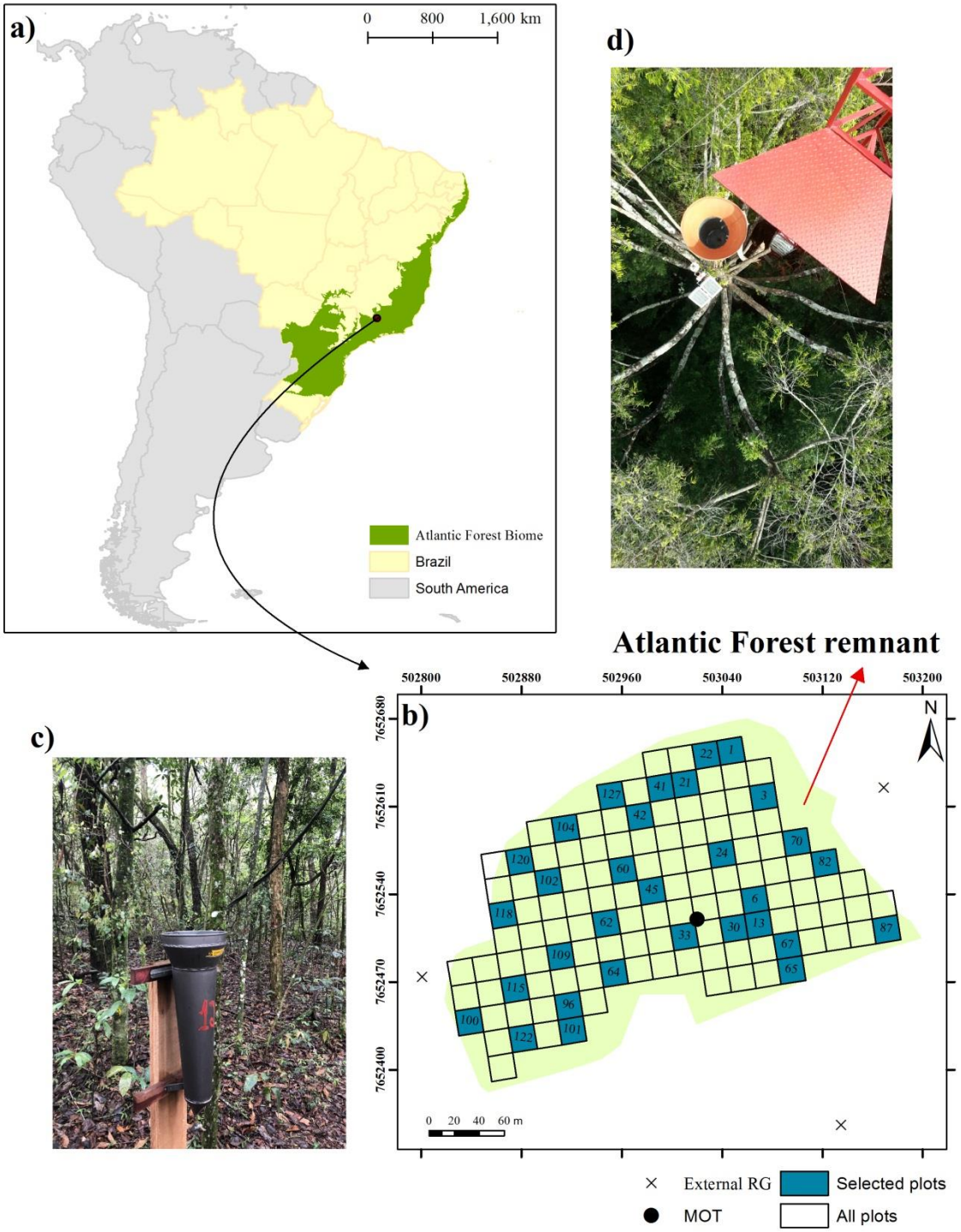

Figure 1. (a) Atlantic Forest remnant geographical location; (b) the plots distribution, external rain gauges (RG), and meteorological tower (MOT) location; (c) a rain gauge for monitoring throughfall; (d) the rain gauge installed on the top of the MOT.

The climate is characterized by rainy summers and dry winters with well-defined rainfall seasonality. The wet season extends from October to March and is responsible

for ~80% of the rainfall, whereas the dry season lasts from April to September. The average monthly vertical water balance (rainfall minus potential evapotranspiration) ranges from -75.9 mm in August to 158.6 mm in December. The average maximum and minimum temperatures are 27.2 ± 1.6 °C and 15.4 ± 2.5 °C, respectively. Wind intensity is greatest in September (2.9 m s^{-1}) and least in February, May, and June (2.2 m s^{-1}), with slight variations throughout the year. Easterly wind directions prevail in the rainy season and northeasterly directions in the dry season. Average sunshine per day ranges from 4.9 hours in December to 8.0 hours in August, highlighting the influence of clouds during the rainy season. The climate is temperate Cwa according to the Köppen classification. These climatological features are based on the 1981-2010 time series from a weather station placed 2 km from the Atlantic Forest remnant provided by the National Institute of Meteorology (*INMET*).

2.2 Gross rainfall and throughfall monitoring

GR was collected from October 2013 to September 2019 using both totalizing and tipping bucket rain gauges. Both gauges were installed on the top of a 22 m meteorological tower (MOT) (Figure 1d) and presented good agreement between their readings (R^2 = 0.95; Junqueira Junior et al., 2019). The tipping gauge measured rainfall at 0.2 mm resolution (Campbell Scientific CR10X) and stored it in a 10-minute time-step in a Hobbo datalogger. The water collected in the totalizing gauge was drained into a 60-L bin placed at the base of the MOT. The readings were performed with graduated cylinders of measuring volumes ranging from 0.1 L to 1.0 L. Next, three totalizer rain gauges were installed surrounding the Atlantic Forest remnant to correct inconsistencies in the GR dataset (Rodrigues et al., 2021a) (Figure 1b).

Throughfall (TF) was measured using 31 rain gauges across inventory plots (Figure 1c). These plots were selected because they represent the main tree species distribution and the terrain features (Oliveira et al., 2021). Such gauges have a collected area of 378.5 cm^2 and were installed 150 cm above the floor to avoid splash-in (Rodrigues et al., 2021a). The gauges were equipped with meshes to avoid clogging with leaves and debris. The meshes were cleaned at least once a week during the rainy season to guarantee representativeness of the measuring observed by Junqueira Junior et al. (2019). This representativeness refers to a low standard error in the non-roving distribution of the 31 gauges, and periodic maintenance was needed to maintain the suitability of the present configuration.

Throughfall and gross rainfall were monitored four hours after the rainfall event to guarantee total dryness of the canopy. The monitoring was carried out the next morning for events that had started in the late afternoon.

2.3 Standardized Precipitation Index (SPI)

The Standardized Precipitation Index (SPI) is a probabilistic approach to characterize drought occurrence, frequency, and duration based on a time series of rainfall (McKee et al., 1993). The interesting aspect about this index is that rainfall deficit or surplus can be highlighted together with its return period. The SPI was selected because it has been widely applied in both Brazillian Savanna (Junqueira et al., 2020) and Atlantic Forest biomes (Silva and Mello, 2021) for water resource management. The second reason is because SPI standardizes the rainfall for a location and period of interest (Quiring, 2009), which enables the results of this study (regarding drought occurrence) to be compared with others dealing with throughfall spatial variability worldwide.

The steps for computing SPI were: (i) a monthly time series of rainfall (provided by *INMET*) was accumulated on the scale of a hydrological year (from October to September) from 1961 to 2019, resulting in a total of 58 hydrological years. SPI is strongly influenced by the time series length and more than 50 years is recommended to avoid distortions (Quiring, 2009); (ii) The Gamma-2-parameter probability function was fitted to this time series and its adequacy was assessed using the Anderson-Darling test (Anderson and Darling, 1952, 1954) at 5% probability level; (iii) the respective probability was applied to an inverse standard normal distribution ($\mu = 0$; $\sigma = 1$) (McKee et al., 1993). The positive and negative deviations are the SPI and indicate rainfall surplus and deficit, respectively. Monthly rainfall was integrated from October to September to account for drought occurrence in the hydrological year scale, which covers the period from 1961/1962 to 2018/2019 in order to analyze the studied period in the context of prolonged drought. Different time scales indicate different impacts of rainfall deficits on water availability, characterizing the agricultural, meteorological, and hydrological droughts (Quiring, 2009). Although long periods (such as the hydrological year) are preferred for water resource management, prolonged droughts increase forest dynamics, making the use of the hydrological year scale adequate to assess their effect on throughfall. Further evidence for considering long periods is that forests have a delayed response to droughts (Anderegg et al., 2020; Rodrigues et al., 2021b).

The persistent dry weather can also be shown by comparing the gross rainfall (GR), air temperature (T), and air relative humidity (RH) of the 2013-2019 period (study period) to the regional climatological average (1981-2010). Moreover, the maximum rainfall intensity of one hour (i_{max}) was selected from each rainfall event to

assess the likely differences on rainfall variability in the presence (or absence) of droughts.

2.4 Spatial variability and time stability

The spatial variability of throughfall was assessed on an event scale by means of the coefficient of variation (CV) and the 31-rain-gauge datasets collected in the study period. The time stability was assessed through the Time Stability Indicator (TSI), which is a function of the mean relative difference (MRD_j) and the standard deviation of the relative difference ($\sigma_{RD_{ij}}$) (Minet et al., 2013; Vachaud et al., 1985):

$$RD_{i,j} = \frac{TF_{i,j} - \overline{TF_i}}{\overline{TF_i}} \quad (1)$$

$$\overline{TF_i} = \frac{1}{m}\sum_{j=1}^{m} TF_{ij} \quad (2)$$

$$MRD_j = \frac{1}{n}\sum_{i=1}^{n} RD_{ij} \quad (3)$$

$$\sigma_{RD_j} = \sqrt{\frac{1}{n-1}\sum_{i=1}^{n}\left(RD_{i,j} - MRD_j\right)^2} \quad (4)$$

In which: RD_{ij} is the relative difference of time *i* in the rain gauge position *j*; $\overline{TF_i}$ is the spatial mean of TF on time *i*; MRD_j is calculated for all rain gauges and represents the behavior of TF in the position *j* in relation to the spatial average TF. $MRD_j > 0$ represents wetter locations, $MRD_j < 0$ drier locations, and $MRD_j \sim 0$ locations with TF amount close to the forest average. MRD_j represents the plots of the Atlantic Forest remnant that are wetter, dryer, or closer to the spatial average TF. However, the standard deviation of the relative positions indicates how much the TF spatial pattern

varies between events (Vachaud et al., 1985). Therefore, it is not appropriate to only rely on MRD_j to define time stability because its variability ($\sigma_{RD_{ij}}$) is also important. Therefore, TSI was developed to integrate the effect of MRD_j and $\sigma_{RD_{ij}}$:

$$TSI = \sqrt{\left(MRD_j\right)^2 + \left(\sigma_{RD_j}\right)^2} \quad (5)$$

The lower the TSI value, the more time stable the location is. Assessing TSI differs from MRD because it describes the persistence of the spatial distribution (i.e. the TF time stability), whereas MRD describes the expected TF spatial distribution throughout the study period. Two approaches were considered to assess the TF time stability: (i) the single (from 2013/2014 to 2018/2019) and (ii) the integrated (2013/2015, 2015/2017, 2017/2019, 2013/2016, 2016/2019, 2013/2017, 2013/2019) hydrological years.

2.5 Forest structure

Forest structure variables used in this study were obtained from a permanent plot network sampled in the Atlantic Forest remnant. A total of 126 plots of 20 x 20 m (400 m^2) were established in the fragment in 1987. These plots were re-measured in the years 1992, 1996, 2001, 2006, 2010, 2015, and 2017. All arboreal individuals with a diameter at breast height (DBH) ≥ 5 cm were identified and measured in each plot (Souza et al., 2021). For the trees which presented tillering, we transformed the diameter to a unique value according to the following equation (Macdicken et al. 1991):

$$D = \sqrt{d_{n1}^2 + d_{n2}^2 + \cdots + d_n^2} \quad (6)$$

In which: D is the transformed diameter, and d_n is the tillered tree diameter.

Botanical material was collected and exsiccates were made for species identification. Tree nomenclature was standardized using the "Flora do Brasil" according to the APG IV classification system (BFG, 2021; The Angiosperm Phylogen Group, 2016). We selected the 31 abovementioned plots from the field survey (Figure 1b) (i.e. each of the 31 forest plots that contained a rain gauge).

We calculated the following variables for each plot from the forest inventory data of 2010, 2015, and 2017: aboveground biomass (AGB), basal area (G), mean diameter at breast height (DBH), coefficient of variation from the mean DBH (CV DBH), number of trees per hectare (N ha^{-1}), species richness (S), Shannon diversity index (H), and Pielou evenness index (J) (Table 1). The aboveground biomass for each plot was determined by each forest inventory year (i.e. 2010, 2015, and 2017) using the equation proposed by Chave et al. (2014) through the *Biomass* package (Réjou-Méchain et al., 2017) in R language (R Core team, 2020). The equation provides individual tree AGB by considering the tree diameter (*D*) and wood density (*WD*), as well as the site coordinates which enable estimating the measure of environmental stress (E). To do so, the wood density is achieved from "The Global Wood Density database" (GWD). Therefore, the plot AGB was obtained as the sum of the AGB of the trees within the plot.

Table 1. Description of forest variables measured in the forest inventory of an Atlantic Forest remnant.

Variable	Description	Formula
DBH (cm)	Mean diameter at breast height - Represents the mean value of the tree's diameter measured at 1.30 meters high in relation to the ground level of each plot.	-
G (m^2 ha^{-1})	Basal area – Represents the cross-sectional area of trees at breast height; provides the occupation level by wood in an area.	$G = \sum_{i=1}^{n} g_i = \sum_{i=1}^{n} \frac{\pi \, . \, DBH^2}{40000}$ *DBH* in cm
CV DBH (%)	Coefficient of variation of the diameter at breast height - Expresses the variability of diameters within each plot.	$CV = \frac{s}{\overline{DBH}}$ Where: *s* is the standard deviation.
AGB (Mg ha^{-1})	Aboveground biomass - Defined as all living tree woody biomass, expressed as a mass per unit area.	AGB = exp (−2.024 − 0.896 ∗ *E* + 0.920 ∗ log (*WD*) + 2.795 ∗ log (*D*) − 0.0461∗ (log $(D)^2$)) (Chave et al., 2014)
N (individuals ha^{-1})	Represents tree density at the site, i.e., the number of individuals per plot in hectares.	-
S	Species richness - Expresses the number of species sampled in a specific area.	-
H (nats ind^{-1})	Shannon diversity index - Diversity index based on the proportional abundance of the community species. In other words, it represents the measurement of the quantity of different species	$H = \frac{\left[N.ln(N) - \sum_{i-1}^{S} n_i ln(n_i)\right]}{N}$

	in a specific area.	Where: N is the total number of tree individuals sampled in each plot; n_i is the number of tree individuals sampled of the i-th species; S is the number of species sampled in each plot; ln is the natural logarithm.
J (nats ind^{-1})	Pielou evenness index - Express the number of individuals distribution in relation to the species.	$J = \frac{H}{Hmax}$ Where: $H\ max$ is the maximum diversity ($\ln(S)$); S is the number of species sampled at each plot.

2.6 Multivariable analyses

We followed the protocol presented in Figure 2 in order to conduct the analyses correlating MRD and forest strucucture data. We ran this protocol for both the < 10 mm and the > 10 mm set of events. Therefore, we first ran a Principal Components Analysis (PCA) (Pearson, 1901; Hotelling, 1933; Jolliffe, 1973) of the annual mean relative difference (MRD) data (MRD-13/14, MRD-14/15, MRD-15/16, MRD-16/17, MRD-17/18, and MRD-18/19) and a PCA for the annual Time Stability Indicator (TSI) data (TSI-13/14, TSI-14/15, TSI-15/16, TSI-16/17, TSI-17/18, and TSI-18/19) in order to deal with a set of multiple variables. PCA is a much-used unconstrained ordination analysis, and is considered the best way to reduce the dimensionality of multivariate data to determine what statistically and practically matters. Moreover, this analysis is widely used as an exploratory tool which helps to visualize patterns out of multivariate data. The basic assumptions of PCA are: (i) multiple variables (multiple variables are required to perform the analysis); (ii) variables should be measured at continuous level, although ordinal variables are frequently used (see Hoshiyar et al., 2021); (iii) sample adequacy: generally, at least 5 to 10 cases per variable is recommended for PCA analysis; (iv) linear relationships among variables (it is assumed that the relationships between variables are linear, since PCA is based on Person's correlation coefficients); and (v) no significant outliers. Assumptions i, ii, and iii were obviously met. Since the variables are scaled prior to the analysis, assumptions iv and v were also met (see Tables S1, S2, S3, and S4 and Figures S1, S2, S3, and S4).

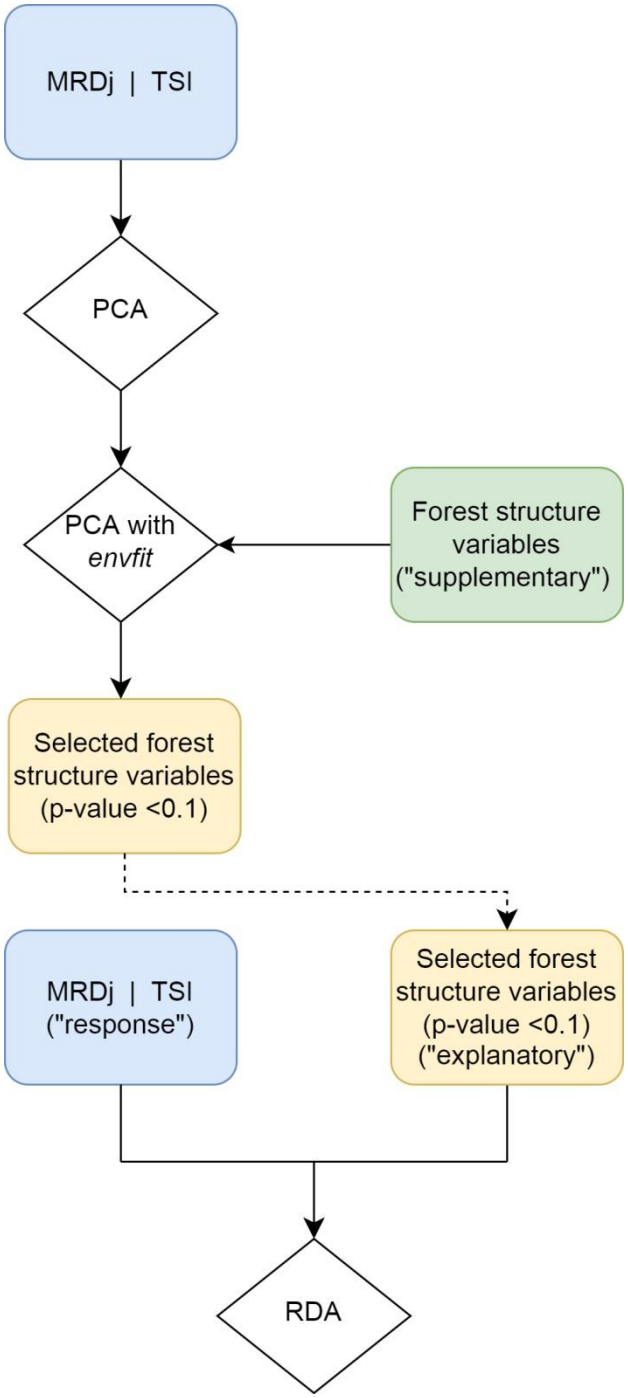

Figure 2. Flowchart of the statistical analyses used to represent the correlations between annual mean relative difference of throughfall (MRDj) and time stability indicator (TSI) and forest structure variables in a Atlantic Forest remnant. *envfitenvfit*

Thus, we used the *envfit* function ("vegan" package for R; Oksanen et al., 2020) in aiming to interpret the meaning of the PCA outputs with the available forest variables

(DBH-10, N-10, G-10, CV DBH-10, AGB-10, S-10, H-10, J-10, DBH-15, N-15, G-15, CV DBH-15, AGB-15, S-15, H-15, J-15, DBH-17, N-17, G-17, CV DBH-17, AGB-17, S-17, H-17, and J-17) and to only select a subset of forest variables that appear to be important for the PCA arrangements. The *envfit* function is designed to calculate regression of supplementary (not "explanatory") variables on ordination axes of uncontrained ordination and test the significance of these regressions by a permutation test. Therefore, the forest variables were projected onto the PCA ordination diagrams as supplementary variables (i.e. regressions of each forest variable were independently fit to ordination axes and their significance was tested by a permutation test, with the number of permutations = 999).

Next, we used redundancy analyses to represent the relationship between the MRD and the forest variables, as well as the relationship between TSI and the forest variables. Redundancy analysis (RDA) reduces the multivariable universe to an easier-to-understand two- or three-dimensional space, where the variations of the response variables can be related to those of the explanatory variables (ter Braak and Looman, 1994). Therefore, RDA is a contrained ordination technique (ordination with covariates or predictors) used to explain a dataset "Y" using a dataset "X" (Legendre et al., 2011). We used the forest dataset ("X") as the explanatory variable of the scaled MRD dataset ("Y") (as well as the scaled TSI dataset), only including those variables in the forest set ("X") whose vectors were significantly or marginally significant (p-value <0.1) according to the *envfit* outputs for each case (Tables S5, S6, S7, and S8). The assumptions of RDA are rather the same as the PCA and have been met for our data (Tables S1, S2, S3, and S4).

One of the main advantages of both PCA and RDA is the diagram ("biplot") which enables visually interpreting multiple correlations. The variables are typically positively correlated when two vectors are close in the diagram and form a small angle.

3. Results

3.1 Prolonged drought during the study period

The adequacy of the Gamma PDF to model the frequency distribution of the hydrological year rainfall series was confirmed through the Anderson-Darling test (Figure 3a). Therefore, the SPI can be applied to assess drought conditions in the study region.

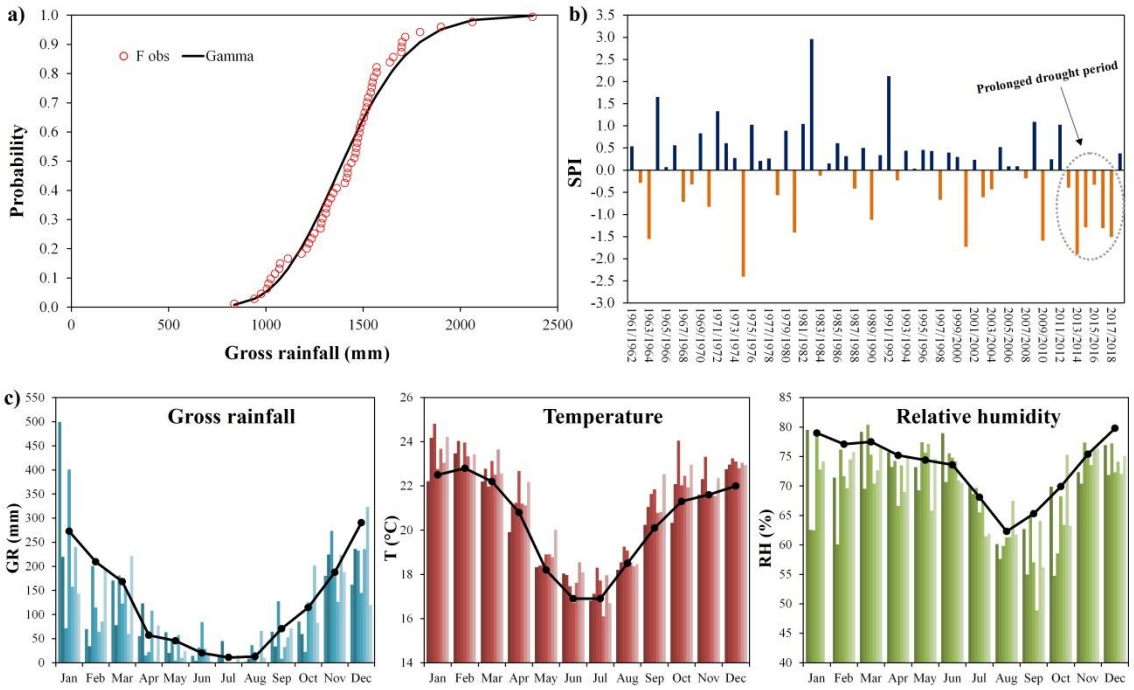

Figure 3. (a) The SPI accumulated frequency (F obs) and the Gamma probability distribution; (b) the Standardized Precipitation Index (SPI); and (c) the monthly gross rainfall (GR), air temperature (T), and relative humidity (RH) (blue, red, and green bars,

respectively) for the study period (2013-2019), with the climatological average (1981-2010) (black dotted lines). Dark to light bars represent 2013 to 2019 monthly values.

Dry and wet hydrological years interspersed up to 2011/2012, indicating drought seasonality occurrence in the region. However, a prolonged drought period could be observed at the end of the time series (Figure 3b). Such a prolonged meteorological drought impacts the Atlantic Forest hydrology, as highlighted by Rodrigues et al. (2021b) and Souza et al. (2021), and is therefore expected to interfere in the throughfall time stability. Thus, the study period was split into two to assess the effects of droughts on the throughfall time stability: (i) prolonged drought period (October 2013 to September 2018) and (ii) non-drought period (October 2018 – September 2019). Table S1 depicts the SPI classification in accordance with the World Meteorological Organization (WMO) (World Meteorological Organization – WMO, 2012).

GR and RH were below average for most of the months during the study period, whereas temperature was greater than average (Figure 3c). Overall, GR was 250 mm less than the climatological year average. RH ranged from 58.4% to 74.8% and from 62.3% to 79.8% for the 2013-2019 and 1981-2010 periods, respectively. Moreover, T ranged from 17.2 °C to 23.6°C in the study period, whereas T ranged from 16.9 °C to 22.8 °C for the climatological average. The behavior of GR, T, and RH indicated that the study period was drier and hotter than the average long-term conditions of the region.

The box plots regarding rainfall intensity highlight the different distribution of maximum rainfall intensity between the prolonged drought and non-drought period (Figure 4). A greater concentration of light rainfall events was observed in the prolonged drought period, in which the first, second, and third quartiles were 0.25 mm h^{-1}, 1.78 mm h^{-1}, and 5.08 mm h^{-1}, respectively. Conversely, they were 0.76 mm h^{-1},

3.05 mm h^{-1}, and 7.87 mm h^{-1} during the non-drought period, respectively. However, heavier rainfall events were observed in the prolonged drought period, characterizing a greater variability of rainfall intensities (Figure 4). This is confirmed by the greater coefficient of variation in the prolonged drought (CV = 141%) versus that in the non-drought period (CV = 108%).

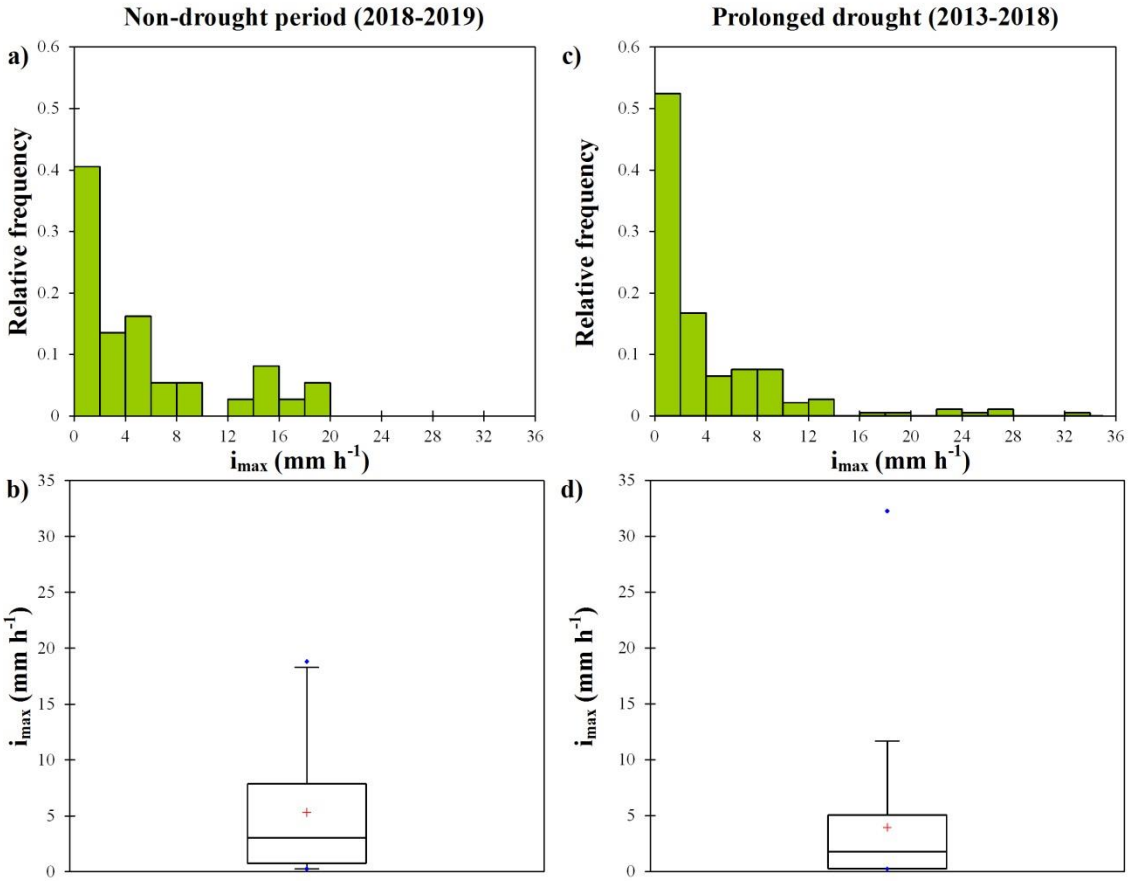

Figure 4. Histogram and box plot of the maximum rainfall intensity (i_{max}) for the prolonged drought (c, d) and non-drought (a, b) periods, respectively.

3.2 Canopy water balance

Box-plot and filtering techniques highlighted 25 rainfall events out of 427 (encompassing 6 hydrological years) as outliers. These events were then removed before the analyses. Annual gross rainfall (GR) ranged from 860 mm (2013/2014) to 1422 mm (2018/2019). Throughfall (TF) ranged from 707 mm to 1135 mm (2013/2014 and 2018/2019, respectively) and represented up to 84.5% of GR (2016/2017). Most of

the throughfall occurred in the wet season (up to 94.2% in 2015/2016). GP and TF in the prolonged drought period added up to 5232 mm and 4097 mm, respectively, with TF/GP of 78.3%. In contrast, GP and TF in the non-drought period were 1422 mm and 1135 (TF/GP = 79.8%), respectively.

On the event scale, the TF/GR ratio increased with gross rainfall, regardless of the period analyzed (prolonged drought or non-drought periods) (Figure 5). TF/GR ranged from 2.4% to 99.1% and from 19.8% to 98.1% in the prolonged drought and non-drought periods, respectively. The TF/GR followed logarithmic behavior in both analyzed periods, with GR describing 60.7% of the TF/GR variability in the non-drought period (Figure 5b). In contrast, only 33.4% of TF/GR variability was described by GR in the prolonged drought period (Figure 5b). The logarithimic tendency was similar for small rainfall events (GR < 10 mm) and became different beyond this threshold. Moreover, GR represented 99% and 97% of TF's variability in the prolonged drought and non-drought periods, respectively (Figure 5a). The linear pattern is the same regardless of the rainfall amount (< or > 10 mm), highlighting an overall relationship between these two variables.

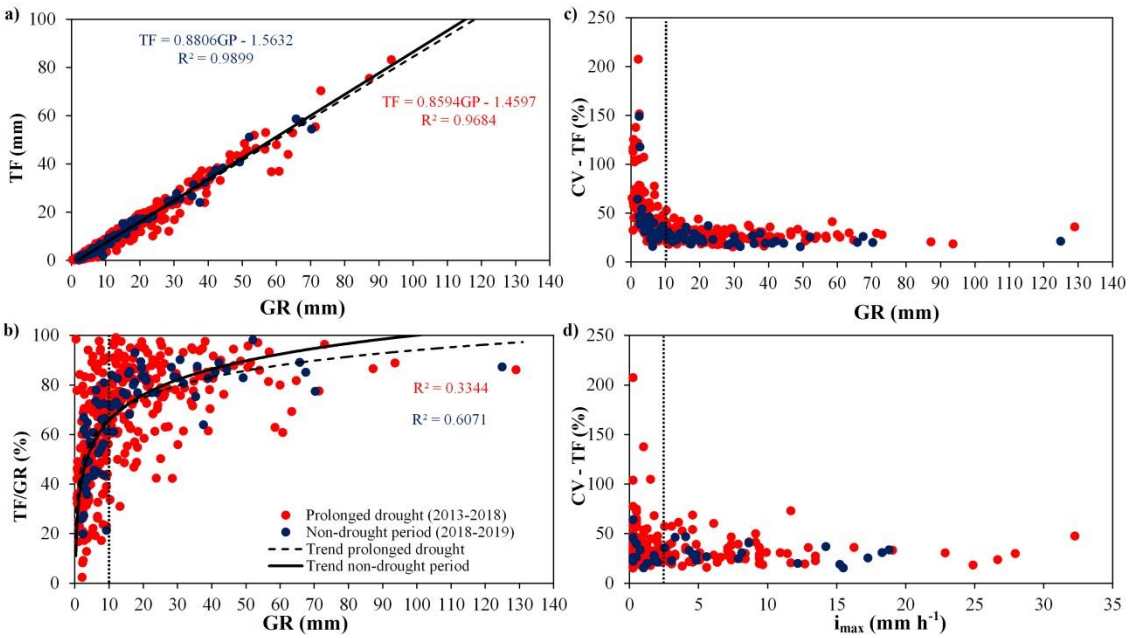

Figure 5. (a) Linear relationship between TF and GR, (b) The ratio of throughfall (TF)

to gross rainfall (GR), (c) relationship beteween throughfall spatial variability (measured by the coefficient of variation (CV)) and gross rainfall, and (d) relationship between throughfall spatial variability and maximum rainfall intensity (i_{max})

Evaporation from canopy interception accounted for an average 22.4% of GR, ranging from 153.4 mm (17.8%) to 333.8 mm (27.7%) in 2013/2014 and 2015/2016, respectively. Canopy evaporation in the prolonged drought added up to 1135 mm, accounting for 21.7% of GR, whereas 287 mm (20.2% of GR) was observed in the non-drought period. As shown in Figure 3a, the range of canopy evaporation was larger in the prolonged drought (0.9% to 97.6%) than in the non-drought periods (1.9% to 80.2%).

3.3 Gross rainfall, period length, and throughfall time stability

The TF spatial variability (represented by the coefficient of variation) decreased up to the threshold of GR = 10 mm and stabilized at CV = 25%, regardless of drought or non-drought condition (Figure 5c), i.e. greater spatial variability occurs for events < 10 mm, even under different climatological conditions (Table S1).

The wet and dry plots were more acute for events below the threshold (GR = 10 mm), whereas MRD_j was closer to 0 for GR > 10 mm (Figures 6 and 7). The greater TF time stability is remarkable for greater amounts of gross rainfall (GR) due to the lower fluctuations of MRD_j (Figure 7). This is confirmed by TSI, which was 0.25±0.09 and 0.49±0.21 when only considering events above and below the threshold (GR = 10 mm), respectively. Overall, the TF spatial pattern is more sensitive to changes in GR for events < 10 mm, since water input to the remnant becomes more homogeneous as long as gross rainfall increases. Plots representing the remnant TF average (MRD < 1%) varied between the study years and rainfall amount. Regarding GR < 10 mm, plots 70,

70, 118, 109, 122, and 65 represented the TF spatial average for 2013/2014, 2014/2015, 2015/2016, 2016/2017, 2017/2018, and 2018/2019 periods, respectively. In contrast, plots 1, 67, 3, 62, 24, 64, and 60 could be used to determine the TF spatial average in 2013/2014, 2014/2015, 2015/2016, 2016/2017, 2017/2018, and 2018/2019, respectively, for GR > 10 mm.

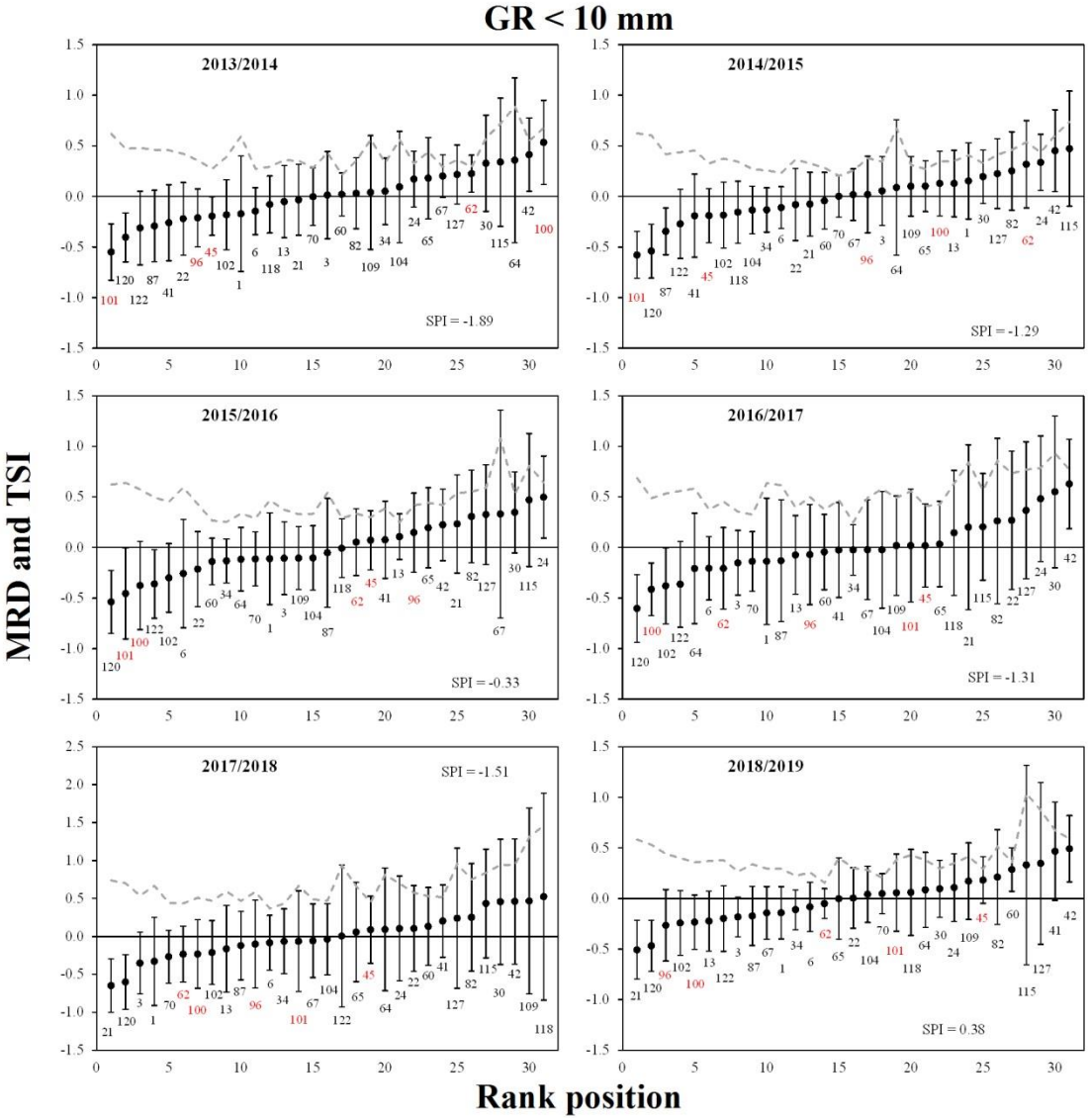

Figure 6. Throughfall time stability regarding gross rainfall (GR) < 10 mm throughout six hydrological years (2013-2019). Temporal stability index (TSI): gray dashed line; mean relative difference (MRD): black dots; standard deviation of MRD ($\sigma_{RD_{ij}}$): vertical bars; SPI: the Standardized Precipitation Index.

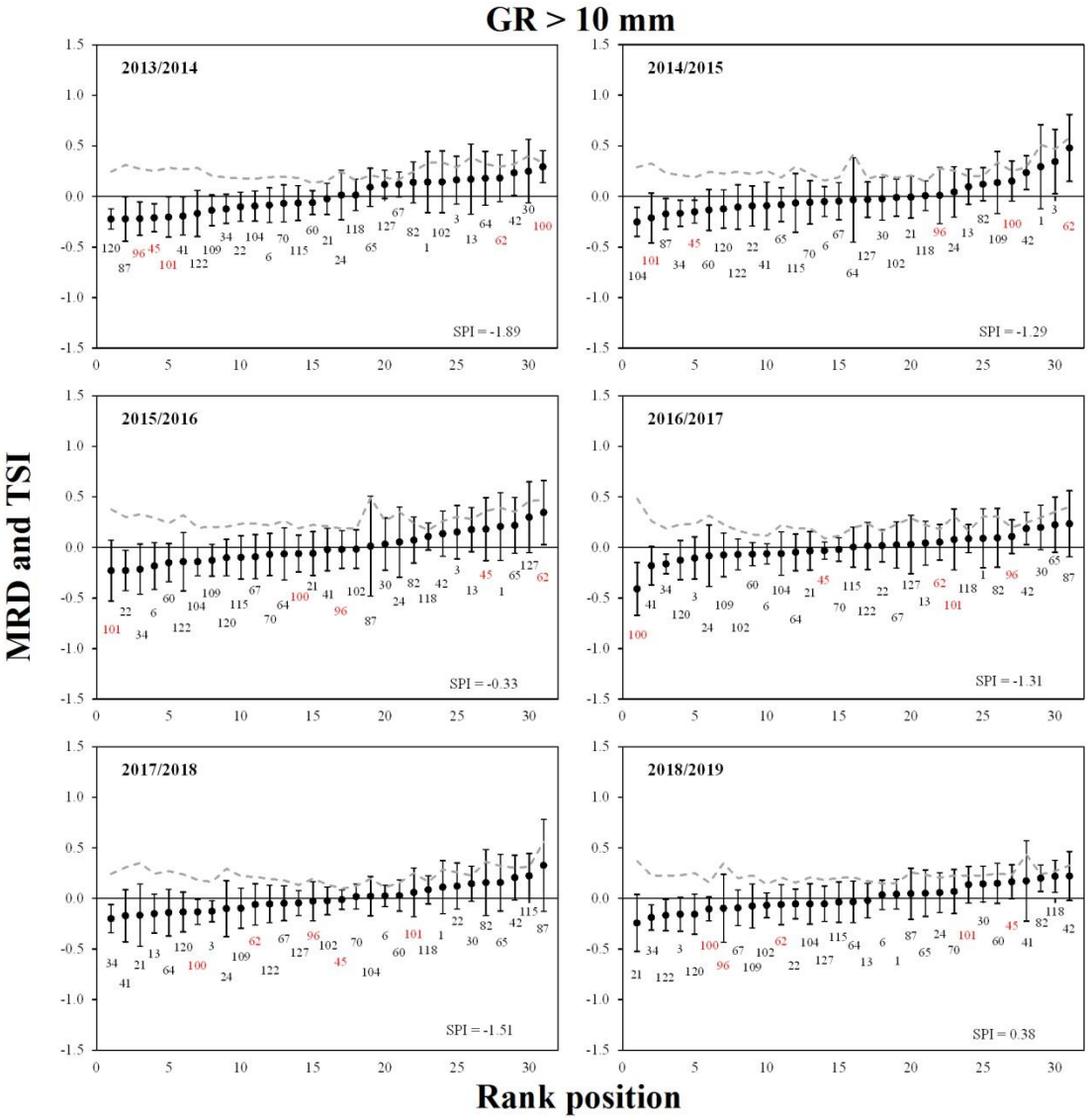

Figure 7. Throughfall time stability regarding gross rainfall (GR) > 10 mm throughout six hydrological years (2013-2019). Temporal stability index (TSI): gray dashed line; mean relative difference (MRD): black dots; standard deviation of MRD ($\sigma_{RD_{ij}}$): vertical bars; SPI: the Standardized Precipitation Index.

Although there were no differences in the metric ranges, the relative positions of the inventory plots changed throughout the hydrological years (Figures 6, 7, and S2). The most drastic changes in the rank position were observed in plots 45, 62, 96, 100, and 101, which changed betweem wet and dry positions. Plots 45, 96, and 101 ranged from 19% (21%), 26% (22%), and 57% (43%) drier to 18% (16%), 14% (5%), and 6%

(9%) wetter than the remnant TF average for GR < 10 mm (for GR > 10 mm). Moreover, plots 62 and 100 ranged from 42% (41%) and 53% (38%) wetter to 15% (15%) and 41% (39%) drier than the TF spatial average for GR < 10 mm (for GR > 10 mm). In contrast, plot 120 was drier than the TF spatial average, while plot 42 was wetter than the TF spatial average, regardless of the measurement time. We also integrated different time periods to verify the influence of the the dataset lengths on the time stability of TF spatial variability. The rank position of the inventory plots changed among the different lengths regardless of the rainfall amount, highlighting different time evolutions of TF spatial variability for the integrated datasets (from two hydrological years to the entire period) (Table 2 and Figures S3 and S4).

Table 2. The driest, wettest, and closest to the spatial average TF plots for different period lengths and gross rainfall (GR).

	2013/ 2014	2014/ 2015	2015/ 2016	2016/ 2017	2017/ 2018	2018/ 2019	2013/ 2015	2015/ 2017	2017/ 2019	2013/ 2016	2016/ 2019	2013/ 2017	2013/ 2019
GR < 10 mm													
Driest plots	101	101	120	120	21	21	101	120	21	101	120	120	120
	120	120	101	100	120	120	120	100	120	120	21	101	101
	60	70	118	34	102	62	60	34	6	60	34	60	34
Average stable plots	-	-	13	-	45	70	70	13	104	70	-	70	70
	-	-	-	-	70	-	-	-	-	-	-	-	45
	42	42	115	30	109	41	115	30	115	24	30	24	115
Wettest plots	100	115	24	42	118	42	42	24	42	115	42	42	42
GR > 10 mm													
	2013/ 2014	2014/ 2015	2015/ 2016	2016/ 2017	2017/ 2018	2018/ 2019	2013/ 2015	2015/ 2017	2017/ 2019	2013/ 2016	2016/ 2019	2013/ 2017	2013/ 2019
Driest plots	101	101	120	120	21	21	101	120	21	101	120	120	120
	120	120	101	100	120	120	120	100	120	120	21	101	101
	60	6	96	45	127	6	60	96	70	70	6	60	70
Average stable plots	21	67	102	70	45	1	70	13	6	118	70	70	45
	-	127	-	6	70	-	-	-	-		-	118	60
	30	3	127	65	115	118	62	127	118	62	30	62	30
Wettest plots	100	62	62	87	87	42	42	42	42	42	42	42	42

3.4 *Rainfall intensity, droughts, and the throughfall time stability*

Regarding the maximum rainfall intensity, the TF spatial variability decreased up to the threshold of i_{max} = 2.5 mm h^{-1} stabilizing at CV = 25% (Figure 5d) in both prolonged drought and non-drought periods, i.e. the greater spatial variability occurs for i_{max} < 2.5 mm h^{-1} in the presence and absence of droughts.

The spatial variability of TF is more time stable in the non-drought than in the prolonged drought period as indicated by the lower fluctuation of MRD_j (Figure 8). This is reinforced by the TSI of 0.30 ± 0.11 and 0.41 ± 0.13 in the non-drought and prolonged drought period, respectively. Regarding the threshold (i_{max} = 2.5 mm h^{-1}), TSI was 0.30 ± 0.13 and 0.29 ± 0.08 for events below and above the threshold in the non-drought period, respectively. A greater instability of the TF spatial variability was observed during lighter (i_{max} < 2.5 mm h^{-1}) than heavier rainfall events in the prolonged drought period indicated by TSI of 0.45 ± 0.12 and 0.37 ± 0.14, respectively. Plots representing the remnant TF average (MRD < 1%) were different regarding rainfall intensity and the presence (or absence) of droughts. For i_{max} < 2.5 mm h^{-1}, plots 21 and 64 (prolonged drought period) and 1 (non-drought period) can be considered as representative of TF spatial average. For i_{max} > 2.5 mm h^{-1}, plots 96 and 1 represented the TF spatial average in the prolonged drought and non-drought periods, respectively.

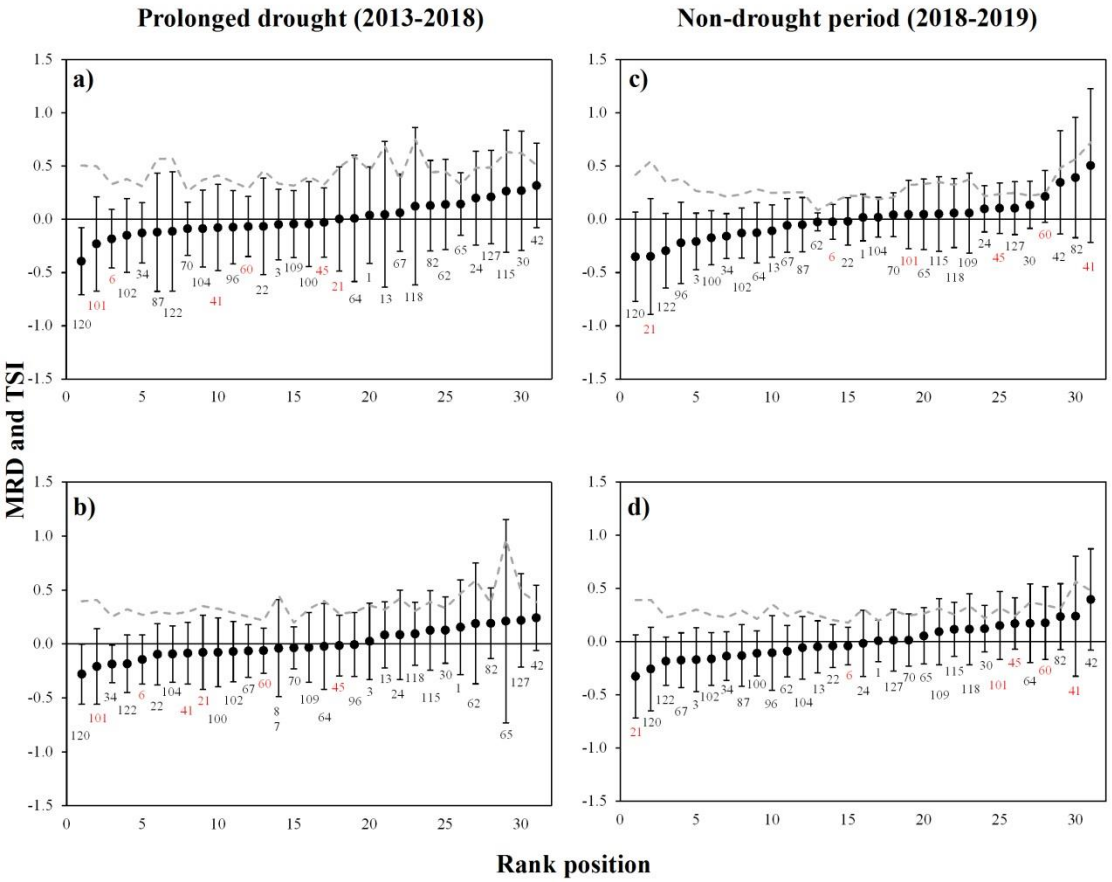

Figure 8. Throughfall time stability regarding maximum rainfall intensity (i_{max}) < 2.5 mm h^{-1} (a, c) and > 2.5 mm h^{-1} (b, d) for the prolonged drought and non-drought periods, respectively. Temporal stability index (TSI): gray dashed line; mean relative difference (MRD): black dots; standard deviation of MRD ($\sigma_{RD_{ij}}$): vertical bars.

The presense (or absence) of droughts defined the relative postions of the plots (Figure 8). Changes in plots 101, 6, 41, 60, 45, and 21 were more relevant because they changed between wet and dry positions when the study period was split into prolonged drought and non-drought periods. For instance, plots 101, 41, 60 and 6 became wetter in the non-drought period, while plot 21 became drier. This pattern was observed for i_{max} < 2.5 mm h^{-1} and > 2.5 mm h^{-1} (Figure 8). Overall, these plots concentrated at drier and wetter positions in the prolonged drought and non-drought periods, respectively, highlighting the influence of rainfall intensity distribution (Figure 4) in the relative spatial distribution of TF

3.5 Forest structure and the throughfall time stability

The PCA with *envifit* selected forest variables correlated with variations in MRD and TSI data. MRD PCA for < 10 mm events only pointed out the number of trees (N10, N15, and N17) as being important for MRD data arrangement (Table S5), whereas MRD PCA for > 10 mm selected the number of trees, the plot mean diameter and the evenness index (N10, N15, N17, DBH10, DBH15, DBH17, and J17) (Table S6). TSI PCA for < 10 mm events pointed out basal area, aboveground biomass, plot mean diameter, diversity and evenness as important for TSI events (G10, G15, G17, CV_DBH10, H10, H15, J10, J15, DBH17, AGB10, AGB15, and AGB17) (Table S7), whereas TSI PCA for >10 events only selected tree occupation/cover variables (DBH10, DBH15, DBH17, G10, G15, G17, AGB10, AGB15, and AGB17) (Table S8).

The redundancy analysis (RDA) highlighted different interactions between forest and rainfall redistribution (MRD) when the threshold (GR = 10 mm) was considered (Figure 9). RDA for GR < 10 mm shows that the first and second axes explained nearly 95% of the constrained variation in the data. Three forest structure variables presented significant ($p < 0.1$) contributions to explain variation in the TF matrix: N-10, N-15, and N-17 with positive correlations to MRD (Figure 9a). RDA for GR > 10 mm demonstrates that the first and second axes explained nearly 79% of the constrained variation in the data. A total of 8 forest structure variables showed significant ($p<0.1$) contributions to explain variation in the TF matrix: N-10, N-15, and N-17, with overall positive correlations to MRD and DBH-10, DBH-15, DBH-17, J-15, and J-17 with negative correlations to MRD (Figure 9b).

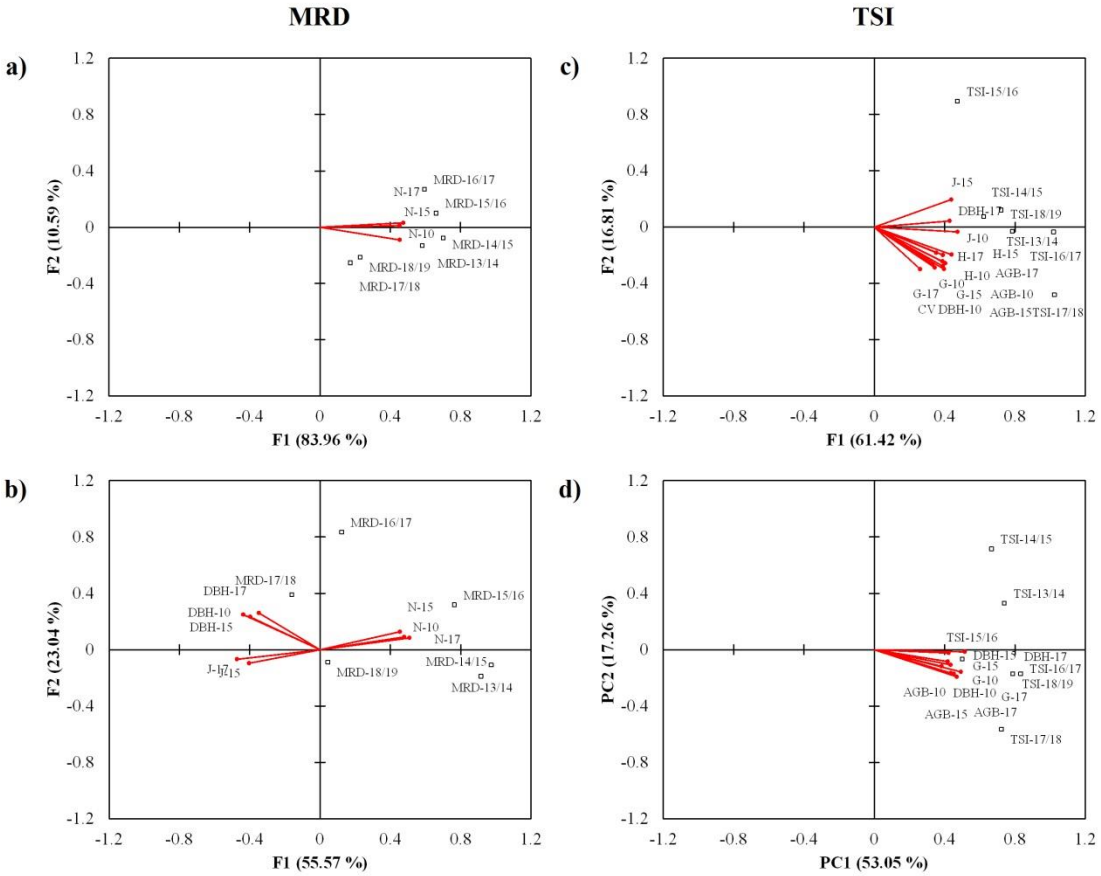

Figure 9. Redundancy analysis (RDA) biplot of throughfall variables (MRD and TSI) constrained by forest structure variables (using three years of data from the Atlantic Forest stand). Red vectors are the significant ($p < 0.1$) forest variables according to the *envfit* function. The RDA was carried out regarding rainfall events < 10 mm (a, c) and > 10 mm (b, d). TSI: time stability index; MRD: mean relative difference.

The RDA showed a different influence of forest structure on the TF time stability regarding TSI. For GR < 10 mm, the first and second axes explained 78.2% of the constrained variation with fourteen variables responsible for such variability: G-10, CVDBH-10, AGB-10, H-10, J-10, G-15, CVDBH-15, AGB-15, H-15, J-15, G-17, DBH-17, AGB-17, and H-17 ($p<0.1$) with positive correlations to TSI. On the other hand, DBH-10, AGB-10, G-10, DBH-15, AGB-15, G-15, DBH-17, AGB-17, and G-17 ($p<0.1$) were responsible for explaining 70.3% of the constraining variation in the two axes with positive correlations to TSI for GR > 10 mm (Figure 9).

4. Discussion

4.1 Canopy-rainfall interactions and the TF spatial variability

Although studies have demonstrated the influence of rainfall intensity and amount in throughfall behavior (Liu et al., 2019; Sheng and Cai, 2021; Su et al., 2019; Zhang et al., 2019; Zhu et al., 2021), we did not find a difference in the CV tendency regardless of the drought intensity (Figure 5c,d). Moreover, the frequency of rainfall events was similar among the study years (Figure S1). This means that the forest structure and architecture determined the spatial variability of throughfall, not the rainfall distribution. For gross rainfall < 10 mm, the canopy is still filling, and water entering the forest is mainly due to the existence of gaps (free throughfall), the formation of some preferential dripping points (Staelens et al., 2006), and drops splashing from the canopy (Levia et al., 2019). As rainfall progresses, the canopy reservoir fills and more water is routed to the forest floor (Carlyle-Moses et al., 2010; Rodrigues et al., 2021a). Spatial variability decreases as long as more dripping points occur and stabilizes for events higher than 10 mm (CV ~ 25%) when the canopy is saturated and the water drains into all dripping pathways (Allen et al., 2013; Fathizadeh et al., 2014).

The same pattern was observed in other forest worldwide (Sheng and Cai, 2021; Staelens et al., 2006; Su et al., 2019; Zhu et al., 2021), only differing by the threshold and the stable CV (Table S2). For instance, Fan et al. (2015) observed a threshold of 20 mm in a pine forest, decreasing to a stable CV of 16.5%. In a mixed deciduous forest, Staelens et al. (2006) observed a threshold of 10 mm and a stable CV of 19% and 11% for the leafed and leafless periods, respectively. Sheng and Cai (2021), Zhu et al.

(2021), and Su et al. (2019) observed a stable CV of ~20% in a boreal, semi-arid mountain forests, and mixed evergreen-deciduous broadleaved forests, respectively. The greater stable CV value (25%) observed in the Atlantic Forest remnant may be due to its higher species diversity and stratified canopy (Terra et al., 2018a), which create different zones for throughfall (Carlyle-Moses and Lishman, 2015). Moreover, the greater stable CV value could also be a consequence of the non-roving approach used in this study, since roving rain gauges (after each rainfall event) may decrease the throughfall spatial variability (Fan et al., 2015). However, Junqueira Junior et al. (2019) and Rodrigues et al. (2021a) confirmed the adequacy of the spatial distribution of rain gauges to represent the TF spatial variability in the forest remnant. Therefore, the more noticeable CV value can be related to the complexity of the Atlantic Forest remnant.

The increase in TF/GR ratio supports the assumptions about the formation of more drainage pathways as the canopy gets fuller, increasing the transformation of GR into TF up to a stable ratio of ~82% (Figure 5b). Although TF linearly increases with GR (Figure 5a), the TF/GR stabilization indicates that the canopy has reached its maximum drainage capacity. Beyond this point, no more drainage pathways are formed and the water entering the forest as TF is a function of the maximum drainage capacity, the canopy openness, and the weather conditions. Therefore, the canopy-rainfall interactions are minimized and the observed variability is mainly due to atmosphere dynamics rather than forest structure for GR > 10 mm.

TF/GR variability is driven by canopy evaporation, which is a function of the available energy during and between events (Rodrigues et al., 2021a). Rodrigues et al. (2021a) called attention to the importance of the energy stored in biomass and air within the Atlantic Forest remnant in both drought and non-drought conditions. However, external energy arrives by advection and increases canopy evaporation during droughts

(Rodrigues et al., 2021a), which explains the differences in the TF/GP fluctuations between the two analyzed periods (Figure 5b). This fluctuation can also partly be explained by the semi-deciduous characteristic of the Atlantic Forest remnant (Oliveira-Filho and Fontes, 2000) due to the natural leaf loss seasonality, which is intensified during prolonged droughts (Rodrigues et al., 2021b). Furthermore, wind direction and intensity contribute to the increase in variability through the rain-shadow phenomenon (Fan et al., 2015). Although evaporation, leaf shedding, and wind patterns are important in the variability of TF/GR for events < 10 mm, the acuteness of the increase on the TF/GR ratio is mainly due to canopy filling, which leads to new dripping points and the greater contribution of TF (Figure 5b).

4.2 Influence of forest structure on the time stability of TF spatial variability

The redundancy analysis of MRD (Figure 9) pointed out the forest characteristics that drive the overall TF spatial distribution in the study period (2013-2019), highlighting the characteristics which improve water input. More populated plots (i.e. plots with a higher number of trees) in our study area input more water to the forest, regardless of the rainfall amount (Figure 9). Plots with higher numbers of individuals usually indicate those that are recovering from a disturbance (i.e. gaps created by fallen trees), and therefore have higher densities of young trees (Martins et al., 2004; Oliveira-Filho et al., 1997). Reduced canopy interception is observed in young trees due to their small crown (Terra et al., 2018a; Wullaert et al., 2009), funnel-shaped branches (Germer et al., 2006; Su et al., 2019), and greater canopy openness (Martins et al., 2004).

For GR > 10 mm, the higher dominance of certain tree species (lower J values) also increases throughfall (Figure 9). Tree species in tropical forests show a wide range

of anatomic and architectural traits (Poorter et al., 2006), which can either boost rainfall interception (Terra et al., 2018a) or increase throughfall. Therefore, plots with greater water inputs via throughfall are probably dominated by species with improved drainage capacity. Moreover, higher mean tree diameter (in 2010, 2015, and 2017) had a negative effect on throughfall for GR > 10 mm (Figure 9). This is expected, since the more trees there are per area in tropical forests, the thinner they tend to be (Hallé et al.,1978; Ngueguim et al., 2018).

The greater rainfall-canopy interaction before saturation (GR < 10 mm) highlights the effect of canopy openness for TF since free throughfall is more relevant in events with lower rainfall amounts (Staelens et al., 2006). The importance of canopy openness for TF decreased in large events as also observed by Zimmerman et al. (2009). Therefore, the canopy drainage capacity becomes more relevant than the rainfall-canopy interaction to spatially distribute throughfall after canopy saturation. This is reinforced by the importance assigned to tree species (Figure 9), which points out the species-specific characteristics that improves canopy drainage (Levia and Frost, 2006). This information can support decisions toward reforestation by selecting tree species that increase water input.

Forest structure and architecture drive the time stability of TF spatial variability in the Atlantic Forest remnant, as indicated by the RDA plot considering the TSI (Figure 9). Regardless of the gross rainfall amount (< 10 mm or > 10 mm), the larger the area occupied by the tree boles in a plot (as indicated by AGB and G), the less time stable the plot was. This means that throughfall time stable conditions are related to lesser biomass per area. The biomass of the Atlantic Forest remnant is increasing as it moves toward an advanced successional stage (Souza et al., 2021). This is likely the explanation for the importance assigned to DBH, because the temporal increase in

biomass was greatest in the large diameters classes in the study remnant (Souza et al., 2021), which is consistent with the abovementioned importance of tree occupation for TF time instability.

In contrast, the importance of H and J for GR < 10 mm can be attached to the onset of new dripping points, which increases the time instability of TF spatial distribution. Since tropical forests have a wide range of species with different canopy storage capacity, leaf properties (such as shape, orientation, and texture), branch architecture, canopy structure and hydrophobicity, and bark roughness (Levia and Frost, 2006; Nanko et al., 2014; Poorter et al., 2006; Terra et al., 2018a), the diversity and dominance of certain species provide a distinct time for starting canopy drainage (Allen et al., 2013). This condition, in combination with varying rainfall amounts, resulted in a variety of spatial configurations of dripping pathways since forest canopy is unsaturated when GR < 10 mm. These different configurations of dripping points decreased TF time stability, i.e. TF spatial variability was unstable for GR < 10 mm. This is confirmed by the non-significance of H and J in the RDA for GR > 10 mm. Beyond this rainfall amount, all dripping points had already started, homogenizing the time evolution of the TF spatial distribution.

RDA highlights linear relationships between explanatory and response variables (ter Braak and Looman, 1994) and some cautions should be taken when dealing with rainfall partitioning. The canopy is a complex environment due to the heterogeneity of species, leaf characteristics, branch angulation, water storage capacity, and seasonality (leaf shedding in the dry period), among others. The association of the abovementioned characteristics can lead to non-linear responses, which cannot be observed using RDA (Legendre et al., 2011; ter Braak and Looman, 1994). Therefore, some connections and potential drivers of the throughfall spatial distribution could have been left out.

However, RDA was used as an exploratory analysis to shed light on the importance of considering forest dynamics when dealing with the throughfall time stability. The results of this study will supplement future studies on forest hydrology and point to the need for considering forest dynamics and weather conditions. Future works should also increase the time resolution of the measured forest structure variables (to track inter-season variation) and implement scanning technologies (such as LiDar) for a 3D characterization of the canopy.

4.3 Influence of rainfall intensity on the time stability of TF spatial variability

The different distribution of the maximum rainfall intensity between the non-drought and prolonged drought periods (Figure 4) affected the time stability of the TF spatial variability (Figure 8). The TF spatial variability was less time stable in the prolonged drought period, in which a greater variability of i_{max} (CV = 141%) was observed. This instability increased even more for rainfall events with $i_{max} < 2.5$ mm h^{-1} (Figure 8). Canopy-rainfall interactions are greater (Figure 5d) for light events because they can either saturate or unsaturate the canopy. Long events with low intensity saturate the canopy, activate all dripping pathways (as previously stated), and decrease the TF spatial variability. Conversely, unsaturation is likely to occur in short events with low intensity (Yan et al., 2021). Different spatial configurations of dripping pathways are formed depending on the rainfall amount, intensity, and duration. This drives the throughfall redistribution in each event, changing the spatial distribution over time (Figure 8). Therefore, more unstable time conditions can be expected as long as droughts, with a concentration of light events, become more frequent.

The TF spatial variability was more time stable for $i_{max} > 2.5$ mm h^{-1}. Intense events have greater kinetic energy, which reduces canopy storage capacity (Calder et

al., 1996) and increases TF (Yan et al., 2021), i.e. the canopy is easily saturated in these events. The TF spatial variability tends to homogenize with greater TF (Figure 5d), decreasing TSI (Figure 8). However, greater TSI values were observed during the prolonged drought period. This was likely due to the occurrence of heavier events since the i_{max} was limited to 20 mm h^{-1} in the non-drought period (Figure 4). Higher rainfall intensities splash more water from the canopy (Nanko et al., 2006), which can either be recaptured or become throughfall, depending on the canopy thickness (Nanko et al., 2008). More splashes from the canopy added to the diversity of canopy structures (Terra et al., 2018a) increased the TF spatial variability in the Atlantic Forest remnant during the prolonged drought period. However, the relative contribution of each throughfall type (free, drip, and splash) in the time stability needs further investigation. For instance, the formation of splash throughfall is greater at the onset of events (Levia et al., 2019) and its random distribution likely increases spatial variability. Therefore, future studies dealing with diverse and dynamic environments (as in tropical forests) should consider partitioning throughfall (as well as their respective size and volume) because it is another source of spatial variability that can affect the time stability of throughfall (Levia et al., 2019, 2017; Nanko et al., 2016).

4.4 Forest-drought feedback and TF time stability

Long-term meteorological droughts can affect forest structure, function, and ecosystem services by leading to higher individual tree loss and lower tree growth, ultimately reducing forest productivity (Anderegg et al., 2013). The duration and aggressiveness of such events influence water and soil nutrient availability and consequently change structure and composition of the forest (He and Dijkstra, 2014). Trees are long-lived organisms, and so they are expected to be more vulnerable to rapid changes in climate (Brodribb et al., 2020).

The Atlantic Forest remnant where our study was conducted is adapted to climate seasonality, and therefore to a certain level of periodic drought (Souza et al., 2021). However, the region went through various stages of abnormal drought during 2013-2019 (Figure 3), which certainly impacted its structural dynamics. Although the remnant has been reported to show a long term increase in biomass, decreasing tree density and increasing abundance of late-successional plants, which are indicators of the late-successional stage due to protection (Souza et al., 2021), we observed a strong increase in the loss of trees along with basal area (negative net change) in the 2015-2017 interval (Figure 10). This may have been intensified by drought conditions, corroborating previous studies on forest changes under severe and long droughts (Berenguer et al., 2021; Phillips et al., 2009). These changes in the forest structure have the potential to modify the inputs of water because the TF spatial variability is connected to forest structure, as previously highlighted (Figure 9). Therefore, the time stability of the TF spatial variability disappears as long as the lengths of the monitoring period extends, because the longer the monitoring period, the higher the probability that natural changes in forest structure will affect the spatial distribution of TF.

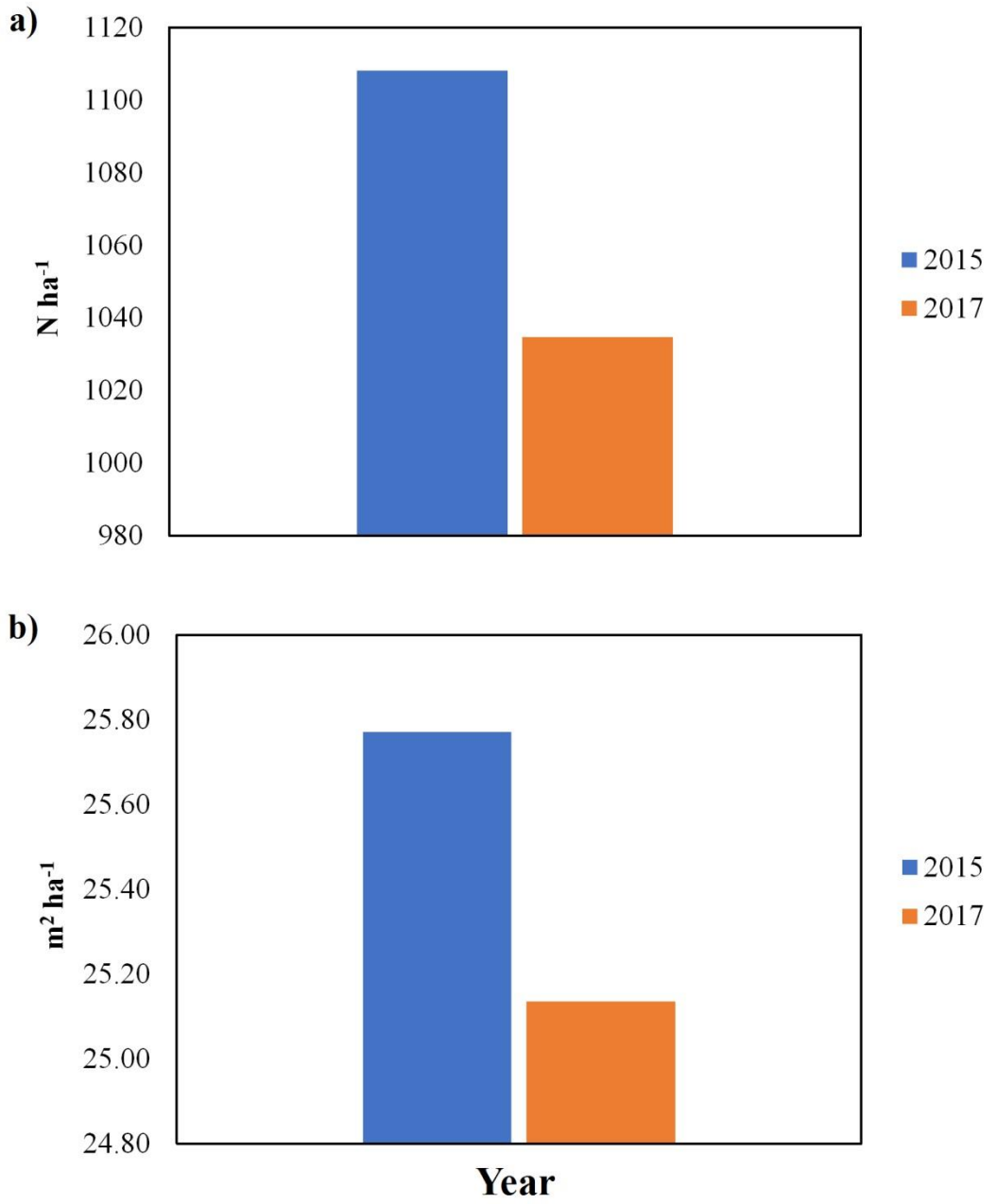

Figure 10. The number of individuals and basal area calculated based on the forest inventory of the years of 2015 and 2017.

The influence of the different study periods (and the length of the periods) is in accordance with the abovementioned changes in the TF spatial variability. Different configurations of the rank positions highlighted the changes in the TF spatial variability as long as the monitoring period was modified (Table 2 and Figures S3 and S4), i.e. this claims that TF time stable conditions are unfeasible in a dynamic environment because

the TF spatial distribution changes over time. Moreover, attention must be paid to the feedback effects of forest moisture stress on climate change. The more forests dry up, the more likely they are to accelerate climate change through carbon losses and changing surface energy balances (Phillips et al., 2009). Climate scenarios for the study area indicate that extreme weather events will increase in the future, making longer dry periods more likely (Nehren et al. 2019). In turn, paleoenvironmental studies show that changes in precipitation patterns during the Late Quaternary have repeatedly led to shifts in the transition zone between the Cerrado and the Atlantic Forest biomes, and that even small changes in water balance affect the fragile ecological balance (Kirchner et al. 2015). Future studies could also track possible changes in species composition in face of such events, as an increase in abundance of drought-tolerant species is likely to happen (Esquivel-Muelbert et al., 2018).

4.5 Misinterpretation of throughfall time stability in previous studies

Throughfall time stability is related to forest structure and architecture (Figure 6), and therefore changes in the forest configuration modify the spatial distribution of throughfall. Three main factors are able to modify the forest structure: (i) anthropogenic activities (i.e. logging and fire); (ii) ecological succession (i.e. gaps created by falling trees and differences in forest structure in forest edge *versus* forest interior); and (iii) natural disturbances (i.e. droughts). The investigated Atlantic Forest remnant is in an advanced successional stage and has been under protection since 1986 (Souza et al., 2021), which means that some throughfall instability, as indicated by the variability in the rank position throughout the years (Figure 6 and 7), is due to natural changes in the forest structure over time. These changes may be exacerbated by prolonged drought

conditions that the forest has experienced (Figure 3), which could have increased both tree mortality and biomass losses in the past years (Figure 10). Such behavior questions the previous statement of TF time stability and precludes the definition of a specific position to represent the remnant average TF (Vachaud et al., 1985), as claimed by most of the published studies (Table S2). In this regard, claiming throughfall time stability without considering structural changes can lead to misinterpretation.

Several studies have argued about the throughfall time stability in different types of forests around the world, indicating positions which could be used to monitor the throughfall spatial average (Table S2). Moreover, the importance of weather characteristics (e.g., rainfall intensity, duration and amount, and wind speed) on throughfall time stability (Liu et al., 2019; Zhang et al., 2019; Zhu et al., 2021) have also been highlighted. However, canopy structure has been recognized to be more important than weather characteristics for throughfall spatial and temporal dynamics (Nanko et al., 2016; Sheng and Cai, 2021; Staelens et al., 2006; Wullaert et al., 2009). The significance has already been linked to leafed and leafless periods (or growing and dormant periods) because a shift in the spatial distribution was observed when both periods were evaluated separately (Staelens et al., 2006; Zimmermann et al., 2008). Since the hydrological year scale encompasses wet and dry periods, some instability in the spatial variability of throughfall (Figures 6 and 7) can be attached to the semi-deciduousness of the Atlantic Forest stand.

However, most studies consider a short monitoring period, such as a season or just one hydrological year, whereas longer studies (> 4 years) are scarce (Table S2). Because the response to drought conditions is delayed (see Forest-drought feedbacks and the TF time stability topic), significant changes in the forest structure (and canopy composition) were not ascertained in the studies with short monitoring periods. Even

forests which have not faced stressful droughts, short periods were also unable to account for forest succession. This caused a false impression of throughfall time stability for different time intervals and period lengths (Table 2 and Figures S2, S3, and S4). Future studies should apply temporal variograms to appraise the period length that the time stability of throughfall persists (Zimmermann et al., 2009). This approach will highlight the maximum period length in which throughfall time stability could be considered without the risk of misinterpretation. Moreover, it will also provide insights into throughfall spatial variability between different time intervals (Zimmermann et al., 2009).

Most studies did not split the events (i.e. GR > 10 mm and < 10 mm) before assessing the throughfall time stability. The canopy-rainfall interaction is greater for GR < 10 mm as a consequence of rainfall amount and formation of dripping points, causing instability in the throughfall spatial variability. When all events are put together to account for time stable positions, the abovementioned interactions are smoothed due to events > 10 mm, homogenizing the water inputs within the forest (Figures 5c, 6, and 7). Zimmermann and Zimmermann (2014) pointed out increased relative errors (> 40%) in the mean throughfall estimates for small events due to a greater canopy-rainfall interaction in heterogeneous forests (such as tropical forests). These authors recommended boosting the number of gauges to decrease throughfall uncertainty, mainly when dealing with small events. Therefore, beyond the abovementioned importance of splitting the analyses into saturated (GR >10 mm) and unsaturated (GR < 10 mm) canopy for a correct assessment of time stability, we recommend future studies to improve their monitoring set according to Zimmermann and Zimmermann (2014). Incorrect accounting for the throughfall spatial variability is another source of

uncertainty in defining time stable positions, mainly regarding small events in tropical forests.

Additional precautions should be taken as long as drier years become more frequent and intense. More instability of the TF spatial variability can be expected during droughts due to the greater variability of maximum rainfall intensity (as highlighted by the greater coefficient of variation) and presence of lighter events (Figure 4). Light events create canopy saturation and unsaturation episodes, increasing the time instability of the throughfall spatial variability. This instability is also due to the decreased canopy storage capacity and increased splash throughfall as a consequence of heavier events (i_{max} > 20 mm h^{-1}). Therefore, indicating overall stable positions will become even harder during droughts.

5. Conclusion

The throughfall spatial variability decreased with gross rainfall amount because a greater canopy-rainfall interaction occurred prior to canopy saturation (GR < 10 mm). The different spatial configuration of dripping points, which depends on rainfall amount and specie-specific characteristics, added to the greater importance of canopy openness (free throughfall is more relevant in events with lower rainfall amounts), increased the temporal changes of the spatial distribution before canopy saturation (i.e. throughfall is more time instable for small events). Forest structure also demonstrated importance for the throughfall spatial variability after canopy saturation, highlighting species which either booster rainfall interception (drier plots) or improve canopy drainage (wetter plots). However, tropical forests are in constant development, either ecologically succeeding or adaptating to natural/anthropogenic disturbances (e.g., droughts, logging,

and fire). This development changes forest structure, and therefore the throughfall time stability, i.e. defining time stable positions is not straightforward because the throughfall spatial distribution changes with forest dynamics, as highlighted by the differences in the time stable positions for different periods lengths. These results can only be tracked by long monitoring periods and claiming time stability in shorter periods (one year or less) can lead to misinterpretation.

The throughfall spatial variability was less time stable in the prolonged drought period than in the non-drought period. The greater concentration of events with light intensities and the presence of more extreme events (heavy intensities > 20 mm h^{-1}) are responsible for increasing time instability. Light events can either saturate or unsaturate the canopy depending on their duration (long or short events). This creates different spatial configurations of throughfall distribution, affecting the spatial variability over time. Moreover, the heavier the event, the lower the storage capacity of the canopy and the greater the amount of splash throughfall formed. This increases the throughfall input and the randomness of the spatial distribution. In a climate change scenario where droughts become more intense and frequent, more throughfall time instability can be expected as long as the observed distribution of rainfall intensities (in the prolonged drought) is maintained.

Future works should consider the effects of droughts and forest dynamics on throughfall time stability. Considering the abovementioned issues will prevent misinterpreting time stability and provide a more precise definition of time stable positions.

Funding: This work was supported by the Improvement of Higher Educational Personnel – CAPES [grant number 88882.306661/2018-01]; and FAPEMIG [grant number PPMX-545/18].

6. References

Allen, S.T., Brooks, J.R., Keim, R.F., Bond, B.J., Mcdonnell, J.J., 2013. The role of pre-event canopy storage in throughfall and stemflow by using isotopic tracers. Ecohydrology 7, 858–868. https://doi.org/10.1002/eco.1408

Anderegg, W. R. L., Trugman, A. T., Badgley, G., Anderson, C. M., Bartuska, A., Ciais, P., Cullenward, D., Field, C. B., Freeman, J., Goetz, S. J., Hicke, J. A., Huntzinger, D., Jackson, R. B., Nickerson, J., Pacala, S., Randerson, J. T., 2020. Climate-driven risks to the climate mitigation porential of forests. Science 368, 1-9. https://doi.org/10.1126/science.aaz7005

Anderegg, W.R.L., Kane, J.M., Anderegg, D.L., 2013. Consequences of widespread tree mortality triggered by drought and temperature stress. Nat. Clim. Chang. 3, 30–36. https://doi.org/10.1038/NCLIMATE1635

Anderson, T.W., Darling, D.A., 1954. A Test of Goodness of Fit. J. Am. Stat. Assoc. 49, 765–769.

Anderson, T.W., Darling, D.A., 1952. Asymptotic theory of certain “goodness of fit” criteria based on stochastic processes. Ann. Math. Stat. 23, 193–212. https://doi.org/10.1214/aoms/1177733256

Aubry-kientz, M., Dutrieux, R., Ferraz, A., Saatchi, S., Hamraz, H., Williams, J.,

Coomes, D., Piboule, A., Vincent, G., 2019. A comparative assessment of the performance of individual tree crowns delineation algorithms from ALS data in tropical forests. Remote Sens. 11, 1–21. https://doi.org/10.3390/rs11091086

Berenguer, E., Lennox, G.D., Ferreira, J., Malhi, Y., Aragão, L.E.O.C., Barreto, J.R., Espírito-Santo, F.D.B., Figueiredo, A.E.S., França, F., Gardner, T.A., Joly, C.A., Palmeira, A.F., Quesada, C.A., Rossi, L.C., Seixas, M.M.M., Smith, C.C., Witney, K., Barlow, J., 2021. Tracking the impacts of El Niño drought and fire in human-modified Amazonian forests. PNAS 119, 1–8. https://doi.org/10.1073/pnas.2019377118

BFG - Brazil Flora Group, 2021. Brazilian Flora 2020 project - Projeto Flora do Brasil 2020. v393.274. Instituto de Pesquisas Jardim Botanico do Rio de Janeiro. Dataset/Checklist. https://doi.org/10.15468/1mtkaw

Bialkowski, R., Buttle, J.M., 2015. Stemflow and throughfall contributions to soil water recharge under trees with differing branch architectures. Hydrol. Process. 29, 4068–4082. https://doi.org/10.1002/hyp.10463

Brodribb, T.J., Powers, J., Cochard, H., Choat, B., 2020. Hanging by a thread? Forests and drought. Science 368, 261–266. https://doi.org/10.1126/science.aat7631

Calder, I.R., Hall, R.L., Rosier, P.T.W., Bastable, H.G., Prasanna, K.T., 1996. Dependence of rainfall interception on drop size: 2. Experimental determination of the wetting functions and two-layer stochastic model parameters for five tropical species. J. Hydrol. 185, 379–388.

Carlyle-Moses, D.E., Lishman, C.E., 2015. Temporal persistence of throughfall heterogeneity below and between the canopies of juvenile lodgepole pine (Pinus

contorta). Hydrol. Process. 29, 4051–4067. https://doi.org/10.1002/hyp.10494

Carlyle-Moses, D.E., Park, A.D., Cameron, J.L., 2010. Modelling rainfall interception loss in forest restoration trials in Panama. Ecohydrology 3, 272–283. https://doi.org/10.1002/eco

Chave, J., Réjou-Méchain, M., Búrquez, A., Chidumayo, E., Colgan, M.S., Delliti, W.B.C., Duque, A., Eid, T., Fearnside, P.M., Goodman, R.C., Henry, M., Martínez-Yrízar, A., Mugasha, W.A., Muller-Landau, H.C., Mencuccini, M., Nelson, B.W., Ngomanda, A., Nogueira, E.M., Ortiz-Malavassi, E., Pélissier, R., Ploton, P., Ryan, C.M., Saldarriaga, J.G., Vieilledent, G., 2014. Improved allometric models to estimate the aboveground biomass of tropical trees. Glob. Chang. Biol. 20, 1–14. https://doi.org/10.1111/gcb.12629

Choat, B., Brodribb, T.J., Brodersen, C.R., Duursma, R.A., López, R., Medlyn, B.E., 2018. Triggers of tree mortality under drought. Nature 558, 531-539. https://doi.org/10.1038/s41586-018-0240-x

Coelho, C.A.S., Oliveira, C.P., Ambrizzi, T., Reboita, M.S., Carpenedo, C.B., Campos, J.L.P.S., Tomaziello, A.C.N., Pampuch, L.A., Custódio, M.S., Dutra, L.M.M., Rocha, R.P., Rehbein, A., 2016. The 2014 southeast Brazil austral summer drought: regional scale mechanisms and teleconnections. Clim. Dyn. 46, 3737–3752. https://doi.org/10.1007/s00382-015-2800-1

Crockford, R.H., Richardson, D.P., 2000. Partitioning of rainfall into throughfall, stemflow and interception: effect of forest type, ground cover and climate. Hydrol. Process. 14, 2903–2920. https://doi.org/10.1002/1099-1085(200011/12)14:16/17<2903::AID-HYP126>3.0.CO;2-6

Dean, W., 1995. A Ferro e Fogo: a história e a devastação da Mata Atlântica Brasileira, first ed. Schwarcz Ltda., São Paulo.

Ellison, D., Morris, C.E., Locatelli, B., Sheil, D., Cohen, J., Murdiyarso, D., Gutierrez, V., Noordwijk, M. van, Creed, I.F., Pokorny, J., Gaveau, D., Spracklen, D. V., Tobella, A.B., Ilstedt, U., Teuling, A.J., Gebrehiwot, S.G., Sands, D.C., Muys, B., Verbist, B., Springgay, E., Sugandi, Y., Sullivan, C.A., 2017. Trees, forests and water: cool insights for a hot world. Glob. Environ. Chang. 43, 51–61. https://doi.org/10.1016/j.gloenvcha.2017.01.002

Esquivel-Muelbert, A., Baker, T.R., Dexter, K.G., Lewis, S.L., Brienen, R.J.W., Feldpausch, T.R., Lloyd, J., Monteagudo-Mendoza, A., Arroyo, L., Álvarez-Dávila, E., Higuchi, N., Marimon, B.S., Marimon-Junior, B.H., Vilanova, E., Gloor, E., Malhi, J.C., Barlow, J., Bonal, D., Cardozo, N.D., Erwin, T., Fauset, S., Hérault, B., Laurance, S., Poorter, L., Qie, L., Stahl, C., Sullivan, M.J.P., ter Steege, H., Vos, V.A., Zuidema, P.A., Almeida, E., Oliveira, E.A., Andrade, A., Vieira, S.A., Aragão, L., Araujo-Murakami, A., Arets, E., Aymard, G.A., Baraloto, C., Camargo, P.B., Barroso, J.G., Bongers, F., Boot, R., Camargo, J.L., Castro, W., Moscoso, V.C., Comiskey, J., Valverde, F.C., Costa, A.C.L., Pasquel, J.A., Fiore, A.D., Duque, L.F., Elias, F., Engel, J., Llampazo, G.F., Galbraith, D., Fernández, R.H., Coronado, E.H., Hubau, W., Jimenez-Rojas, E., Lima, A.J.N., Umetsu, R. K., Laurance, W., Lopez-Gonzales, G., Lovejoy, T., Cruz, O.A.M., Morandi, P.S., Neill, D., Vargas, P.N., Camacho, N.C.P., Gutierrez, A.P., Pardo, G., Peacock, J., Peña-Claros, M., Peñuela-Mora, M.C., Petronelli, P., Pickavance, G.C., Pitman, N., Prieto, A., Quesana, C., Ramírez-Angulo, H., Réjou-Méchain, M., Correa, Z.R., Roopsind, A., Rudas, A., Salomão, R., Silva, N., Espejo, J.S., Singh, J., Stropp, J., Terborgh, J., Thomas, R., Toledo, M., Torrez-Lezama, A., Gamarra,

L.V., Meer, P.J., Heijden, G., Hout, P., Martinez, R.V., Vela, C., Vieira, I.C.G., Phillips, O.L., 2018. Compositional response of Amazon forests to climate change. Glob. Chang. Biol. 25, 39–56. https://doi.org/10.1111/gcb.14413

Fan, J., Oestergaard, K.T., Guyot, A., Jensen, D.G., Lockington, D.A., 2015. Spatial variability of throughfall and stemflow in an exotic pine plantation of subtropical coastal Australia. Hydrol. Process. 29, 793–804. https://doi.org/10.1002/hyp.10193

Fathizadeh, O., Attarod, P., Keim, R.F., Stein, A., Amiri, G.Z., Darvishsefat, A.A., 2014. Spatial heterogeneity and temporal stability of throughfall under individual Quercus brantii trees. Hydrol. Process. 28, 1124–1136. https://doi.org/10.1002/hyp.9638

Germer, S., Elsenbeer, H., Moraes, J.M., 2006. Throughfall and temporal trends of rainfall redistribution in an open tropical rainforest, south-western Amazonia (Rondônia, Brazil). Hydrol. Earth Syst. Sci. 10, 383–393. https://doi.org/10.5194/hess-10-383-2006

Guan, K., Wolf, A., Medvigy, D., Caylor, K.K., Pan, M., Wood, E.F., 2013. Seasonal coupling of canopy structure and function in African tropical forests and its environmental controls. Ecosphere 4, 1–21. https://doi.org/10.1890/ES12-00232.1

Guo L., Mount G., Hudson S., Lin H., Levia D., 2020. Pairing geophysical techniques improves understanding of the near-surface Critical Zone: visualization and confirmation of preferential routing of stemflow along coarse roots. Geoderma 357, 1-12. https://doi.org/10.1016/j.geoderma.2019.113953

Guswa, A.J., Spence, C.M., 2011. Effect of throughfall variability on recharge: application to hemlock and deciduous forests in western Massachusetts.

Ecohydrology 5, 563-574. https://doi.org/10.1002/eco.281

Hallé, F., Oldeman, R.A.A., Tomlinson, P.B., 1978. Tropical Trees and Forests: An Architectural Analysis, first ed. Springer, Berlin.

He, M., Dijkstra, F.A., 2014. Drought effect on plant nitrogen and phosphorus: a meta-analysis. New Phytol. 204, 924–931. https://doi.org/10.1111/nph.12952

Helman, D., Lensky, I.M., Yakir, D., Osem, Y., 2017. Forests growing under dry conditions have higher hydrological resilience to drought than do more humid forests. Glob. Chang. Biol. 23, 2801–2817. https://doi.org/10.1111/gcb.13551

Hoshiyar, A., Kiers, H.A.L., Gertheiss, J., 2021. Penalized non-linear principal component analysis for ordinal variables with an application to international classification of functioning core sets. arXiv:2110.02805v1.

Hotelling, H., 1933. Analysis of complex of statistical variables into principal components. J. Educ. Psychol. 24, 417–441. https://doi.org/10.1037/h0071325

Jolliffe, I.T., 1973. Discarding variables in a principal component analysis. II: Real data. J. R. Stat. Soc. 22, 21–31. https://doi.org/10.2307/2346300

Joly, C.A., Metzger, J.P., Tabarelli, M., 2014. Experiences from the Brazilian Atlantic Forest: ecological findings and conservation initiatives. New Phytol. 204, 459–473. https://doi.org/10.1111/nph.12989

Junqueira, R., Viola, M.R., Amorim, J.S., Mello, C.R., 2020. Hydrological response to drought occurences in a Brazilian Savanna basin. Water 9, 1 – 11. https://doi.org/10.3390/resources9100123

Junqueira Junior, J.A., Mello, C.R., Mello, J.M., Scolforo, H.F., Beskow, S., McCarter,

J., 2019. Rainfall partitioning measurement and rainfall interception modelling in a tropical semi-deciduous Atlantic forest remnant. Agric. For. Meteorol. 275, 170–183. https://doi.org/10.1016/j.agrformet.2019.05.016

Junqueira Junior, J.A., Mello, C.R., Owens, P.R., Mello, J.M., Curi, N., Alves, G.J., 2017. Time-stability of soil water content (SWC) in an Atlantic Forest - Latosol site. Geoderma 288, 64–78. https://doi.org/10.1016/j.geoderma.2016.10.034

Keim, R.F., Link, T.E., 2018. Linked spatial variability of throughfall amount and intensity during rainfall in a coniferous forest. Agric. For. Meteorol. 248, 15–21. https://doi.org/10.1016/j.agrformet.2017.09.006

Kirchner, A., Nehren, U., Behling, H., Heinrich, J., 2015. Mid- and late Holocene fluvial dynamics in the tropical Guapi-Macacu catchment, Southeast Brazil: The role of climate change and human impact. Palaeogeogr. Palaeoclimatol. Palaeoecol. 426, 308-318. https://doi.org/10.1016/j.palaeo.2015.03.015

Legendre, P., Oksanen, J., ter Braak, C.J.F., 2010. Testing the significance of canonical axes in redundancy analysis. Methods Ecol. Evol. 2, 269–277. https://doi.org/10.1111/j.2041-210X.2010.00078.x

Levia, D.F., Nanko, K., Amasaki, H., Giambelluca, T.W., Hotta, N., Iida, S., Mudd, R.G., Nullet, M.A., Sakai, N., Shinohara, Y., Sun, X., Suzuki, M., Tanaka, N., Tantasirin, C., Yamada, K., 2019., Throughfall partitioning by trees. Hydrol. Process. 33, 1698 – 1708. https://doi.org/10.1002/hyp.13432

Levia, D.F., Hudson, S.A., Llorens, P., Nanko, K., 2017. Throughfall drop size distributions: a review and prospectus for future research. Wires. Water 4, 1–18. https://doi.org/10.1002/wat2.1225

Levia, D., Germer, S., 2015. A review of stemflow generation dynamics and stemflow-environment interactions in forest and schrublands. Rev. Geophys. 53, 673-714. https://doi.org/10.1002/2015RG000479

Levia, D.F., Frost, E.E., 2006. Variability of throughfall volume and solute inputs in wooded ecosystems. Prog. Phys. Geogr. 30, 605–632. https://doi.org/10.1177/0309133306071145

Liu, J., Liu, W., Li, W., Zeng, H., 2019. How does a rubber plantation affect the spatial variability and temporal stability of throughfall? Hydrol. Res. 50, 1–15. https://doi.org/10.2166/nh.2018.028

Liu, J., Zhang, Z., Zhang, M., 2018. Impacts of forest structure on precipitation interception and run-off generation in a semiarid region in northern China. Hydrol. Process. 32, 2362–2376. https://doi.org/10.1002/hyp.13156

Llorens, P., Domingo, F., 2007. Land use and land cover change after agricultural abandonment. J. Hydrol. 335, 37–54.

Macdicken, K.G., Wolf, G.V., Briscoe, C.B., 1991. Standard research methods for multipurpose trees and shrubs, first ed. Winrock International, USA.

Mantovani, V.A., Terra, M.C.N.S., Mello, C.R., Rodrigues, A.F., Oliveira, V.A., Pinto, L.O.R., 2021. Spatial and temporal patterns in carbon and nitrogen inputs by net precipitation in Atlantic Forest, Brazil. For. Sci. 1–12. https://doi.org/10.1093/forsci/fxab056

Martins, S.V., Júnior, R.C., Rodrigues, R.R., Gandolfi, S., 2004. Colonization of gaps produced by death of bamboo clumps in a semideciduous mesophytic forest in south-eastern Brazil. Plant Ecol. 172, 121–131.

https://doi.org/10.1023/B:VEGE.0000026030.93687.c4

McKee, T.B.; Doesken, N.J.; Kleist, J., 1993. The relationship of drought frequency and duration to time scales. Proc. Conf. Appl. Climatol. 17, 179–183.

Mello, C.R., Ávila, L.F., Lin, H., Terra, M.C.N.S., Chappell, N.A., 2019. Water balance in a neotropical forest catchment of southeastern Brazil. Catena 173, 9–21. https://doi.org/10.1016/j.catena.2018.09.046

Metzger, J.C., Filipzik, J., Michalzik, B., Hildebrandt, A., 2021. Stemflow infiltration hotspots create soil microsites near tree stems in an unmanaged mixed beech Forest. Front. For. Glob. Chang. 4, 1–14. https://doi.org/10.3389/ffgc.2021.701293

Minet, J., Verhoest, N.E.C., Lambot, S., Vanclooster, M., 2013. Temporal stability of soil moisture patterns measured by proximal ground-penetrating radar. Hydrol. Earth Syst. Sci. Discuss. 10, 4063–4097. https://doi.org/10.5194/hessd-10-4063-2013

Molina, A.J., Llorens, P., Garcia-Estringana, P., Heras, M.M., Cayuela, C., Gallart, F., Latron, J., 2019. Contributions of throughfall, forest and soil characteristics to near-surface soil water-content variability at plot scale in a mountainous Mediterranean area. Sci. Total Environ. 647, 1421–1432. https://doi.org/10.1016/j.scitotenv.2018.08.020

Myers, N., Mittermeier, R.A., Mittermeier, C.G., Fonseca, G.A.B., Kent, J., 2000. Biodiversity hotspots for conservation priorities. Nature 403, 853–858. https://doi.org/10.1038/35002501

Nanko, K., Hudson, S.A., Levia, D.F., 2016. Differences in throughfall drop size distribution in the presence and absence of foliage. Hydrol. Sci. J. 61, 620–627.

https://doi.org/10.1080/02626667.2015.1052454

Nanko, K., Onda, Y., Ito, A., Moriwaki, H., 2011. Spatial variability of throughfall under a single tree: Experimental study of rainfall amount, raindrops, and kinetic energy. Agric. For. Meteorol. 151, 1173–1182. https://doi.org/10.1016/j.agrformet.2011.04.006

Nanko, K., Onda, Y., Ito, A., Moriwaki, H., 2008. Effect of canopy thickness and canopy saturation on the amount and kinetic energy of throughfall: An experimental approach. Geophys. Res. Lett. 35, 1 – 5. https://doi.org/10.1029/2007GL033010

Nanko, K., Hotta, N., Suzuki, M., 2006. Evaluating the influence of canopy species and meteorological factors on throughfall drop size distribution. J. Hydrol. 329, 422–431. https://doi.org/10.1016/j.jhydrol.2006.02.036

Nehren, U., Kirchner, A., Lange, W., Follador, M., Anhuf, D., 2019. Natural hazards and climate change Impacts in the state of Rio de Janeiro: A landscape historical analysis, in: Nehren, U., Schlüter, S., Raedig, C., Sattler, D., Hissa, H. (Hrsg.), Strategies and tools for a sustainable rural Rio de Janeiro. Springer Ser.Environment.Management, Cham, pp. 313-330.

Ngueguim, J.R., Solefack, M.C.M., Betti., J.L. Floristic and structural traits of tree vegetation in three sites with different level of disturbance in dense humid forest of Cameroon. J. Ecol. Nat. 10, 239–249. https://doi.org/10.5897/JENE2018.0685

Nobre, C.A., Marengo, J.A., Seluchi, M.E., Cuartas, L.A., Alves, L.M., 2016. Some Characteristics and impacts of the drought and water crisis in southeastern Brazil during 2014 and 2015. J. Water Resour. Prot. 8, 252–262. https://doi.org/10.4236/jwarp.2016.82022

Oksanen, J., Blanchet, F.G., Friendly, M., Kindt, R., Legendre, P., McGlinn, D., Michin, P. R., O'Hara, R.B., Simpson, G. L., Solymos, P., Stevens, M.H.S., Szoecs, E., Wagner, H., 2020. vegan: Community Ecology Package. R package version 2.5-7. https://CRAN.R-project.org/package=vegan

Oliveira, V.A., Rodrigues, A.F., Morais, M.A.V., Terra, M.C.N.S., Guo, L., Mello, C.R., 2021. Spatiotemporal modelling of soil moisture in an Atlantic forest through machine learning algorithms. Eur. J. Soil Sci. 1–19. https://doi.org/10.1111/ejss.13123

Oliveira-Filho, A.T., Fontes, M.A.L., 2000. Patterns of floristic differentiation among Atlantic Forests in Southeastern Brazil and the influence of climate. Biotrop. 32, 793–810. https://doi.org/10.1111/j.1744-7429.2000.tb00619.x

Oliveira-Filho, A.T., Mello, J.M., Scolforo, J.R.S., 1997. Effects of past disturbance and edges on tree community structure and dynamics within a fragment of tropical semideciduous forest in south-eastern Brazil over a five-year period (1987-1992). Plant Ecol. 131, 45–66. https://doi.org/10.1023/A:1009744207641

Pearson, K., 1901. On lines and planes of closest fit to systems of points in space. London and Edinburgh Philos. Mag. J. Sci. 2, 559 – 572. https://doi.org/10.1080/14786440109462720

Phillips, O.L., Aragão, L.E.O.C., Lewis, S.L., Fisher, J.B., Lloyd, J., López-gonzález, G., Malhi, Y., Monteagudo, A., Peacock, J., Quesada, C.A., Heijden, G. Van Der, Almeida, S., Amaral, I., Arroyo, L., Aymard, G., Baker, T.R., Bánki, O., Blanc, L., Bonal, D., Brando, P., Chave, J., Cristina, Á., Oliveira, A. De, Cardozo, N.D., Czimczik, C.I., Feldpausch, T.R., Freitas, M.A., Gloor, E., Higuchi, N., Jiménez,

E., Lloyd, G., Meir, P., Mendoza, C., Morel, A., Neill, D.A., Nepstad, D., Patiño, S., Peñuela, M.C., Prieto, A., Ramírez, F., Schwarz, M., Silva, J., Silveira, M., Thomas, A.S., Steege, H., Stropp, J., Vásquez, R., Zelazowski, P., Dávila, E.A., Andelman, S., Andrade, A., Chao, K., Erwin, T., Fiore, A. Di, C, E.H., Keeling, H., Killeen, T.J., Laurance, W.F., Cruz, A.P., Pitman, N.C.A., Vargas, P.N., Ramírez-angulo, H., Rudas, A., Salamão, R., 2009. Drought sensitivity of the Amazon Rainforest. Science 323, 1344–1347. https://doi.org/10.1126/science.1164033

Poorter, L., Bongers, L., Bongers, F., 2006. Architecture of 54 moist-forest tree species: traits, trade-offs, and functional groups. Ecology 87, 1289–1301. https://doi.org/10.1890/0012-9658(2006)87[1289:AOMTST]2.0.CO;2

Pressland, A.J., 1976. Soil moisture redistribution as affected by throughfall and stemflow in an arid zone shrub community. Aust. J. Bot. 24, 641–649. https://doi.org/10.1071/BT9760641

Quiring, S.M., 2009. Monitoring drought: An evaluation of meteorological drought indices. Geogr. Compass. 3, 64–88. https://doi.org/10.1111/j.1749-8198.2008.00207.x

R Core Team, 2020. R: A Language and environment for statistical computing. R. Foundation for Statistical Computing, Vienna. ISBN 3-900051-07-0. URL http://www.R-project.org.

Réjou-Méchain, M., Tanguy, A., Piponiot, C., Chave, J., Hérault, B., 2017. BIOMASS: an R package for estimating above-ground biomass and its uncertainty in tropical forests. Methods Ecol. Evol. 8, 1163–1167. https://doi.org/10.1111/2041-

210X.12753

Ribeiro, M.C., Metzger, J.P., Martensen, A.C., Ponzoni, F.J., Hirota, M.M., 2009. The Brazilian Atlantic Forest: How much is left, and how is the remaining forest distributed? Implications for conservation. Biol. Conserv. 142, 1141–1153. https://doi.org/10.1016/j.biocon.2009.02.021

Rodrigues, A.F., Mello, C.R., Nehren, U., Ribeiro, J.P.C., Mantovani, V.A., Mello, J.M., 2021a. Modeling canopy interception under drought conditions: The relevance of evaporation and extra sources of energy. J. Environ. Manage. 292. https://doi.org/10.1016/j.jenvman.2021.112710

Rodrigues, A.F., Mello, C.R., Terra, M.C.N.S., Beskow, S., 2021b. Water balance of an Atlantic forest remnant under a prolonged drought period. Cienc. e Agrotecnologia 45, 1–13. https://doi.org/10.1590/1413-7054202145008421

Rodrigues, A.F., Mello, C.R., Terra, M.C.N.S., Silva, V.O., Pereira, G.A., Silva, R.A., 2020. Soil water content and net precipitation spatial variability in an Atlantic forest remnant. Acta Sci. - Agron. 42. https://doi.org/10.4025/actasciagron.v42i1.43518

Ryan, M.G., 2015. Tree mortality: Large trees losing out to drought. Nat. Plants 1, 1–3. https://doi.org/10.1038/nplants.2015.150

Schlesinger, W.H., Dietze, M.C., Jackson, R.B., Phillips, R.P., Rhoades, C.C., Rustad, L.E., Vose, J.M., 2016. Forest biogeochemistry in response to drought. Glob. Chang. Biol. 22, 2318–2328. https://doi.org/10.1111/gcb.13105

Sheng, H., Cai, T., 2021. Spatial variability of throughfall in a Larch (Larix gmelinii) Forest in Great Kingan Mountain, northeastern China. Forests 12, 1–13.

https://doi.org/10.3390/f12040393

Silva, V.O., Mello, C.R., 2021. Meteorological droughts in part of southeastern Brazil: Understanding the last 100 years. An. Acad. Bras. Ciênc. 93, 1–17. https://doi.org/10.1590/0001-3765202120201130

Souza, C.R., Maia, V.A., Aguiar-Campos, N., Santos, A.B.M., Rodrigues, A.F., Farrapo, C.L., Gianasi, F.M., Paula, G.G.P., Fagundes, N.C.A., Silva, W.B., Santos, R.M., 2021. Long-term ecological trends of small secondary forests of the atlantic forest hotspot: A 30-year study case. For. Ecol. Manage. 489. https://doi.org/10.1016/j.foreco.2021.119043

Staelens, J., De Schrijver, A., Verheyen, K., Verhoest, N.E.C., 2006. Spatial variability and temporal stability of throughfall water under a dominant beech (Fagus sylvatica L.) tree in relationship to canopy cover. J. Hydrol. 330, 651–662. https://doi.org/10.1016/j.jhydrol.2006.04.032

Stogsdill, W.R., Wittwer, R.F., Hennessey, T.C., Dougherty, P.M., 1989. Relationship between throughfall and stand density in a *Pinus taeda* Plantation. For. Ecol. Manag. 29, 105–113.

Su, L., Xie, Z., Xu, W., Zhao, C., 2019. Variability of throughfall quantity in a mixed evergreen-deciduous broadleaved forest in central China. J. Hydrol. Hydromech. 67, 225–231. https://doi.org/10.2478/johh-2019-0008

Teixeira, G.M., Figueiredo, P.H.A., Salemi, L.F., Ferraz, S.F.B., Ranzini, M., Arcova, F.C.S., Cicco, V. De, Rizzi, N.E., 2021. Regeneration of tropical montane cloud forests increases water yield in the Brazilian Atlantic Forest. Ecohydrology 15, 1–11. https://doi.org/10.1002/eco.2298

ter Braak, C.J.F., Looman, C.W.M., 1994. Biplots in Reduced-Rank Regression. Biometrical J. 36, 983–1003.

Terra, M.C.N.S., Mello, C.R., Mello, J.M., Oliveira, V.A., Nunes, M.H., Silva, V.O., Rodrigues, A.F., Alves, G.J., 2018a. Stemflow in a neotropical forest remnant: vegetative determinants, spatial distribution and correlation with soil moisture. Trees 32, 323–335. https://doi.org/10.1007/s00468-017-1634-3

Terra, M.C.S.N., Santos, R.M., Prado Júnior, J.A., Mello, J.M., Scolforo, J.R.S., Fontes, M.A.L., Schiavini, I., Reis, A.A., Bueno, I.T., Magno, L.F.S., ter Steege, H., 2018b. Water availability drives gradients of tree diversity, structure and functional traits in the Atlantic-Cerrado-Caatinga transition, Brazil. J. Plant Ecol. 11, 803–814. https://doi.org/10.1093/jpe/rty017

The Angiosperm Phylogeny Group, Chase, M.W., Christenhuszm, J.M., Fay, M.F., Byng, J.W., Judd, W.S., Soltis, D.E., Mabberley, D.J., Sennikov, A.N,. Soltis, P.S., Stevens, P.F., 2016. An update of the Angiosperm Phylogeny Group classification for the orders and families of flowering plants: APG IV. Bot. J. Linn. Soc. 181, 1–20. https://doi.org/10.1111/boj.12385.

Tonello, K., Rosa, A.G., Pereira, L.C., Matus, G.N., Guandique, M.E.G., Navarrete, A. A., 2021. Rainfall partitioning in the Cerrado and its influence on net rainfall nutrient fluxes. Agric. For. Meteorol. 303, 1-12. https://doi.org/10.1016/j.agrformet.2021.108372

Vachaud, G., Silans, A.P.D.E., Balabanis, P., Vauclin, M., 1985. Temporal stability of spatially measured soil water probability density function. Soil Sci. Soc. Am. J. 49, 822–828.

Van Stan J.T., Hildebrandt A., Friesen J., Metzger J.C., Yankine S.A., 2020. Spatial variability and temporal stability of local net precipitation patterns. In: Van Stan, II J., Gutmann E., Friesen J. (eds) Precipitation partitioning by vegetation. Springer, Cham. https://doi.org/10.1007/978-3-030-29702-2_6

World Meteorological Organization - WMO. Standardized precipitation index user guide. 2012. Available in: <http://www.wamis.org/agm/pubs/SPI/WMO_1090_EN.pdf>. Access in: June, 12, 2021.

Wullaert, H., Pohlert, T., Boy, J., Valarezo, C., Wilcke, W., 2009. Spatial throughfall heterogeneity in a montane rain forest in Ecuador: extent, temporal stability and drivers. J. Hydrol. 377, 71–79. https://doi.org/10.1016/j.jhydrol.2009.08.001

Yan, T., Wang, Z., Liao, C., Xu, W., Wan, L., 2021. Effects of the morphological characteristics of plants on rainfall interception and kinetic energy. J. Hydrol. 592, 1–15. https://doi.org/10.1016/j.jhydrol.2020.125807

Zhang, H., Wu, H., Li, J., He, B., Liu, J., Wang, N., Duan, W., Liao, A., 2019. Spatial-temporal variability of throughfall in a subtropical deciduous forest from the hilly regions of eastern China. J. Mt. Sci. 16, 1788–1801. https://doi.org/10.1007/s11629-019-5424-9

Zhang, M., Liu, N., Harper, R., Li, Q., Liu, K., Wei, X., Ning, D., Hou, Y., Liu, S., 2017. A global review on hydrological responses to forest change across multiple spatial scales: Importance of scale, climate, forest type and hydrological regime. J. Hydrol. 546, 44–59. https://doi.org/10.1016/j.jhydrol.2016.12.040

Zhang, Y., Wang, X., Hu, R., Pan, Y., 2016. Throughfall and its spatial variability beneath xerophytic shrub canopies within water-limited arid desert ecosystems. J.

Hydrol. 539, 406–416. https://doi.org/10.1016/j.jhydrol.2016.05.051

Zhang, Y., Wang, X., Hu, R., Pan, Y., Paradeloc, M., 2015. Rainfall partitioning into throughfall, stemflow and interception loss by two xerophytic shrubs within a rain-fed re-vegetated desert ecosystem, northwestern China. J. Hydrol. 527, 1084–1095.

Zhu, X., He, Z., Du, J., Chen, L., Lin, P., Tian, Q., 2021. Spatial heterogeneity of throughfall and its contributions to the variability in near-surface soil water-content in semiarid mountains of China. For. Ecol. Manage. 488, 1–12. https://doi.org/10.1016/j.foreco.2021.119008

Zimmermann, A., Zimmermann, B., 2014. Requirements for throughfall monitoring: The roles of temporal scale and canopy complexity. Agric. For. Meteorol. 189–190, 125–139. http://dx.doi.org/10.1016/j.agrformet.2014.01.014

Zimmermann, A., Zimmermann, B., Elsenbeer, H., 2009. Rainfall redistribution in a tropical forest: Spatial and temporal patterns. Water Resour. Res. 45, 1-18. https://doi.org/10.1029/2008WR007470

Zimmermann, A., Germer, S., Neill, C., Krusche, A. V, Elsenbeer, H., 2008. Spatio-temporal patterns of throughfall and solute deposition in an open tropical rain forest. J. Hydrol. 360, 87–102. https://doi.org/10.1016/j.jhydrol.2008.07.028

7. Supplementary Material

Table S1. Pearson coefficient correlation for MRDj data used in the PCA for small rainfall events (GR < 10 mm) in the Atlantic Forest remnant.

	MRD-13/14	MRD-14/15	MRD-15/16	MRD-16/17	MRD-17/18	MRD-18/19
MRD-13/14	1	0.807753	0.511616	0.36708	0.337268	0.315945
MRD-14/15	0.807753	1	0.710708	0.5356	0.394799	0.415502
MRD-15/16	0.511616	0.710708	1	0.746348	0.432505	0.409264

MRD-16/17	0.36708	0.5356	0.746348	1	0.630024	0.591104
MRD-17/18	0.337268	0.394799	0.432505	0.630024	1	0.80852
MRD-18/19	0.315945	0.415502	0.409264	0.591104	0.80852	1

Table S2. Pearson coefficient correlation for MRDj data used in the PCA for rainfall events with gross precipitation > 10 mm in the Atlantic Forest remnant.

	MRD-13/14	MRD-14/15	MRD-15/16	MRD-16/17	MRD-17/18	MRD-18/19
MRD-13/14	1	0.638877	0.511751	0.043459	0.005336	0.062621
MRD-14/15	0.638877	1	0.606198	0.015569	-0.09677	-0.04901
MRD-15/16	0.511751	0.606198	1	0.360595	0.100243	0.234276
MRD-16/17	0.043459	0.015569	0.360595	1	0.716613	0.397088
MRD-17/18	0.005336	-0.09677	0.100243	0.716613	1	0.53829
MRD-18/19	0.062621	-0.04901	0.234276	0.397088	0.53829	1

Table S3. Pearson coefficient correlation for TSI data used in the PCA for small rainfall events (GR < 10 mm) in Atlantic Forest remnant.

	TSI-13/14	TSI-14/15	TSI-15/16	TSI-16/17	TSI-17/18	TSI-18/19
TSI-13/14	1	0.587917	0.127826	0.235208	0.265127	0.270514
TSI-14/15	0.587917	1	0.234486	0.349661	0.244912	0.526435
TSI-15/16	0.127826	0.234486	1	0.34256	-0.03134	0.339151
TSI-16/17	0.235208	0.349661	0.342559	1	0.470336	0.371058
TSI-17/18	0.265127	0.244912	-0.03134	0.470336	1	0.400504
TSI-18/19	0.270514	0.526435	0.339151	0.371058	0.400504	1

Table S4. Pearson coefficient correlation for TSI data used in the PCA for rainfall events with gross precipitation > 10 mm in Atlantic Forest remnant.

	TSI-13/14	TSI-14/15	TSI-15/16	TSI-16/17	TSI-17/18	TSI-18/19
TSI-13/14	1	0.505657	0.054914	0.302366	0.138155	0.176704
TSI-14/15	0.505657	1	0.14323	0.359967	0.046769	0.143627
TSI-15/16	0.054914	0.14323	1	0.337435	-0.04474	0.200386
TSI-16/17	0.302366	0.359967	0.337435	1	0.314773	0.185113
TSI-17/18	0.138155	0.046769	-0.04474	0.314773	1	0.330296

TSI-18/19	0.176704	0.143627	0.200386	0.185113	0.330296	1

Table S5. Output of the *envfit* function of forest structure data onto the MRDj PCA for small rainfall events (GR < 10 mm) in the Atlantic Forest remnant.

	PC1	PC2	r^2	Pr(>r)	
DBH-10	-0.29375	-0.95588	0.1278	0.157	
N-10	0.88732	0.46115	0.218	0.036	*
G-10	0.78592	-0.61833	0.0996	0.246	
CV_DBH-10	0.38783	-0.92173	0.0131	0.821	
AGB.10	0.64001	-0.76837	0.1085	0.215	
S.10	0.76035	0.64952	0.0269	0.694	
H-10	0.90227	0.43117	0.0115	0.853	
J-10	-0.81005	-0.58636	0.0144	0.811	
DBH-15	-0.46609	-0.88474	0.0935	0.265	
N-15	0.88241	0.47048	0.2114	0.042	*
G-15	0.90395	-0.42763	0.0936	0.263	
CV_DBH-15	-0.3169	-0.94846	0.0117	0.834	
AGB-15	0.7417	-0.67074	0.0901	0.276	
S-15	0.89068	0.45462	0.0419	0.545	
H-15	0.99841	0.05633	0.0176	0.79	
J-15	-0.92438	-0.38148	0.0832	0.297	
DBH-17	-0.33773	-0.94124	0.0621	0.407	

N-17	0.84873	0.52883	0.2427	0.025	*
G-17	0.96031	-0.27893	0.0863	0.28	
CV_DBH-17	-0.82051	-0.57164	0.0341	0.624	
AGB-17	0.76164	-0.648	0.0669	0.388	
S-17	0.90714	0.42082	0.0731	0.35	
H-17	0.98221	0.18781	0.0209	0.746	
J-17	-0.93953	-0.34246	0.1378	0.121	
Signif. codes: 0 ‘***’ 0.001 ‘**’ 0.01 ‘*’ 0.05 ‘.’ 0.1 ‘ ’ 1					

Table S6. Output of the *envfit* function of forest structure data onto the MRDj PCA for rainfall events with gross precipitation > 10 mm in the Atlantic Forest remnant.

	PC1	PC2	r^2	Pr(>r)	
DBH-10	0.37398	-0.92744	0.2294	0.021	*
N-10	-0.78047	0.62519	0.2226	0.037	*
G-10	-0.30933	-0.95096	0.0702	0.362	
CV_DBH-10	0.16706	-0.98595	0.0254	0.688	
AGB.10	-0.16168	-0.98684	0.0915	0.259	
S.10	-0.41092	0.91167	0.0422	0.546	
H-10	-0.60423	0.79681	0.0258	0.702	
J-10	0.70382	-0.71038	0.0138	0.818	
DBH-15	0.42543	-0.90499	0.1804	0.061	.
N-15	-0.82863	0.5598	0.2056	0.047	*
G-15	-0.60196	-0.79852	0.0842	0.292	
CV_DBH-15	0.18464	-0.98281	0.0284	0.655	
AGB-15	-0.38245	-0.92398	0.0921	0.261	
S-15	-0.8311	0.55612	0.0432	0.565	
H-15	-0.99999	0.00358	0.0103	0.869	
J-15	0.83574	-0.54912	0.1663	0.078	.
DBH-17	0.31367	-0.94953	0.1547	0.1	.
N-17	-0.74555	0.66645	0.252	0.023	*
G-17	-0.80392	-0.59474	0.0544	0.451	
CV_DBH-17	0.54263	-0.83997	0.0266	0.694	

AGB-17	-0.43405	-0.90089	0.0539	0.442	
S-17	-0.74358	0.66865	0.1003	0.248	
H-17	-0.90449	0.4265	0.0264	0.685	
J-17	0.80468	-0.59372	0.2234	0.032	*
Signif. codes: 0 ‘***’ 0.001 ‘**’ 0.01 ‘*’ 0.05 ‘.’ 0.1 ‘ ’ 1					

Table S7. Output of the *envfit* function of forest structure data onto the TSI PCA for small rainfall events (GR < 10 mm) in Atlantic Forest remnant.

	PC1	PC2	r^2	Pr(>r)	
DBH-10	-0.93542	0.35355	0.1063	0.213	
N-10	0.66627	0.74571	0.0147	0.813	
G-10	-0.63054	0.77616	0.2321	0.025	*
CV_DBH-10	-0.5188	0.8549	0.167	0.088	.
AGB.10	-0.66421	0.74754	0.2749	0.012	*
S.10	-0.68977	0.72403	0.1169	0.185	
H-10	-0.83485	0.55048	0.2386	0.021	*
J-10	-0.96478	0.26307	0.2091	0.041	*
DBH-15	-0.98455	0.17508	0.1291	0.146	
N-15	0.84573	0.53361	0.0263	0.684	
G-15	-0.63724	0.77066	0.2054	0.037	*
CV_DBH-15	-0.58211	0.81311	0.1571	0.104	
AGB-15	-0.67686	0.73612	0.2535	0.02	*
S-15	-0.54697	0.83715	0.1384	0.125	
H-15	-0.8009	0.59879	0.1994	0.049	*
J-15	-0.97598	-0.21787	0.2022	0.051	.
DBH-17	-0.98556	0.16934	0.1936	0.042	*
N-17	0.96948	0.24518	0.0245	0.689	
G-17	-0.71458	0.69956	0.2316	0.02	*

CV_DBH-17	-0.53764	0.84318	0.1081	0.209	
AGB-17	-0.71339	0.70077	0.255	0.018	*
S-17	-0.58444	0.81144	0.1155	0.17	
H-17	-0.81239	0.58311	0.1501	0.106	
J-17	-0.93032	-0.36676	0.1153	0.183	
Signif. codes: 0 ‘***’ 0.001 ‘**’ 0.01 ‘*’ 0.05 ‘.’ 0.1 ‘ ’ 1					

Table S8. Output of the *envfit* function of forest structure data onto the TSI PCA for rainfall events with gross precipitation > 10 mm in the Atlantic Forest remnant.

	PC1	PC2	r^2	Pr(>r)	
DBH-10	-0.74874	-0.66286	0.2112	0.04	*
N-10	0.02186	0.99976	0.058	0.445	
G-10	-0.84945	-0.52767	0.2089	0.051	.
CV_DBH-10	-0.48704	-0.87338	0.131	0.144	
AGB.10	-0.76411	-0.64509	0.2665	0.022	*
S.10	-0.80582	0.59216	0.0535	0.47	
H-10	-0.99853	-0.05425	0.0784	0.344	
J-10	-0.66325	-0.7484	0.1248	0.16	
DBH-15	-0.88273	-0.46989	0.1987	0.056	.
N-15	0.46162	0.88708	0.0176	0.771	
G-15	-0.84686	-0.53182	0.2272	0.033	*
CV_DBH-15	-0.53279	-0.84625	0.1481	0.108	
AGB-15	-0.77348	-0.63382	0.2819	0.017	*
S-15	-0.98867	0.15013	0.0262	0.713	
H-15	-0.95838	-0.2855	0.0638	0.411	
J-15	-0.84436	-0.53577	0.0705	0.362	
DBH-17	-0.89938	-0.43716	0.2892	0.011	*
N-17	0.71847	0.69556	0.015	0.797	
G-17	-0.81046	-0.58579	0.3125	0.011	*

CV_DBH-17	-0.4586	-0.88864	0.1061	0.215	
AGB-17	-0.7388	-0.67393	0.3265	0.009	**
S-17	-0.98536	-0.17049	0.026	0.678	
H-17	-0.91594	-0.40131	0.0578	0.448	
J-17	-0.76225	-0.64729	0.0397	0.552	
Signif. codes: 0 ‘***’ 0.001 ‘**’ 0.01 ‘*’ 0.05 ‘.’ 0.1 ‘ ’ 1					

Table S9. The Standardized Precipitation Index (SPI), the associated return level, and the WMO classification throughout the study period.

Hydrological year	**SPI**	**Return period (years)**	**WMO classification**
2013/2014	-1.89	34.4	severely dry
2014/2015	-1.29	10.2	moderately dry
2015/2016	-0.33	2.7	near normal
2016/2017	-1.31	10.4	moderately dry
2017/2018	-1.51	15.1	severely dry
2018/2019	0.38	1.5	near normal

Table S10. Studies that have assessed the spatial variability and time stability of throughfall. Their assumptions, methodologies, findings, and conclusions.

The table is on .xlsx format due to its size. Please check out the Supplementary Materials (Table S2 – Supplementary Materials.xlsx)

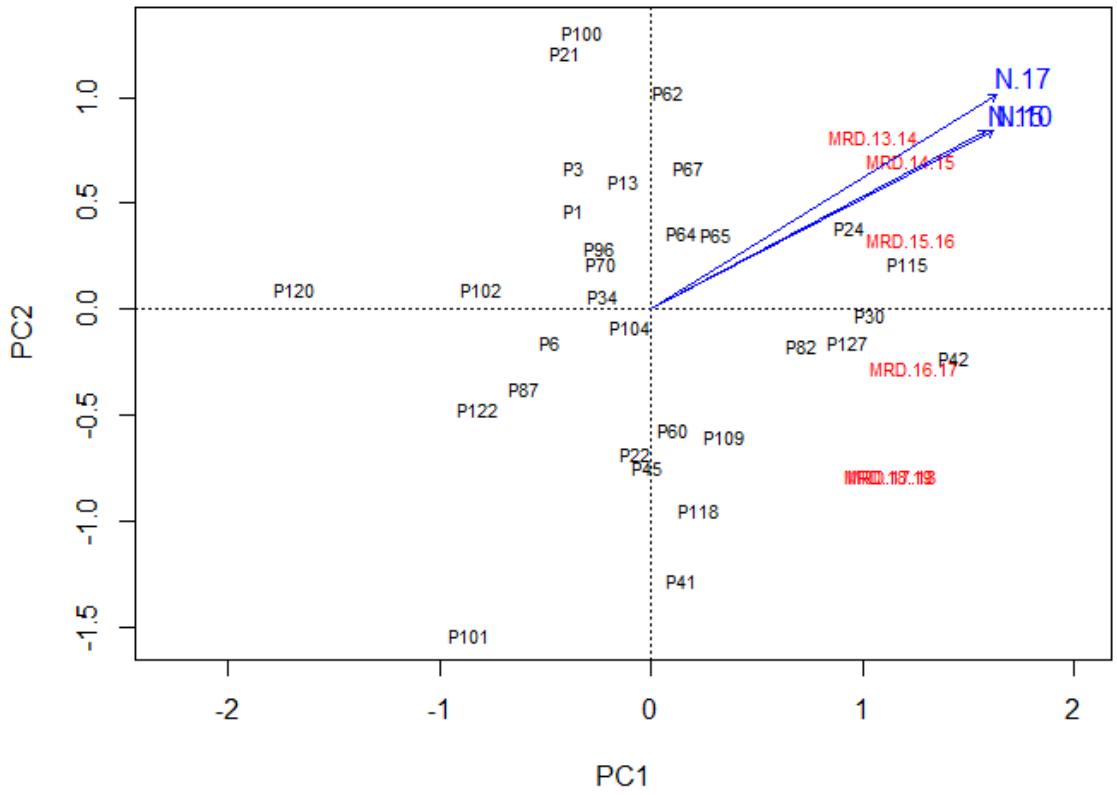

Figure S1. PCA diagram of MRDj data for small rainfall events (GR < 10 mm) in Atlantic Forest remnant. Arrows represent forest structure variables selected by the *envfit* function. Proportion explained by the axes: 1. 61%; 2. 19%.

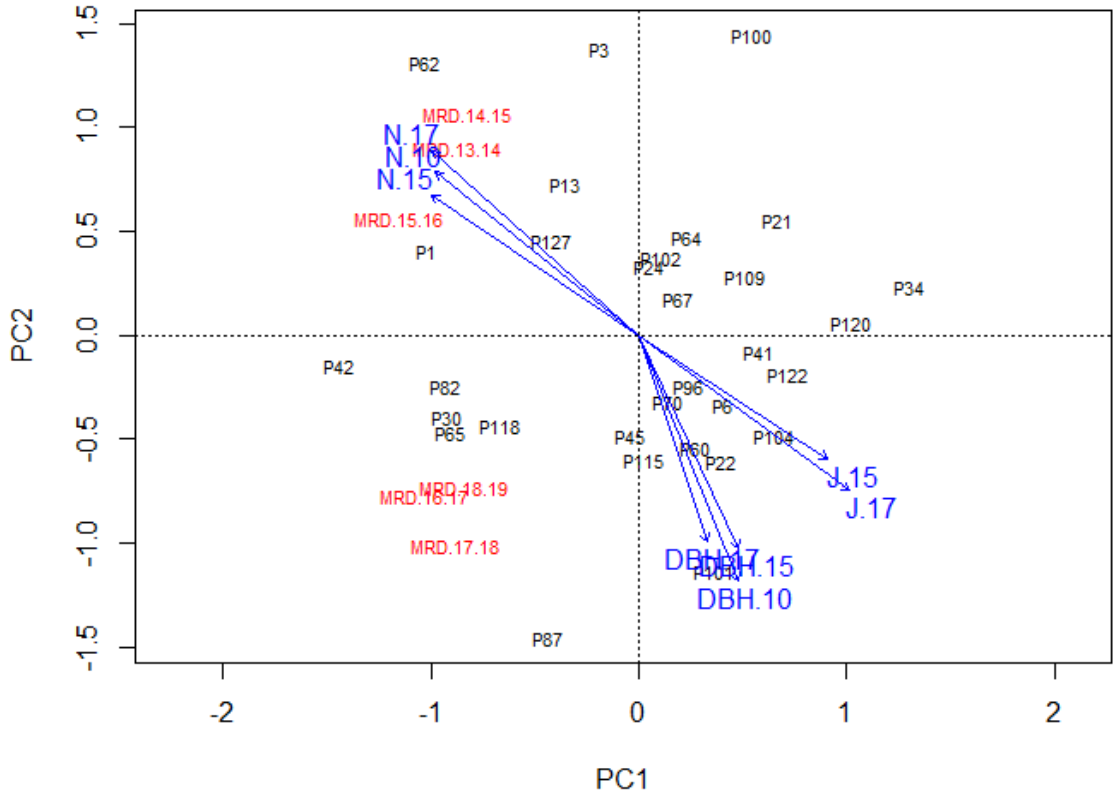

Figure S2: PCA diagram of MRDj data for rainfall events with gross precipitation > 10 mm in Atlantic Forest remnant. Arrows represent forest structure variables selected by the *envfit* function. Proportion explained by the axes: 1. 40%; 2. 33%.

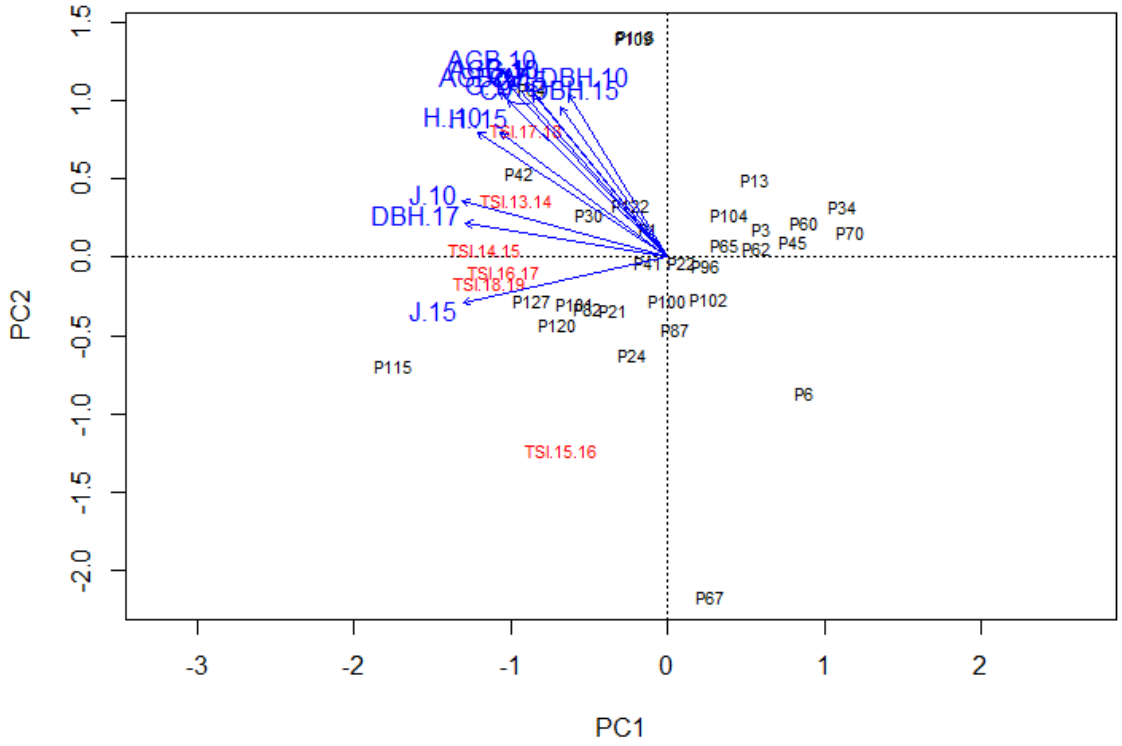

Figure S3. PCA diagram of TSI data for small rainfall events (GR < 10 mm) in Atlantic Forest remnant. Arrows represent forest structure variables selected by the *envfit* function. Proportion explained by the axes: 1. 44%; 2. 17%.

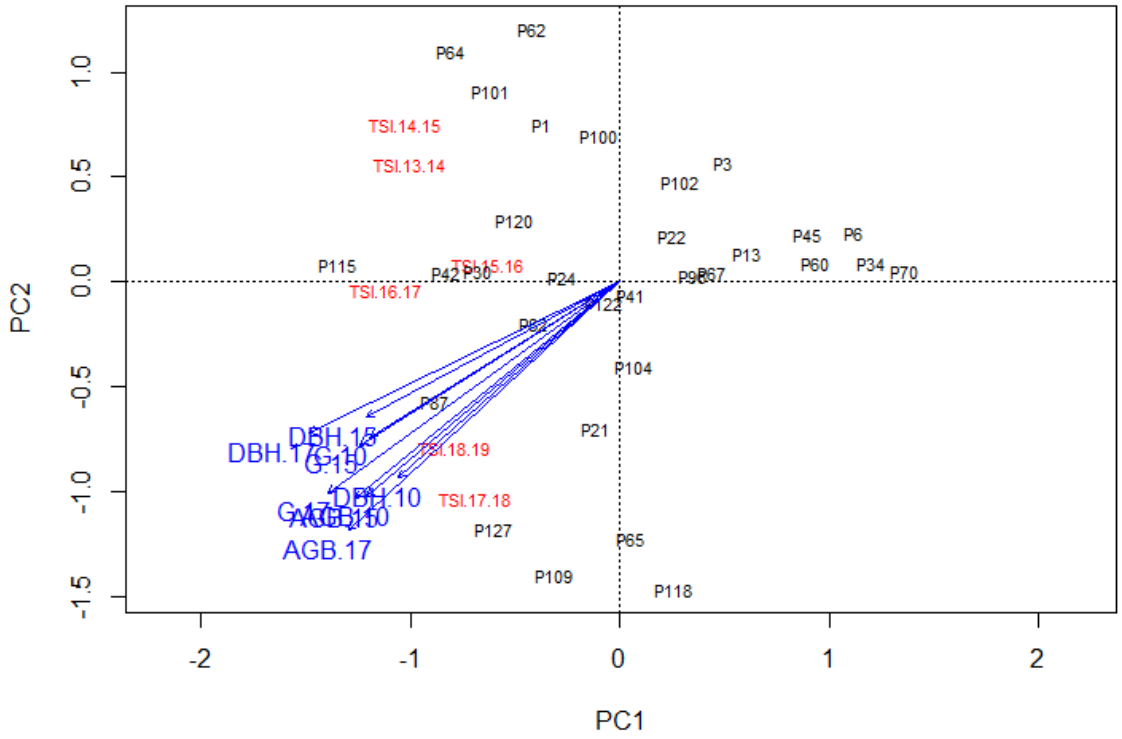

Figure S4. PCA diagram of TSI data for rainfall events with gross precipitation > 10 mm in the Atlantic Forest remnant. Arrows represent forest structure variables selected by the *envfit* function. Proportion explained by the axes: 1. 35%; 2. 19%.

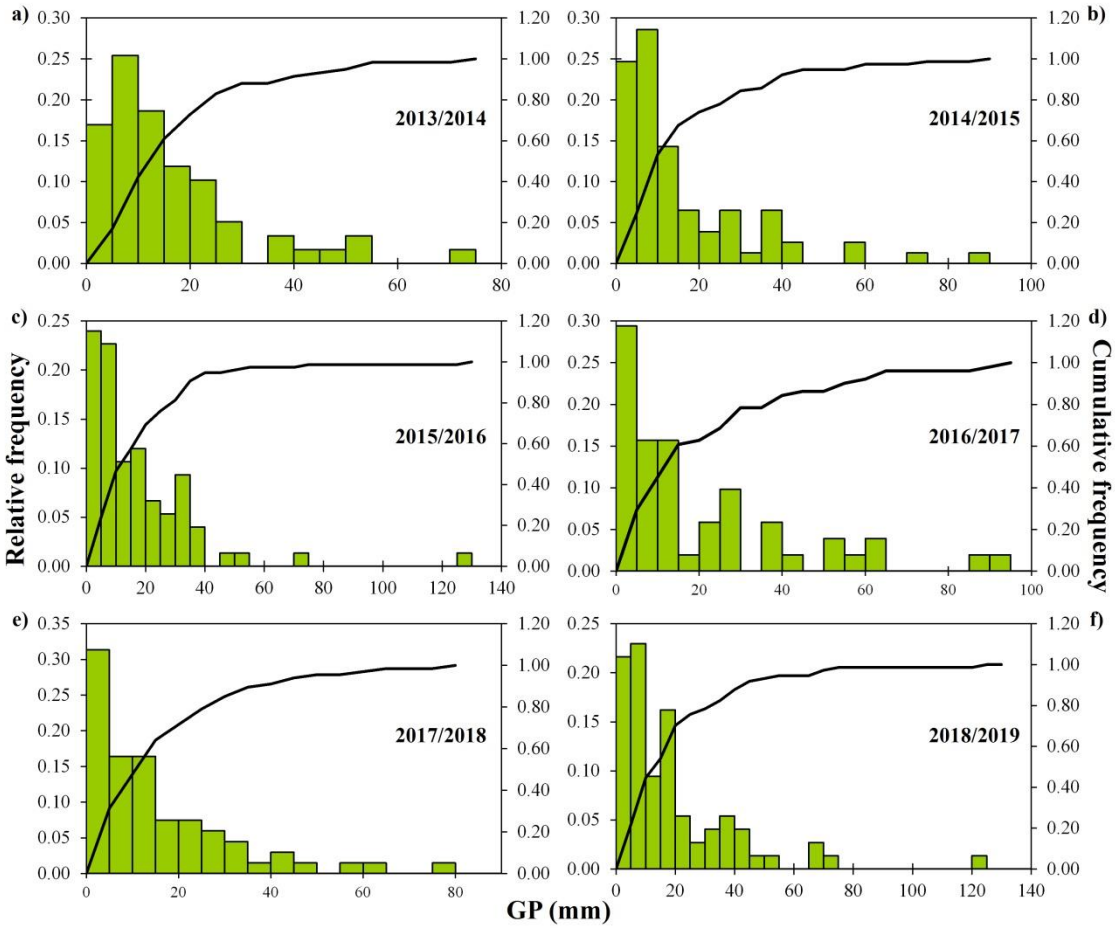

Figure S5. Histograms of gross rainfall (GR) distribution (green bars) and the cumulative frequency of GR occurrence (black line) for the six hydrological years.

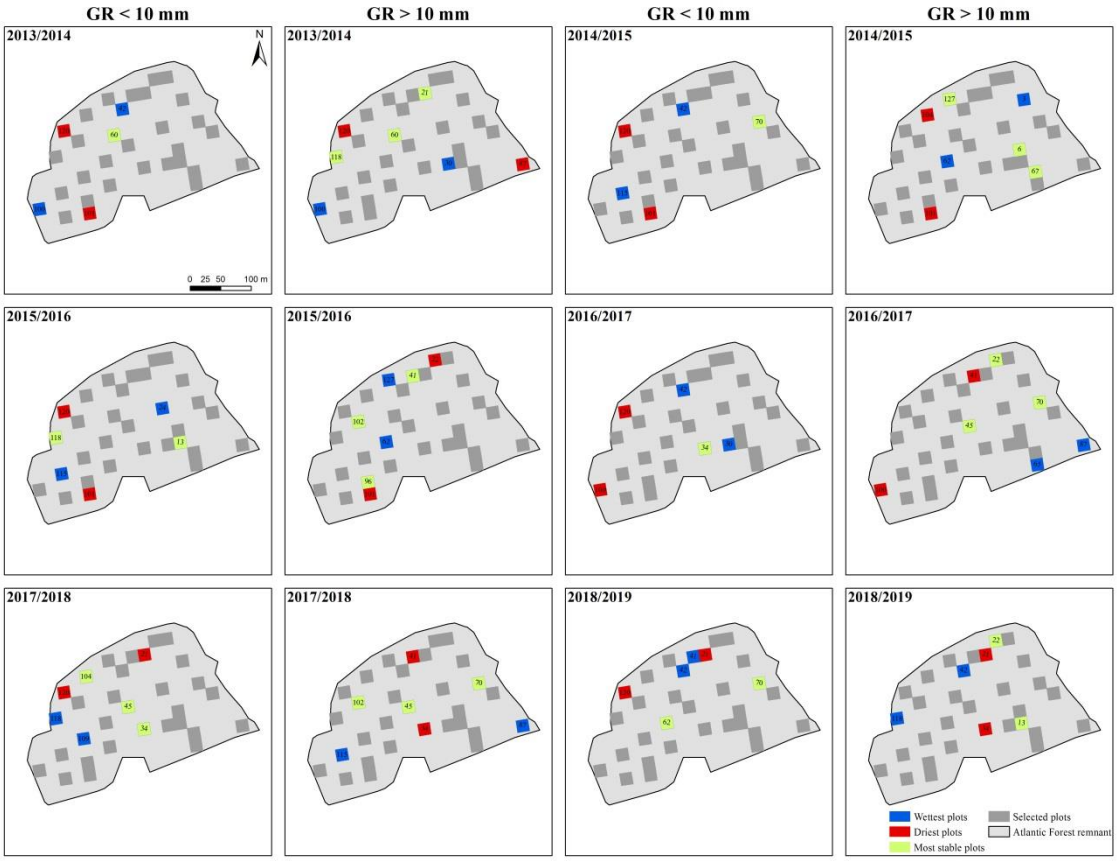

Figure S6. Spatial distribution of the study plots highlighting the wettest, driest, and most time stable plots throughout the six hydrological years and considering gross rainfall (GR) > 10 mm and < 10 mm.

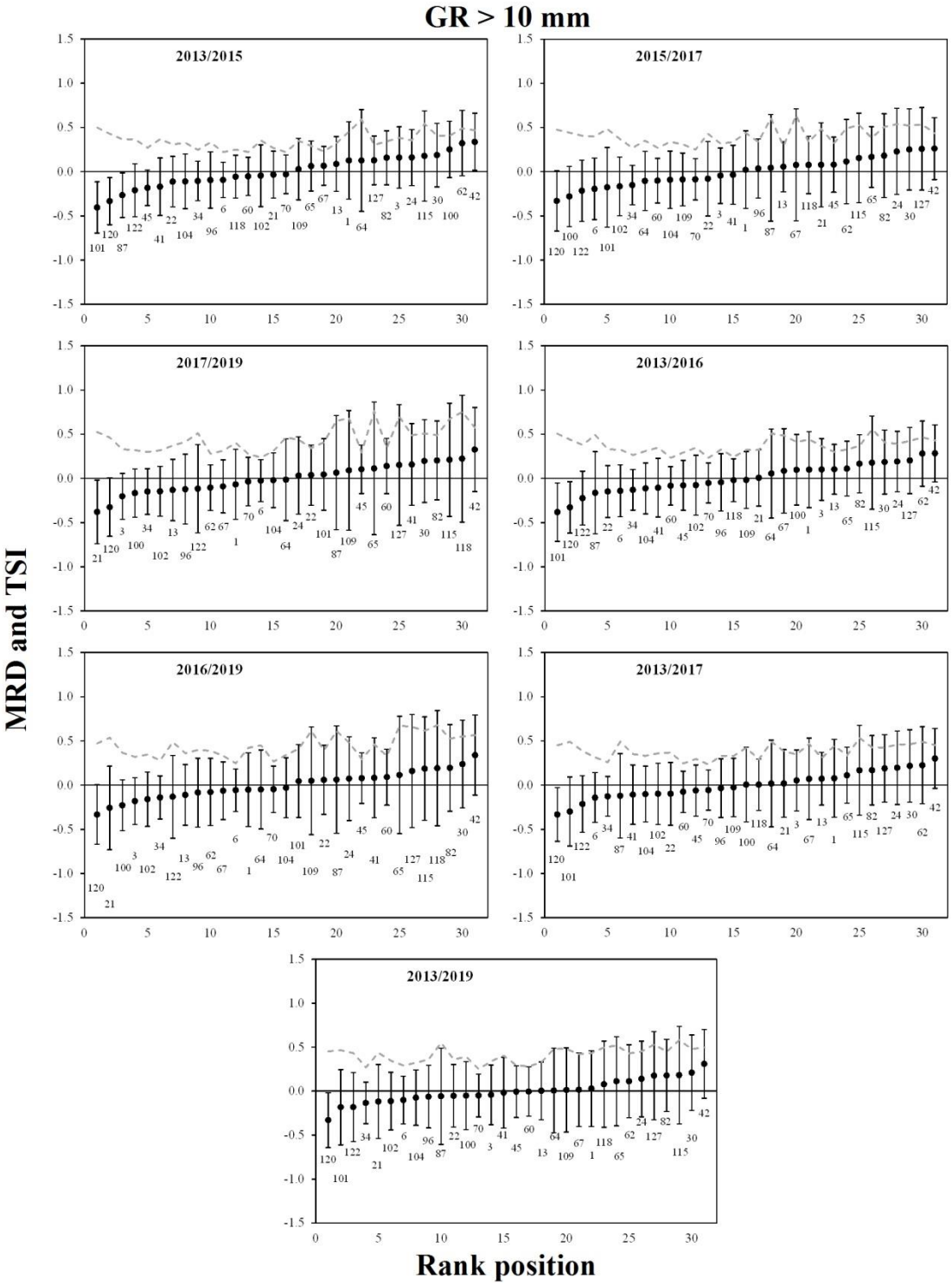

Figure S7. Mean relative difference (MRD) and Temporal Stability Index (TSI) for different period lengths and gross rainfall (GR) > 10 mm.

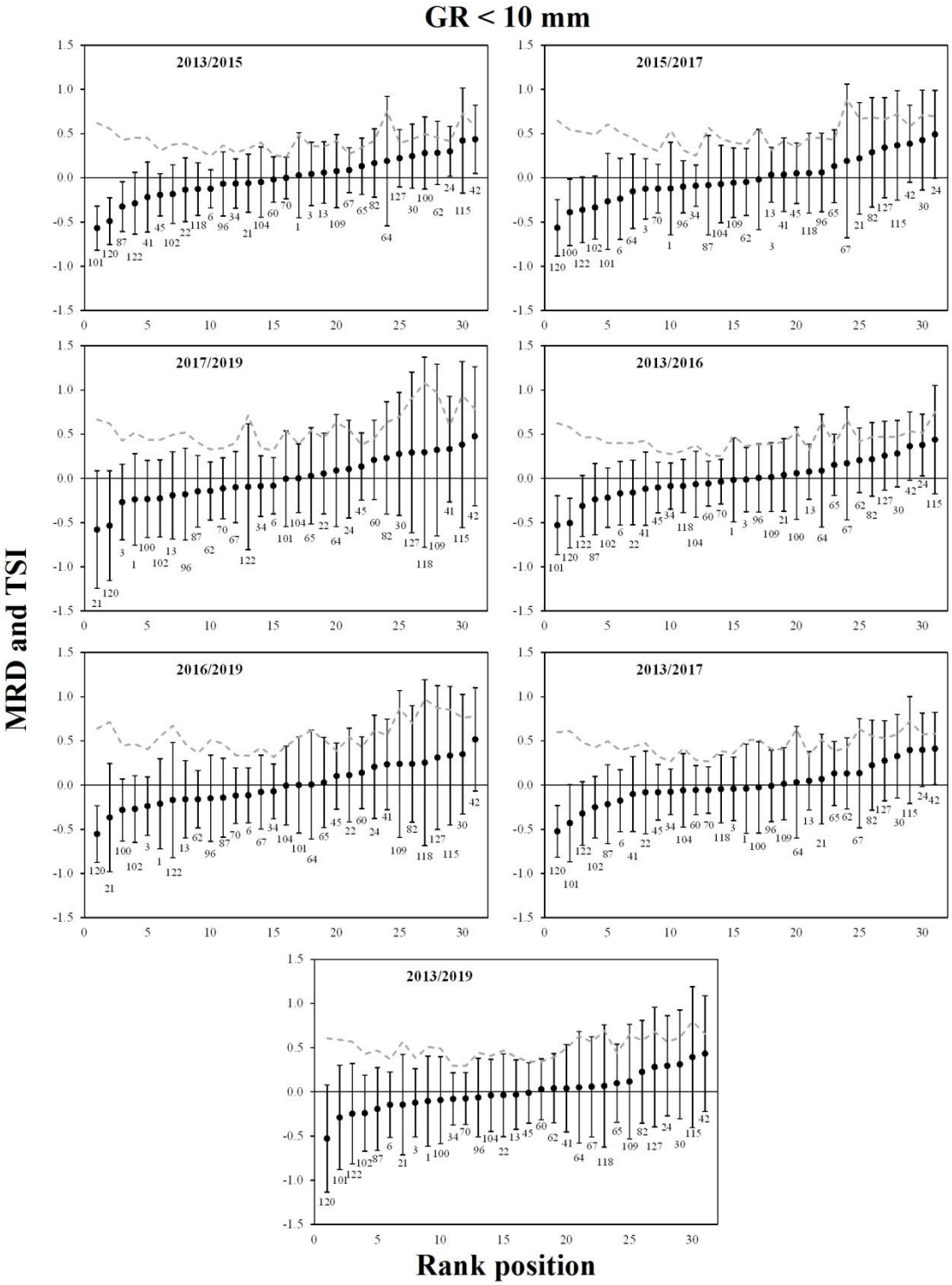

Figure S8. Mean relative difference (MRD) and Temporal Stability Index (TSI) for different period lengths and gross rainfall (GR) < 10 mm.

Final Remarks

This study highlights increasing canopy evaporation during droughts due to greater energy advection from surrounding areas. Droughts also change the spatial distribution of throughfall over time because different species respond differently to water shortage (i.e. leaf loss, mortality, recovering, among others). In such conditions, less water reaches the forest floor following different patterns of spatial distribution, affecting soil water availability, forest transpiration and dynamics, groundwater recharge, and the nutrient cycle. Understanding how forests partition rainfall and redistribute it in both time and space is urgent because canopy-rainfall interactions drive hydrological responses from site to regional scales.

Extreme weather is expected to increase in tropical regions as one of the global warming consequences. Droughts will become more frequent, intense, and lasting, affecting ecosystems dynamics. Therefore, we can expect that the rainfall-canopy interactions are likely to change in the near future due to ecosystem shift to more adapted conditions as a response to increased evaporation and lowered soil water availability. Most of the remaining Atlantic Forest is located in headwater regions that supply water to the wealthiest and most populous region of Brazil. The abovementioned changes in the rainfall partitioning (with lower water reaching the forest floor) are likely to decrease water yield with consequences for people's well-being and livelihood. Decreased water availability can impact agriculture, hydropower plants, water supply, and industry income, among others. However, how much and to which extent the environment, society, and economy will be impacted by changes in rainfall-canopy interactions should be the subject of future studies.

This study is the first glance toward the impacts of dry weather on the rainfall partitioning in tropical regions and calls attention to the importance of this subject to improve ecosystem resilience and water management in the near future. The new insights of this study will support stakeholders in their decisions regarding forest restoration to improve water input as some forest structures and tree characteristics have demonstrated potential to improve throughfall. Therefore, the proper use of such forest characteristics is a powerful tool to mitigate the likely impact of climate change on water yield in tropical watersheds.